Faraday Discussions
Cite this: *Faraday Discuss.*, 2023, **246**, 60

ROYAL SOCIETY OF CHEMISTRY

PAPER

View Article Online
View Journal | View Issue

Unified quantum theory of electrochemical kinetics by coupled ion–electron transfer†

Martin Z. Bazant *

Received 25th May 2023, Accepted 25th May 2023
DOI: 10.1039/d3fd00108c

A general theory of coupled ion–electron transfer (CIET) is presented, which unifies Marcus kinetics of electron transfer (ET) with Butler–Volmer kinetics of ion transfer (IT). In the limit of large reorganization energy, the theory predicts normal Marcus kinetics of "electron-coupled ion transfer" (ECIT). In the limit of large ion transfer energies, the theory predicts Butler–Volmer kinetics of "ion-coupled electron transfer" (ICET), where the charge transfer coefficient and exchange current are connected to microscopic properties of the electrode/electrolyte interface. In the ICET regime, the reductive and oxidative branches of Tafel's law are predicted to hold over a wide range of overpotentials, bounded by the ion-transfer energies for oxidation and reduction, respectively. The probability distribution of transferring electron energies in CIET smoothly interpolates between a shifted Gaussian distribution for ECIT (as in the Gerischer–Marcus theory of ET) to an asymmetric, fat-tailed Meixner distribution centered at the Fermi level for ICET. The latter may help interpret asymmetric line shapes in x-ray photo-electron spectroscopy (XPS) and Auger electron spectroscopy (AES) for metal surfaces in terms of shake-up relaxation of the ionized atom and its image polaron by ICET. In the limit of large overpotentials, the theory predicts a transition to inverted Marcus ECIT, leading to a universal reaction-limited current for metal electrodes, dominated by barrierless quantum transitions. Uniformly valid, closed-form asymptotic approximations are derived that smoothly transition between the limiting rate expressions for ICET and ECIT for metal electrodes, using simple but accurate mathematical functions. The theory is applied to lithium intercalation in lithium iron phosphate (LFP) and found to provide a consistent description of the observed current dependence on overpotential, temperature and concentration. CIET theory thus provides a critical bridge between quantum electrochemistry and electrochemical engineering, which may find many other applications and extensions.

1 Introduction

Charge transfer at the electrode/electrolyte interface is the most fundamental aspect of electrochemical systems, but its understanding remains incomplete. By

Department of Chemical Engineering and Department of Mathematics, Massachusetts Institute of Technology, Cambridge 02139, MA, USA. E-mail: bazant@mit.edu

† This is an extended version of the paper presented at the meeting.

contrast, the bulk properties of electrodes and electrolytes are increasingly investigated and modeled at the molecular level. Their atomic structure and thermodynamic and transport properties can be measured by experiments and accurately predicted by *ab initio* quantum mechanical theories and simulations.[1] For crystalline electrodes and electrolytes, quantum simulations of bulk properties have become so accurate that they are beginning to replace experimental measurements and guide the discovery of new materials.[2] Progress is underway to better understand properties of disordered bulk liquid and solid electrolytes, as well as the molecular structure of electrode/electrolyte interfaces.[3,4]

Faradaic reaction rates at electrode/electrolyte interfaces, however, remain challenging to predict from first principles. This is partly due to the lack of a simple mathematical framework with which to describe both ion transfer (IT) and electron transfer (ET) processes based on quantum mechanics. Here, we develop such a theory for non-adiabatic charge transfer processes, which unifies Butler–Volmer kinetics of IT with Marcus kinetics of ET in a single quantum mechanical framework of coupled ion–electron transfer (CIET).

2 A brief history of electrochemical kinetics

2.1 Ion transfer theory

The standard model of charge transfer kinetics in electrochemistry[5–8] and electrochemical engineering[9,10] is the Butler–Volmer (BV) equation:[11,12]

$$I = I_0(\mathrm{e}^{-\alpha n\tilde{\eta}} - \mathrm{e}^{(1-\alpha)n\tilde{\eta}}) \tag{1}$$

where I is the reduction current, I_0 the exchange current, α the charge-transfer coefficient or symmetry factor, n the number of electrons transferred, and $\tilde{\eta} = e\eta/k_\mathrm{B}T$ the dimensionless activation overpotential η, scaled to the thermal voltage, $k_\mathrm{B}T/e$. The BV equation has remained unchanged for over a century since the seminal work of Tafel,[13,14] Butler,[11,15–18] Bowden[19] and Erdey-Gruz and Volmer[12,20] on the reaction kinetics of electrolysis, motivated by Tafel's limiting law,[13]

$$\ln|I| \sim \begin{cases} -\alpha\tilde{\eta} & \text{as } \tilde{\eta} \to -\infty \\ (1-\alpha)\tilde{\eta} & \text{as } \tilde{\eta} \to \infty \end{cases} \tag{2}$$

The BV equation has since been used to describe faradaic reaction kinetics in all fields of electroanalytical chemistry[6,21] and electrochemical systems,[9,10] including batteries, fuel cells, electrodeposition, corrosion, electrocatalysis, and iontronics (the topic of this *Faraday Discussions* meeting).

The BV equation is almost universally accepted by experimentalists as the model of electrochemical kinetics, although empirical modifications are often required to fit experimental data. For example, in order to reveal pure BV kinetics, it is usually necessary to correct for what are considered spurious "*IR* drops" associated with "film resistance".[9,10] The BV equation has also been extended in many other ways, *e.g.* to account for adsorption isotherms of reaction intermediates,[7,8] Frumkin effects of double-layer charge,[5,22,23] and non-equilibrium thermodynamics of phase transformations.[24]

Despite many successes in fitting experimental data, the BV equation is considered to be phenomenological, and it lacks a consistent theoretical framework with which to interpret fitted parameters or design improved electrode

interfaces. It does not explicitly take into account the microscopic physics of charge transfer, such as charge solvation, ion coordination, double-layer structure, electrode band structure, electronic coupling and quantum tunneling between the acceptor and donor states at interfaces.[25,26] As such, quantitative connections cannot be made between the BV parameters (I_0, α) and material properties, such as dielectric constants, electrode crystal structure, electrolyte chemistry, *etc.*, which could be validated experimentally or predicted by molecular simulations.

Textbook derivations of the BV equation are based on a simple picture of ion transfer (IT) biased by the local electric field,[6–10] as sketched in Fig. 1. The reaction complex explores a landscape of excess chemical potential along a spatial reaction coordinate ξ between the reduced and oxidized states, while transferring n electrons. The chemical part of the activation barrier is assumed to remain constant and at fixed position,

$$\xi_{\ddagger} = \alpha\xi_{\mathrm{O}} + (1 - \alpha)\xi_{\mathrm{R}} \tag{3}$$

as the reaction is biased by a constant local electric field, $E = -\eta_{\mathrm{f}}/(\xi_{\mathrm{R}} - \xi_{\mathrm{O}})$, where η_{f} is the formal overpotential, and $\xi_{\mathrm{R}} - \xi_{\mathrm{O}}$ is the distance for ion transfer, often associated with the thickness of the Stern layer of solvation on the electrode.[27–29] Based on this picture of the reaction mechanism, a thermodynamically consistent derivation of the exchange current yields the formula,

$$I_0^{\mathrm{BV}} = \frac{nek_0^{\mathrm{BV}}(a_{\mathrm{O}}a_{\mathrm{e}}{}^{n})^{1-\alpha}a_{\mathrm{R}}{}^{\alpha}}{\gamma_{\ddagger}} \tag{4}$$

where k_0 is an attempt frequency, $\gamma_{\ddagger}$ is the activity coefficient of the ion-transfer transition state, and a_{O}, a_{R} and a_{e} are the activities of the oxidized state, reduced state, and electrons, defined below.[24]

Although the IT reaction mechanism in Fig. 1 is widely accepted as the justification for BV kinetics, it contains many theoretical inconsistencies. Although η_{f} is varied by changing the potential of electrons in the electrode, the model does not specify exactly when or how electron transfer occurs. Moreover, the activity of electrons is usually neglected by setting $a_{\mathrm{e}} = 1$, and the electrode band structure, which provides electrons over a range of different energies, is not considered at all. The derivation also only applies to moderate overpotentials, much smaller than the chemical energy barrier. As shown in Fig. 1, larger overpotentials would result in barrier-less ion transfer, which cannot be described by classical transition state theory. These limitations of ion transfer theory are well known, but usually overlooked when fitting the BV equation to experimental data. We shall see that the key to resolving these inconsistencies is a quantum mechanical treatment of electron transfer (ET).

2.2 Electron transfer theory

An electrochemical reaction, by definition, involves the transfer of at least one electron between two distinct chemical states. The oxidized state donates an electron, and the reduced state accepts it. In order to conserve charge, there must be ions present in either the reduced or oxidized states, or both. In pure ET reactions, the reactants remain unchanged, except that the oxidized state is

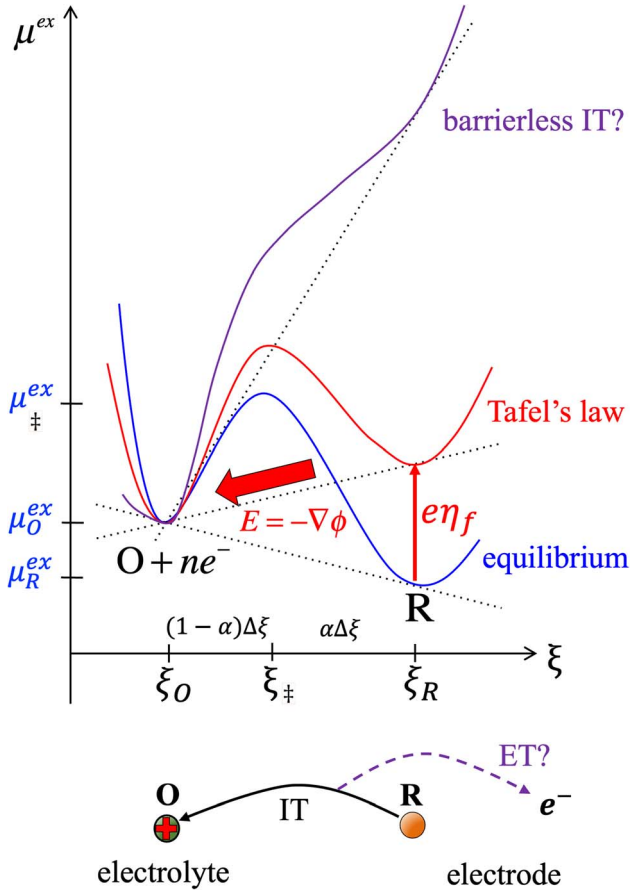

Fig. 1 Phenomenological theory of ion transfer (IT) to explain Butler–Volmer kinetics[6–10] – and its limitations. The reaction complex is hypothesized to move along a classical charge-transfer reaction coordinate ξ (typically the position of an ion) between the reduced state R and the oxidized state O, as n electrons are transferred to the electrode ($R \rightarrow O + ne^-$), in a landscape of excess chemical potential μ^{ex}.[24] The chemical part of the activation barrier, $\mu^{ex}_{\ddagger}$, fixed at position $\xi_\ddagger = \alpha\xi_R + (1-\alpha)\xi_O$, is assumed to be independent of formal overpotential η_f, which is postulated to create a constant electric field, $E = -\eta_f/\Delta\xi$, driving the charge-transfer reaction over a distance, $\Delta\xi = \xi_R - \xi_O$, set by the Stern layer thickness on the electrode. This construction leads to the BV equation (1) and Tafel's limiting law for moderate overpotentials, but the model breaks down at large overpotentials, *e.g.* as shown for $(1-\alpha)ne\eta_f > (\mu^{ex}_{\ddagger} - \mu^{ex}_{O})_{eq}$, when the activation barrier vanishes, and classical transition state theory no longer applies. The model also fails to explain exactly when and how electron transfer (ET) occurs, as the proposed reaction mechanism only accounts for ion transfer (IT). [Adapted from Bazant (2013).[24]]

reduced, and the reduced state oxidized, by the transferring electrons. Such reactions are common in chemistry and biology and are described by quantum mechanical ET theory.[25,26,30–32]

The modern theory of ET kinetics was pioneered by R. A. Marcus starting in 1956[30,33–36] and recognized by the 1992 Nobel Prize in Chemistry.[37] Since quantum-mechanical ET is isoenergetic, Marcus postulated that ET must occur when fluctuations reorganize the solvent (or more generally, the molecular

environment) so as to temporarily align the electron energy levels of the diabatic reduced and oxidized states[38,39] and thus allow ET to occur "in the dark" without absorbing or emitting photons. Importantly, Marcus went beyond earlier models of non-adiabatic ET and solvent-reorganization developed by Weiss[40] to predict a novel Gaussian dependence of the reaction rate on overpotential, by modeling the activation barrier for ET as the intersection of two parabolae describing solvent reorganization in the harmonic approximation.[30,33,36,37] Marcus summarized his theoretical predictions for experimentalists at a Faraday Discussion in 1960,[41] which he later recognized as a turning point in the field.[37]

It is not widely appreciated that the field of quantum electrochemistry predated Marcus by a quarter century. In 1931, R. W. Gurney published the seminal paper on "quantum mechanics of electrolysis" in which he modeled proton transfer and reduction at a metallic electrode as a process of quantum tunneling involving electrons sampled from the Fermi–Dirac distribution,[42] similar to modern formulations in quantum electrochemistry.[6,25,26] Gurney further assumed a linear dependence of the proton transfer energy with position, before and after "neutralization" by the electron, from which he was able to derive Tafel's law.[42] Although the nature of the energy barrier and its dependence on overpotential were not yet clear, Gurney's theory was a radically "new line of attack" in electrochemistry at a time of apparently some lingering doubts about the atomic nature of matter, which he felt compelled to acknowledge in his conclusion: "In deriving these quantities [neutralization potentials] we have used the only available vocabulary – that of molecular spectroscopy. The existence of definite molecules is not, however, a necessary assumption."[42]

In 1936, J. A. V. Butler adapted Gurney's model for specific adsorption of protons on a metal electrode and the linear approximation of the energy landscape for ion transfer (IT) to derive the BV equation.[18] Although quantum aspects of ET were not fully taken into account, the visionary papers of Gurney and Butler were the first to propose a reaction mechanism coupling IT and ET, in the specific case of the Volmer step in the hydrogen evolution reaction in acidic solutions.[43] Below, we shall see that the Gurney–Butler theory corresponds to the limit of infinitely fast ET and holds up to moderately large overpotentials in the Tafel regime.

Starting in the late 1950s, the modern quantum mechanical foundations of ET theory were laid by Hush,[44–46] Levich, Dogonadze, Chizmadzhev and Kuznetsov[26,27,36,47–50] and Marcus[30,36,51,52] with later extensions by Calef and Wolynes,[53,54] Schmickler and Santos,[25,31] Nazmutdinov,[32] Matyushov and Voth,[55,56] and many others. These theories mostly assume adiabatic ET, where a single electron is shared between the reduced and oxidized states in a particular hybrid wavefunction, as the solvent fluctuates to facilitate its gradual transfer. In the opposite limit of non-adiabatic ET, where the electronic coupling is weak, solvent reorganization does not always lead to ET, and independent, rare events of quantum tunneling can occur in parallel between the reactant and all available diabatic electronic states.[38,39]

Despite its many successes, ET theory – by itself – fails to provide a consistent theoretical framework for faradaic reaction kinetics at electrodes. In particular, ET theory cannot explain the vast experimental literature supporting the BV equation and, especially, Tafel's limiting law, eqn (2). This is considered by many

electrochemists to be a fatal flaw in our current understanding of quantum electrochemistry, still awaiting resolution:

"Tafel's law is one of the most tested and verified laws of nature. It is also one with the broadest applicability… The ability to replicate Tafel's law is the first requirement of any theory of electrode kinetics. It represents a filter that may be used to discard models of electron transfer which predict current–potential relationships that are not observed." – J. O. Bockris, A. K. N. Reddy and M. E. Gamboa-Aldeco (p. 1510).[7]

Recent electrochemistry textbooks attempt to resolve this paradox by noting that Marcus theory predicts BV kinetics with $\alpha = 1/2$ (for symmetric ET), if the overpotential is much smaller than the reorganization energy (usually on the order of 100 meV $\approx 4k_BT$),[6,21,25] but this is only an asymptotic limit. The same is true of more sophisticated models of nonlinear solvation,[55,56] related to asymmetric Marcus–Hush kinetics,[57,58] which again rely on the limit of small overpotentials to justify Tafel's law with $\alpha \neq 1/2$.

The persistence of Tafel's law to much larger overpotentials, sometimes spanning many decades in current with overpotentials reaching the 1 V scale of chemical bond breaking, is fundamentally inconsistent with the curved Tafel plots predicted by all ET theories,[6–8,62] as shown in Fig. 2, and cannot be explained by Taylor expansion of the quantum mechanical ET rate equations. Instead, curvature of the Tafel plot is an unavoidable consequence of the nonlinear shape of the free energy landscapes for solvent re-organization in the reduced and oxidized diabatic states, including the parabolic ("harmonic") shapes introduced by Marcus:

"The quantum mechanical formulation of electrode reactions still possesses the Achilles' heel of earlier formulations; it is restricted to nonbond-breaking, seldom occurring outer-sphere reactions and involves the harmonic approximation for the energy variation, which is the main reason it cannot replicate Tafel's law." (*ibid.*, p. 1523).[7]

In contrast, the original Gurney–Butler model of electrolysis suggests that rate-limiting, bond-breaking classical IT is responsible for Tafel's law, but the role of quantum mechanical ET, the defining aspect of electrochemical reactions, still remains to be explained, nearly a century later.

2.3 Toward a theory of coupled ion–electron transfer

Motivated by electrolysis and electrodeposition, new theories of faradaic reaction kinetics have emerged over the past 30 years in which ET is coupled with IT at the electrode/electrolyte interface.[25,31,64] Soon after Marcus received the Nobel Prize, Cukier and Nocera introduced the theory of proton-coupled electron transfer (PCET),[65,66] and Schmickler[67,68] and Koper[69,70] developed quantum mechanical theories of coupled adiabatic ET and bond-breaking IT reaction kinetics at metal electrodes, where interactions of the reactant with the solvent and with the metal depend on its separation from the interface. The literature has focused on situations, such as PCET[71–78] or concerted proton–electron transfer (CPET),[69,79–81] where both protons and electrons are treated quantum mechanically, assuming isolated reactants in a dilute solution at the electrode interface. These theories have also focused on predicting activation energies and exchange current trends, rather than the overpotential dependence of the reaction.

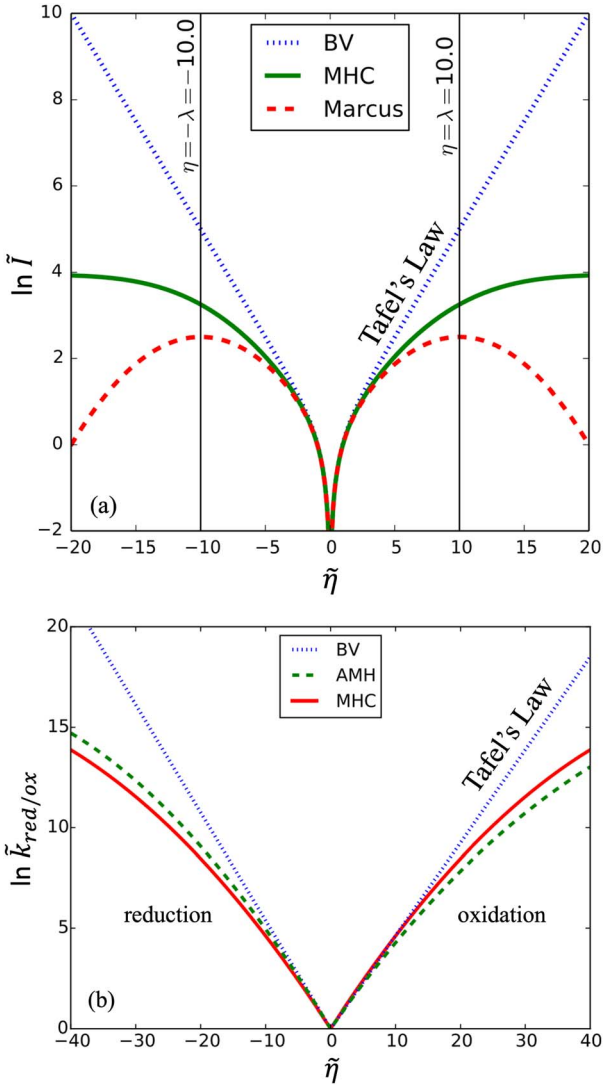

Fig. 2 Failure of quantum theories of electron transfer (ET) to predict Tafel's law as a limit of the Butler–Volmer equation (BV), eqn (1), the most widely used model of electrochemical kinetics.[6,8,10,59] In countless experimental studies, reaction rates of oxidation and reduction, k_{ox} and k_{red}, respectively, as well as the faradaic current I at an electrode, have exhibited persistent exponential dependence on overpotential, η, corresponding to a straight line "Tafel plot" of $\ln|I|$ *vs.* η over several decades of dimensionless current $\tilde{I} = I/I_0$ (scaled to the exchange current, I_0) and overpotential, $\tilde{\eta}$ (scaled to the thermal voltage, $k_B T/e$) up to the scale of chemical bond breaking ($|\eta| \sim 1$ eV). In contrast, all quantum mechanical models of ET predict curved Tafel plots, including (a) symmetric ET for localized electronic states (Marcus kinetics) or metallic electrodes (Marcus–Hush–Chidsey/MHC kinetics) and (b) asymmetric ET for metallic electrodes (asymmetric Marcus–Hush/AMH kinetics). At best, these models can asymptotically match the linear Tafel plot at low overpotentials, $|\eta| \ll \lambda$, much smaller than the Marcus reorganization energy λ, which is typically at the scale of 100 meV $\approx 4k_B T$. [Adapted from (a) Zeng *et al.* (2014)[60] and (b) Zeng *et al.* (2015).[61]]

Much less attention has been paid to situations, such as ion intercalation, where the ions behave classically and experience strong interactions in concentrated solutions and solids, including phase transformations driven by large overpotentials. This requires re-formulating theories of charge transfer, including Butler–Volmer and Marcus kinetics, within a general framework of electrochemical nonequilibrium thermodynamics.[24,82] In electrochemical engineering, ion intercalation has long been viewed as an exclusively IT process, described by BV kinetics[9] and leading to capacitive charge storage, analogous to specific adsorption of ions on surfaces.[83]

In 2014, Peng Bai and the author suggested a different reaction mechanism, in which ion intercalation is a fast IT step, facilitated by a slow ET step between a metallic additive or coating and a poorly conducting host material.[84] (Below, I suggest the term "electron-coupled ion transfer" (ECIT) to describe this reaction mechanism.) In the case of lithium iron phosphate (LFP), we provided experimental evidence that Li^+ intercalation rates extracted from phase-separation dynamics obey Marcus–Hush–Chidsey (MHC) kinetics,[85–87] based on the hypothesis that Li^+ insertion into the crystal is facilitated by non-adiabatic ET from the metallic carbon coating to form a polaron by reducing a neighboring iron redox site (Fe^{3+}/Fe^{2+}),[63] as shown in Fig. 3. This unorthodox picture of ET-limited intercalation was immediately met with skepticism. For example, it was shown that Tafel plots extracted from nonlinear impedance spectra for LFP could "perfectly obey the Butler–Volmer equation",[88] albeit only after fitting series resistances and neglecting known heterogeneities arising from phase separation.[89–91] The importance of IT in LFP was also underscored by my earlier work on driven phase separation modeled by generalized BV kinetics,[24,84,90–94] although the overpotential dependence had never been systematically explored.

Perhaps another reason that quantum-mechanical ET theory was never applied in electrochemical engineering, until recently, was the lack of a simple rate expression to serve as an alternative to the BV equation. Also in 2014, Yi Zeng and I addressed this problem by publishing accurate closed-form approximations for both symmetric MHC kinetics[60] and asymmetric Marcus–Hush (AMH) kinetics[61] using matched asymptotic expansions of the Fermi integrals of the Marcus reaction rate in the limits of large and small reorganization energy. In contrast to various series expansions of the MHC rate,[95,96] the matched asymptotic approximations are uniformly valid for all parameter values.[60] This mathematical simplification enabled ET theory to be used for the first time in simulations of electrochemical systems, such as Li-ion battery cycling[97–99] and electrodeposition.[100–102] For battery simulations, Raymond Smith and I also adapted the generalized MHC formula to include ion-transfer effects in the prefactor,[97] consistent with the ET-limited CIET rate equation presented below, but without any microscopic justification.

Recently, Dimitrios Fraggedakis and the author (building on contributions of Bai, Zeng, Smith, and other students and collaborators) developed the first mathematical theory of coupled ion–electron transfer (CIET), where electrons tunnel quantum mechanically in response to solvent reorganization, coupled with classical ion transfer based on nonequilibrium thermodynamics,[103] based on the two-dimensional diabatic free energy landscape shown in Fig. 4(top). Under certain assumptions, shown below to correspond to ET rate limitation, our theory of the CIET rate for a metal electrode reduces to MHC kinetics with

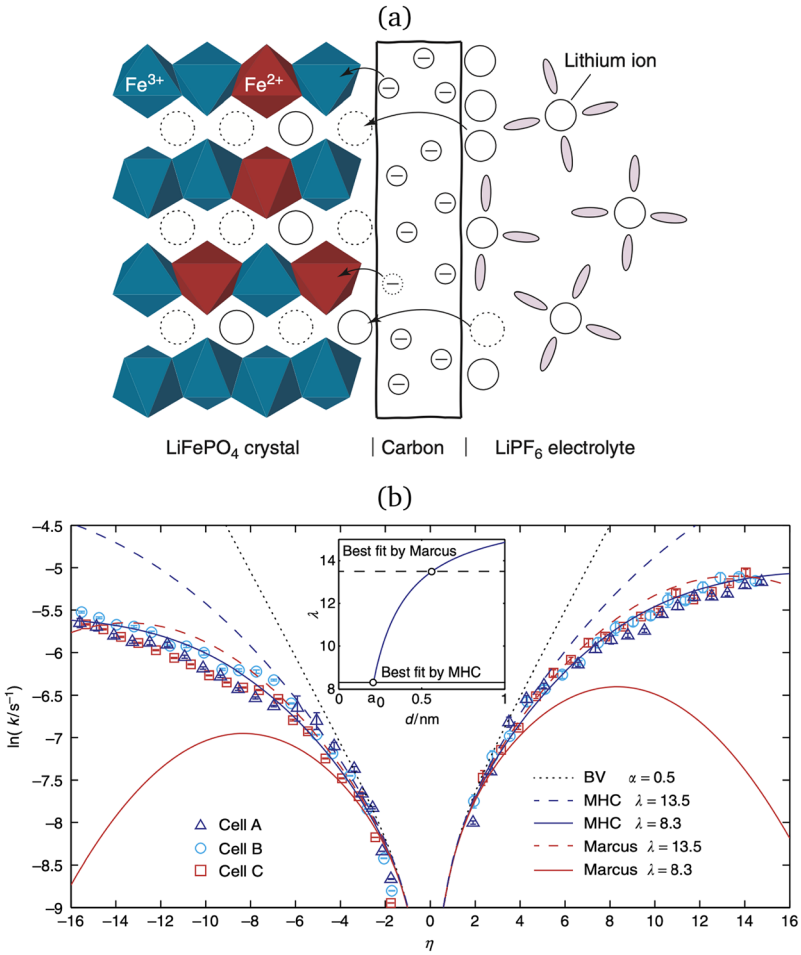

Fig. 3 Kinetics of lithium intercalation in lithium iron phosphate (LFP). (a) Reaction mechanism defined here as "electron-coupled ion transfer (ECIT)", in which ion insertion is limited by electron transfer from the carbon coating to reduce a neighboring iron redox site and form a neutral polaron. (b) Evidence for Marcus kinetics in LFP from Tafel plots of the rate constant for reaction-limited nanoparticle phase transformations *versus* dimensionless overpotential (scaled to k_BT/e = 26 mV), fitted to the Marcus–Hush–Chidsey (MHC) model. [Reproduced from Bai and Bazant (2014).[63]]

a concentration-dependent prefactor. This rate expression has been used in battery simulations,[104] which were able to fit the raw chronoamperometry data of Bai[63] better than BV kinetics, even with a fitted series resistance,[103] as shown in Fig. 4(bottom). This limit of CIET theory was also able to accurately predict the concentration dependence of the lithium intercalation rate in LFP nanoparticles,[105] as revealed by learning the model from a large dataset of *operando* X-ray images,[106] which we revisit at the end of this paper using the general theory. The ET-limited theory has been adapted to successfully describe interphase formation in sodium electrodeposition from solid electrolytes.[100] It has also been used to predict how electronic structure influences the stability of driven

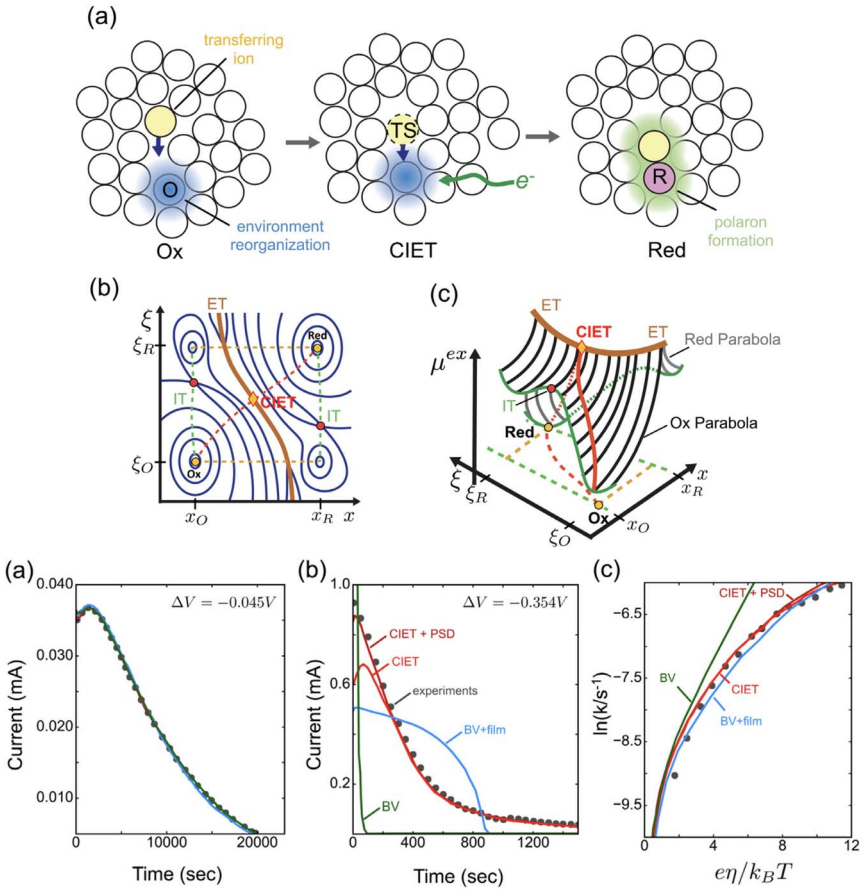

Fig. 4 (Top) (a) Schematic of coupled ion–electron transfer (CIET) with the two-dimensional landscape of excess chemical potential, shown as (b) a contour plot and (c) a surface plot, indicating the diabatic reduced and oxidized states for IT separated by the ET surface at the diabatic crossing, and the minimum energy barrier of the CIET transition state. (Bottom) Simulations of chronoamperometry using the ET-limited CIET (ECIT) model based on MHC kinetics for a single particle and a porous electrode with the measured particle size distribution (PSD), as well as the Butler–Volmer model with and without a fitted film resistance, compared to the raw experimental data of Bai and Bazant[63] for (a) low voltage pulses, (b) high voltage pulses, and (c) the resulting Tafel plot. [Reproduced from Fraggedakis *et al.* (2021).[103]]

electrode interfaces, including intercalation and electrodeposition.[101] Curved Tafel plots and morphological transitions seen in recent experiments on lithium electrodeposition could perhaps also be understood through the lens of CIET,[107] although BV kinetics are more typically observed for electrodeposition and electrocatalysis at metal electrodes. In the original CIET paper, we noted several limits where the CIET barrier could be approximated by that of Butler–Volmer kinetics,[103] but we stopped short of deriving a general theory that could unify BV and Marcus kinetics in a common formalism based on microscopic material properties. That is the focus of the present work.

2.4 Outline

The paper is organized as follows. We begin by developing the general theory of nonadiabatic CIET kinetics in Section 3. We then consider three distinguished limits of the theory corresponding to normal Marcus kinetics for large reorganization energy (Section 4), quantum Butler–Volmer kinetics for large ion-transfer free energies (Section 5), and inverted Marcus kinetics at large overpotentials (Section 6) leading to a universal reaction-limited current for metal electrodes. We proceed to derive uniformly valid approximations for the CIET rate by asymptotic matching of these exact limiting cases in Section 7. Reflecting on these results in Section 8, we derive probability distributions of transferring electron energies from the CIET rate formula. In Section 9, we discuss possible corrections of the theory for adiabatic ET. In Section 10, we summarize our simple analytical approximations for the faradaic current by CIET at a metal electrode. Finally, in Section 11, we revisit the original motivation for CIET theory by re-analyzing experimental data for intercalation rates in LFP nanoparticles. We conclude in Section 12 with a brief outlook on the future of CIET theory.

3 General theory

From the perspective of nonequilibrium thermodynamics, each term in a general faradaic reaction (eqn (7) below) represents an ensemble of chemical species at a certain electrochemical potential (*e.g.* in the grand canonical ensemble at constant temperature and pressure). In my original work re-formulating Marcus kinetics in terms of non-equilibrium thermodynamics,[24] I defined the activity and excess chemical potential of electrons as general concepts, but did not explicitly account for the quantum mechanical properties of electrodes. The theory was extended for integration over the electronic band structure with Smith[104] and, importantly, in the first detailed treatment of CIET kinetics with Fraggedakis.[103] These papers tacitly assumed non-adiabatic ET limited reactions and did not explicitly construct all of the thermodynamic variables in the original theory. Here, we fill in some details, clarify and relax various assumptions, and develop a more general theory of CIET kinetics, which leads to a similar MHC-like formula for the case of ET-limited reactions, while also predicting BV kinetics for the more common case of IT-limited reactions within the same unified quantum framework.

3.1 Nonequilibrium thermodynamics of charge transfer

3.1.1 Electrochemical potentials and overpotentials. The theory begins with three definitions of the (diffusional) electrochemical potential μ_i of species i based on nonequilibrium thermodynamics:[24]

$$\mu_i = \frac{\partial G}{\partial \tilde{c}_i} = \mu_i^{\ominus} + k_{\mathrm{B}}T\ln a_i + z_i e\phi = k_{\mathrm{B}}T\ln\tilde{c}_i + \mu_i^{\mathrm{ex}}. \tag{5}$$

The first is the variational derivative of the free energy functional, $G[\{\tilde{c}_i(\vec{x},t)\},\{\phi_i\},T,P]$, the Gibbs free energy for an open system at temperature T and pressure P, with respect to the dimensionless concentration $\tilde{c}_i(\vec{x},t)$ (scaled to a reference value c_i^{ref}), which expresses the free energy required to create a particle of species i at position $\vec{x}$ and time t. The second definition separates departures

from a reference state electrochemical potential, μ_i^{Θ}, into a short-range chemical contribution depending on the activity a_i and a long-range electrostatic contribution for a species of charge $z_i e$ in the potential of mean force ϕ. The third definition expresses the Boltzmann distribution of concentration, $\tilde{c}_i = \exp((\mu_i - \mu_i^{\mathrm{ex}})/k_{\mathrm{B}}T)$, in the total "excess" chemical potential

$$\mu_i^{\mathrm{ex}} = \mu_i^{\Theta} + k_{\mathrm{B}}T \ln \gamma_i + z_i e\phi, \tag{6}$$

where $\gamma_i = a_i/\tilde{c}_i$ is the activity coefficient. For a set of reactants, μ_i denotes the sum of their electrochemical potentials, while a_i and $\tilde{c}_i$ denote the product of their activities and dimensionless concentrations, respectively.

For the general reduction reaction,

$$\mathrm{O} + \mathrm{e}^- \rightarrow \mathrm{R} \tag{7}$$

the activation overpotential, η, is equal to the free energy of reaction ΔG per charge transferred,

$$e\eta = \Delta G = \mu_{\mathrm{R}} - \mu_{\mathrm{O}} - \mu_{\mathrm{e}}. \tag{8}$$

It is also convenient to define the formal overpotential, η_{f}, based on excess chemical potentials of the reduced and oxidized species,

$$e\eta_{\mathrm{f}} = e\eta + k_{\mathrm{B}}T \ln \frac{\tilde{c}_{\mathrm{O}}}{\tilde{c}_{\mathrm{R}}} = \mu_{\mathrm{R}}^{\mathrm{ex}} - \mu_{\mathrm{O}}^{\mathrm{ex}} - \mu_{\mathrm{e}} \tag{9}$$

Note that in our compact notation for the reaction, eqn (7), the oxidized state O or the reduced state R may involve multiple chemical species, $\sum_j s_j A_j$, in which case its concentration, activity and electrochemical potential are given by:[24]

$$c = \prod_j c_j^{s_j}, \quad a = \prod_j a_j^{s_j}, \quad \mu = \sum_j s_j \mu_j \tag{10}$$

respectively. For example, in the case of the hydrogen evolution reaction in basic solutions,

$$2\mathrm{H_2O} + 2\mathrm{e}^- \rightarrow \mathrm{H_2} + 2\mathrm{OH}^- \tag{11}$$

we have

$$a_{\mathrm{O}} = a_{\mathrm{H_2O}}{}^2,\ \mu_{\mathrm{O}} = 2\mu_{\mathrm{H_2O}},\ a_{\mathrm{R}} = a_{\mathrm{H_2}} a_{\mathrm{OH^-}}{}^2,\ \mu_{\mathrm{R}} = \mu_{\mathrm{H_2}} + 2\mu_{\mathrm{OH^-}} \tag{12}$$

where $a_{\mathrm{H_2O}} \approx 1$, $a_{\mathrm{OH^-}} = 10^{14-\mathrm{pH}}$ (M) and $a_{\mathrm{H_2}} = P_{\mathrm{H_2}}$ (atm). In the case of lithium intercalation in iron phosphate,

$$\mathrm{Li}^+ + \mathrm{e}^- \rightarrow \mathrm{Li_{(int)}} = \mathrm{LiFePO_4} - \mathrm{FePO_4} \tag{13}$$

we have $a_{\mathrm{O}} = a_{\mathrm{Li^+}}$ and $a_{\mathrm{R}} = a_{\mathrm{Li}} = a_{\mathrm{LiFePO_4}}/a_{\mathrm{FePO_4}}$, where, for example, the latter could be described by a regular solution model.[24,108] This example also illustrates our consistent use of diffusional electrochemical potentials in condensed systems,[24] such as $\mu_{\mathrm{Li_{int}}} = \mu_{\mathrm{LiFePO_4}} - \mu_{\mathrm{FePO_4}}$, which expresses the free energy change to create an intercalated lithium ion, while removing a vacancy.

3.1.2 Faradaic current density. The net reduction current density, the rate of electron consumption per active area of the electrode/electrolyte interface, can be expressed as the difference of forward (reduction) and backward (oxidation) current densities,

$$J = e(k_{\mathrm{red}}c_{\mathrm{O}} - k_{\mathrm{ox}}c_{\mathrm{R}}) \tag{14}$$

where k_{red} and k_{ox} are the reduction and oxidation rate constants, which depend on η_{f} and have units of velocity, if we use volumetric concentrations for a first order reaction. More generally, if the reaction has order n_i in a reactant of concentration c_i, then the units of k are velocity times concentration to the power $n_i - 1$. For interfacial reactions, it is more convenient to define the mean area of a reacting site A_{s} and express the current density in terms of dimensionless concentrations, or mean coverages of the surface sites, as

$$J = \frac{e}{A_{\mathrm{s}}}(\nu_{\mathrm{red}}\tilde{c}_{\mathrm{O}} - \nu_{\mathrm{ox}}\tilde{c}_{\mathrm{R}}) \tag{15}$$

where

$$\nu_{\mathrm{red/ox}} = k_{\mathrm{red/ox}}c_{\mathrm{O/R}}^{\mathrm{ref}}A_{\mathrm{s}} \tag{16}$$

is the frequency of reduction or oxidation, whose inverse is the mean time between reaction events at a given surface site. The total current I is the integral of J over the interfacial area A, or simply $I = JA$ for a uniform current density.

As we shall see below, it is natural to scale the CIET reaction frequency to an effective solvent polarization frequency, ν_{s}, for the environment of the donor/acceptor sites near the electrode/electrolyte interface, which sets the scale for ET rates. This frequency scale dominates CIET kinetics at very large overpotentials, which exceed (and effectively eliminate) all barriers to classical IT, leaving only quantum mechanical ET to limit the overall rate. With this insight, we define dimensionless current density as

$$\tilde{J} = \frac{JA_{\mathrm{s}}}{e\nu_{\mathrm{s}}} = \tilde{I} = \frac{IA_{\mathrm{s}}}{e\nu_{\mathrm{s}}A} \tag{17}$$

where the last equality assumes a uniform current density. This allows us to express our results in terms of dimensionless current carried by a pseudo-first-order redox reaction,

$$\tilde{I} = \tilde{k}_{\mathrm{red}}\tilde{c}_{\mathrm{O}} - \tilde{k}_{\mathrm{ox}}\tilde{c}_{\mathrm{R}} \tag{18}$$

where the dimensionless rate constants are given by

$$\tilde{k}_{\mathrm{red/ox}} = \frac{k_{\mathrm{red/ox}}c_{\mathrm{O/R}}^{\mathrm{ref}}A_{\mathrm{s}}}{\nu_{\mathrm{s}}} = \frac{k_{\mathrm{red/ox}}}{\Delta x_{\mathrm{red/ox}}\nu_{\mathrm{s}}} = \frac{\nu_{\mathrm{red/ox}}}{\nu_{\mathrm{s}}} \tag{19}$$

in terms of an effective interfacial thickness, $\Delta x_{\mathrm{red/ox}} = (A_{\mathrm{s}}c_{\mathrm{O/R}}^{\mathrm{ref}})^{-1}$, which converts the solvent polarization frequency ν_{s} into a characteristic reaction velocity, $\Delta x_{\mathrm{red/ox}}\nu_{\mathrm{s}}$.

The interfacial coverages of the reduced and oxidized species at the electrode/electrolyte interface, $\tilde{c}_{\mathrm{O}}$ and $\tilde{c}_{\mathrm{R}}$, will generally be different than in the nearby bulk phases outside the double layer. Assuming each species has bulk activity $a_{i,\mathrm{b}}$ and

undergoes fast adsorption on a set of discrete sites at the interface, we arrive at a generalized Langmuir isotherm,[24]

$$\tilde{c}_i = \frac{a_{i,\mathrm{b}} \mathrm{e}^{-w_i/k_\mathrm{B}T}}{1 + a_{i,\mathrm{b}} \mathrm{e}^{-w_i/k_\mathrm{B}T}} \tag{20}$$

where w_i is the work of surface adsorption ($i = \mathrm{O}, \mathrm{R}$). This general form includes the Temkin isotherm, commonly used in electrochemistry,[7] if w_i has a linear dependence on $\tilde{c}_i$ due to lateral pair interactions, as the regular solution model.[24] Fraggedakis *et al.*[103] assumed $w_\mathrm{O} = w_\mathrm{R}$, but we will consider the general asymmetric case, $w_\mathrm{R} \neq w_\mathrm{O}$. For liquids and solids, surface adsorption is usually fast compared to transport and reaction kinetics, but for high-temperature gas electrodes, surface adsorption can be rate-limiting in the overall electrochemical reaction.[109,110]

3.1.3 Activation barriers for charge transfer. As noted above, radiationless ET is isoenergetic, facilitated by slow thermal fluctuations of the molecular environment that bring the reduced and oxidized states to the transition state. For a given electron energy ε, the reaction complex explores a landscape of excess chemical potential until it overcomes an activation barrier $\mu_\ddagger^\mathrm{ex}$, determined by the reaction mechanism (below).[24] The reduction and oxidation rate constants,

$$\tilde{k}_\mathrm{red}(\varepsilon) \propto \frac{\mathrm{e}^{-\Delta G_\ddagger^\mathrm{red}/k_\mathrm{B}T}}{\gamma_\ddagger} \tag{21}$$

$$\tilde{k}_\mathrm{ox}(\varepsilon) \propto \frac{\mathrm{e}^{-\Delta G_\ddagger^\mathrm{ox}/k_\mathrm{B}T}}{\gamma_\ddagger}, \tag{22}$$

respectively, include activation barriers of excess free energy given by

$$\Delta G_\ddagger^\mathrm{red} = \mu_\ddagger^\mathrm{ex} - \mu_\mathrm{O}^\mathrm{ex} - \mu_\mathrm{e}^\mathrm{ex} \tag{23}$$

$$\Delta G_\ddagger^\mathrm{ox} = \mu_\ddagger^\mathrm{ex} - \mu_\mathrm{R}^\mathrm{ex} \tag{24}$$

as well as a common activity coefficient of the transition state $\gamma_\ddagger$, which accounts for entropic effects on the transition state,[24] such as excluded volume of ions and occupied energy levels of electrons. For consistency with the theory of reaction kinetics based on nonequilibrium thermodynamics,[24] we only require that the free energy barriers are large compared to the thermal energy,

$$\Delta G_\ddagger^\mathrm{red/ox} \gg k_\mathrm{B}T \tag{25}$$

so that barrier crossings are rare events at the scale of molecular vibrations, as in classical transition state theory.[1,111,112]

The transition state activity coefficient contributes an additional universal term, $k_\mathrm{B}T \ln \gamma_\ddagger$, to the excess chemical potential of the transition state, $\mu_\ddagger^\mathrm{ex}$. The excess free energy barriers, $\Delta G_\ddagger^\mathrm{red}$ and $\Delta G_\ddagger^\mathrm{ox}$, generally depend on the excess free energy of reaction,

$$\Delta G^\mathrm{ex} = \mu_\mathrm{R}^\mathrm{ex} - \mu_\mathrm{O}^\mathrm{ex} - \mu_\mathrm{e}^\mathrm{ex} = e\eta_\mathrm{f} + \mu_\mathrm{e} - \mu_\mathrm{e}^\mathrm{ex} \tag{26}$$

so as to satisfy the de Donder relation:[24]

$$\frac{\tilde{k}_{\mathrm{ox}}}{\tilde{k}_{\mathrm{red}}} = \frac{\nu_{\mathrm{ox}}}{\nu_{\mathrm{red}}} = \mathrm{e}^{\eta_{\mathrm{f}}/k_{\mathrm{B}}T} = \frac{\tilde{c}_{\mathrm{O}}}{\tilde{c}_{\mathrm{R}}}\mathrm{e}^{\eta/k_{\mathrm{B}}T}. \tag{27}$$

In principle, the relationship between $\Delta G_{\ddagger}^{\mathrm{red/ox}}$ and ΔG^{ex}, as well as the transition state activity coefficient $\gamma_{\ddagger}$, can be derived from a microscopic model of the reaction mechanism, such as the phenomenological model of classical ion transfer used to derive the BV equation in Fig. 1. Since electrochemical reactions necessarily involve electrons, however, any realistic and predictive model must be based on quantum mechanics.

3.2 Quantum physics of electron transfer

3.2.1 Activity and excess chemical potential of electrons. Electrons participating in the reduction reaction (7) are drawn from the Fermi sea of the electrode with electrochemical potential, $\mu_{\mathrm{e}} = \varepsilon_{\mathrm{F}} - e\phi_{\mathrm{e}}$, where ε_{F} is the Fermi level and ϕ_{e} is the local electrostatic potential. The probability of finding an electron at energy ε is given by the Fermi–Dirac distribution,

$$\tilde{n}_{\mathrm{e}} = \frac{1}{1 + \mathrm{e}^{(\varepsilon-\varepsilon_{\mathrm{F}})/k_{\mathrm{B}}T}} \tag{28}$$

and the probability of finding a hole at the same energy is

$$\tilde{n}_{\mathrm{h}} = 1 - \tilde{n}_{\mathrm{e}} = \frac{1}{1 + \mathrm{e}^{(\varepsilon_{\mathrm{F}}-\varepsilon)/k_{\mathrm{B}}T}} \tag{29}$$

These dimensionless filling fractions for energy levels relate the number densities of electrons and holes (per unit of energy), $n_{\mathrm{e}}(\varepsilon) = \tilde{n}_{\mathrm{e}}(\varepsilon)\rho_{\mathrm{e}}(\varepsilon)$ and $n_{\mathrm{h}}(\varepsilon) = \tilde{n}_{\mathrm{h}}(\varepsilon)\rho_{\mathrm{e}}(\varepsilon)$, respectively, to the electronic density of states, $\rho_{\mathrm{e}}(\varepsilon)$, describing the band structure of the electrode.

Treating electrons in the same framework as ions using eqn (5), we write

$$\mu_{\mathrm{e}} = \mu_{\mathrm{e}}^{\Theta} + k_{\mathrm{B}}T\ln a_{\mathrm{e}} - e\phi_{\mathrm{e}} \tag{30}$$

and define $\mu_{\mathrm{e}}^{\Theta} = \varepsilon_{\mathrm{F}}^{0}$ as the Fermi level of the electrode in a reference state in order to construct the electron activity,

$$a_{\mathrm{e}} = \frac{\tilde{n}_{\mathrm{e}}}{\tilde{n}_{\mathrm{h}}}\mathrm{e}^{\left(\varepsilon-\varepsilon_{\mathrm{F}}^{0}\right)/k_{\mathrm{B}}T} \tag{31}$$

such that $a_{\mathrm{e}} = 1$ for $\varepsilon = \varepsilon_{\mathrm{F}}^{0}$ and $a_{\mathrm{e}} > 1$ for excited states with $\varepsilon > \varepsilon_{\mathrm{F}}^{0}$. We can also define the excess chemical potential of electrons, $\mu_{\mathrm{e}}^{\mathrm{ex}}$, *via*

$$\mu_{\mathrm{e}} - \mu_{\mathrm{e}}^{\mathrm{ex}} = \varepsilon_{\mathrm{F}} - \varepsilon = k_{\mathrm{B}}T\ln\frac{\tilde{n}_{\mathrm{e}}}{\tilde{n}_{\mathrm{h}}} \tag{32}$$

which allows us to express the excess free energy of reaction as

$$\Delta G^{\mathrm{ex}} = e\eta_{\mathrm{f}} + \varepsilon_{\mathrm{F}} - \varepsilon \tag{33}$$

where we use the definition of formal overpotential, eqn (9). In eqn (32), the ratio

$$\frac{\tilde{n}_{\mathrm{e}}}{\tilde{n}_{\mathrm{h}}} = \frac{1 + \mathrm{e}^{-(\varepsilon-\varepsilon_{\mathrm{F}})/k_{\mathrm{B}}T}}{1 + \mathrm{e}^{(\varepsilon-\varepsilon_{\mathrm{F}})/k_{\mathrm{B}}T}} \tag{34}$$

is an effective concentration for reactive electrons, which represents the creation of electron while removing a hole, consistent with the definition of diffusional electrochemical potential for ions. Equivalently, one could write the reduction reaction in a more familiar form as

$$\mathrm{O} + \mathrm{e} \rightarrow \mathrm{R} + \mathrm{h} \tag{35}$$

where $\mathrm{e}^- = \mathrm{e} - \mathrm{h}$ in eqn (7) is the consistent representation of the reactive electron, when defining diffusional chemical potentials. The two approaches lead to the same formula for the nonadiabatic ET rate below, first proposed by Gurney[42] based on eqn (35), but the equivalent formulation of eqn (7) allows us to consistently define the activity coefficient of the transition state, based on the general theory of non-equilibrium thermodynamics of charge transfer kinetics.[24]

3.2.2 Adiabatic *versus* nonadiabatic ET. It is important to distinguish the two types of ET reactions, adiabatic and non-adiabatic, which may be coupled with IT.[25,26] In adiabatic ET, a single electron is shared between strongly coupled reduced and oxidized states in a hybrid orbital, which slowly adjusts as the solvent reorganizes causing the electron probability density to shift its weight between the oxidized (acceptor) and reduced (donor) states. In cases where adiabatic ET is coupled with either classical IT[67–70] or quantum-mechanical proton transfer,[65,66] quantum computations can be performed to construct an energy landscape for specific reactants and solvents, and simple rate expressions can be derived based on a model Hamiltonian,[25,31,32,55,56,113] *e.g.* generalizing the Anderson–Newns model for chemisorption on metals.[114] In this theoretical framework, the nature of the ET reaction is governed by the chemisorption function,[25,31,32,113]

$$\Delta_{\mathrm{e}}(\varepsilon) = \pi {H_{\mathrm{DA}}}^2 \rho_{\mathrm{e}}(\varepsilon) \tag{36}$$

where ${H_{\mathrm{DA}}}^2 = |\langle\psi_{\mathrm{A}}|V_{\mathrm{DA}}|\psi_{\mathrm{D}}\rangle|^2$ is the electronic coupling matrix element between the wavefunctions of the electron donor and acceptor, ψ_{A} and ψ_{D}, respectively, in the interaction potential, V_{DA}. In models of adiabatic ET, chemisorption functions are usually defined separately for each band,[31] but more generally all bands should be included in the total electronic density of states $\rho_{\mathrm{e}}(\varepsilon)$. In the wide-band approximation for metal electrodes[25,31] (the most typical situation for faradaic reactions), the chemisorption function is evaluated at the Fermi level, $\Delta_{\mathrm{e}}(\varepsilon_{\mathrm{F}})$. Adiabatic ET requires strong quantum coupling of the donor and acceptor states, which remains intact under thermal fluctuations, $\Delta_{\mathrm{e}} \gg k_{\mathrm{B}}T$.

In non-adiabatic ET for $\Delta_{\mathrm{e}} \ll k_{\mathrm{B}}T$, the reduced and oxidized quantum states are only weakly coupled and retain their separate "diabatic" chemical identities, until quantum tunneling of electrons from the band structure causes a transition between these states at some energy below the diabatic crossing.[38] In this regime, the barrier profile between the diabatic states could in principle be calculated by constrained density functional theory.[39] The non-adiabatic condition is usually satisfied for outer-sphere ET between well-separated donor and acceptor wavefunctions, as ${H_{\mathrm{DA}}}^2$ decays exponentially with separation distance at the Angstrom scale. Following Levich, Dogonadze and Kuznetsov,[26,27,30,36,48] the quantum tunneling rate can then be approximated as a constant

$$\kappa_{\mathrm{T}} = \frac{2\Delta_{\mathrm{e}}}{\hbar} = \frac{2\pi {H_{\mathrm{DA}}}^2 \rho_{\mathrm{e}}}{\hbar} \tag{37}$$

using first-order perturbation theory (Fermi's Golden Rule),[25,31] where $\hbar = h/2\pi$ and h = Planck's constant. Since the tunneling rate is smaller than the thermal quantum frequency, $\kappa_T \ll k_B T/h$, non-adiabatic electron transfer is a rare event at the scale of molecular vibrations. When non-adiabatic ET is coupled with ion transfer,[103] therefore, it is possible to express the rate as an integral over the band structure of a generalized Marcus rate expression, accounting for both the positions of the ions and the reorganization of the solvent. As the environment fluctuates, the electronic coupling between the reduced and oxidized states remains weak and affects only the prefactor of the reaction rate *via* a constant tunneling probability.

3.2.3 Nonadiabatic CIET kinetics. For non-adiabatic CIET at an electrode, we express the reduction and oxidation rate constants as

$$\tilde{k}_{\mathrm{red}} = \int_{-\infty}^{\infty} \frac{\tilde{\kappa}_{\mathrm{e}}}{\gamma_{\ddagger}} \frac{\tilde{n}_{\mathrm{e}}}{\tilde{n}_{\mathrm{h}}} \mathrm{e}^{-\Delta G_{\ddagger}^{\mathrm{red}}/k_{\mathrm{B}}T} \rho_{\mathrm{e}} \mathrm{d}\varepsilon \tag{38}$$

$$\tilde{k}_{\mathrm{ox}} = \int_{-\infty}^{\infty} \frac{\tilde{\kappa}_{\mathrm{e}}}{\gamma_{\ddagger}} \mathrm{e}^{-\Delta G_{\ddagger}^{\mathrm{ox}}/k_{\mathrm{B}}T} \rho_{\mathrm{e}} \mathrm{d}\varepsilon \tag{39}$$

where $\tilde{\kappa}_{\mathrm{e}}$ is the dimensionless ET coefficient, scaled to the solvent polarization frequency, ν_{s}. This formulation can describe weakly adiabatic ET, where $\tilde{\kappa}_{\mathrm{e}}$ is approximately independent of electron energy,[25,31,52] but it is most accurate for non-adiabatic ET in the limit of weak coupling, described above. In that case, the electron transmission coefficient is independent of electron energy ε and approximately given by,

$$\tilde{\kappa}_{\mathrm{e}} = \frac{{H_{\mathrm{DA}}}^2}{\hbar \nu_{\mathrm{s}} \sqrt{4\pi\lambda k_{\mathrm{B}} T}} \tag{40}$$

where λ is the solvent reorganization energy.[25,26,31,32] More general expressions for $\tilde{\kappa}_{\mathrm{e}}$ are available for weakly adiabatic ET with multiple crossings based on Landau–Zener theory.[26,58,115] Note that $\tilde{\kappa}_{\mathrm{e}} \to 1$ for adiabatic ET.

The present theory contains some significant clarifications and extensions compared to the original CIET theory of Fraggedakis *et al.*[103] In the reduction rate, eqn (38), we have defined the dimensionless concentration of electrons as $\tilde{n}_{\mathrm{e}}/\tilde{n}_{\mathrm{h}}$, to be consistent with our definition of diffusional electrochemical potential of electrons, $\mu_{\mathrm{e}}^{\mathrm{ex}}$, in eqn (32), as well as the dimensionless concentrations of the reduced and oxidized chemical species, $\tilde{c}_{\mathrm{R}}$ and $\tilde{c}_{\mathrm{O}}$, respectively, in the reduction current, eqn (14). The diffusional electrochemical potential enforces the Pauli exclusion principle for fermions by requiring that the creation of a particle always destroys a hole, as expressed by Fermi–Dirac statistics in eqn (32). Consistent with the way the reduction reaction is written, eqn (7), we do not include a hole in the reduced state. However, it is still necessary to integrate over the possible energies of electrons created by the oxidation reaction, eqn (39), since the activation barrier $\Delta G_{\ddagger}^{\mathrm{ox}}$ is electron energy dependent. We also choose the solvent polarization frequency ν_{s} as the natural frequency scale for CIET with non-adiabatic ET, in which case the CIET rate scales with the quantum tunneling frequency, κ_{T}.

In general, the CIET free-energy barriers for oxidation and reduction, $\Delta G_{\ddagger}^{\mathrm{ox}}(\xi,\Delta G^{\mathrm{ex}})$ and $\Delta G_{\ddagger}^{\mathrm{red}}(\xi,\Delta G^{\mathrm{ex}})$, respectively, depend on both the ion transfer coordinate, ξ, and the excess free energy of reaction, $\Delta G^{\mathrm{ex}}(\eta_{\mathrm{f}},\varepsilon)$, which in turn depends on the formal overpotential, η_{f}, and the electron energy, ε, sampled from

the band structure, according to eqn (33). In order to derive these relations, we must postulate a mechanistic model for the CIET transition state, which combines classical IT and quantum mechanical ET.

3.3 Transition state for coupled ion–electron transfer

3.3.1 Activity coefficient of the CIET transition state. We begin by specifying the activity coefficient of the CIET transition state as the product of ionic and electronic terms:

$$\gamma_{\ddagger} = \gamma_{\ddagger}^{\mathrm{IT}} \gamma_{\ddagger}^{\mathrm{ET}} \tag{41}$$

which express general entropic contributions that are assumed not to depend on the microscopic reaction coordinates introduced below. These contributions are rooted in the exclusion of certain states of the molecular reactants, including ions and neutral species, as well as the electrons. The IT term $\gamma_{\ddagger}^{\mathrm{IT}}$ mainly reflects excluded volume constraints on ion transfer, which we assume do not depend on the IT reaction coordinate of the CIET transition state ($\xi_{\ddagger}$ below). For example, in cases of ion adsorption, intercalation or electrodeposition, we could set

$$\gamma_{\ddagger}^{\mathrm{IT}} = \frac{1}{1-\tilde{c}}, \tag{42}$$

so that $(\gamma_{\ddagger}^{\mathrm{IT}})^{-1} = 1 - \tilde{c}$ is equal to the probability of finding a vacancy among reactive ions with coverage $\tilde{c}$ on the electrode/electrolyte interface.[24] Other choices for $\gamma_{\ddagger}^{\mathrm{IT}}$ might express volume exclusion among random loose packings of hard spheres, *e.g. via* the Carnahan–Starling equation of state.[116]

In contrast, there is only one choice for the ET term $\gamma_{\ddagger}^{\mathrm{ET}}$ to enforce the Pauli exclusion principle, which prohibits any two electrons from sharing the same quantum state. By analogy with eqn (42), we must set $\gamma_{\ddagger}^{\mathrm{ET}}$ to the inverse hole concentration,

$$\gamma_{\ddagger}^{\mathrm{ET}} = \frac{1}{\tilde{n}_{\mathrm{h}}(\varepsilon)} = \frac{1}{1-\tilde{n}_{\mathrm{e}}(\varepsilon)} \tag{43}$$

to reflect excluded energy constraints on electron transfer in the electrode. Consistent with the notion of diabatic states in ET theory,[38] we assume that $\gamma_{\ddagger}^{\mathrm{ET}}$ does not depend on the solvent reorganization coordinate at the CIET transition state ($q_{\ddagger}$ below), because the band structure of the electrode remains unchanged by isoenergetic ET. Summarizing these general considerations, we express universal entropic contributions to the excess free energy of the CIET transition state as

$$\mu_{\ddagger}^{\mathrm{ex,ent}} = k_{\mathrm{B}}T \ln \gamma_{\ddagger} = k_{\mathrm{B}}T \ln \gamma_{\ddagger}^{\mathrm{IT}} - k_{\mathrm{B}}T \ln \tilde{n}_{\mathrm{h}}(\varepsilon) \tag{44}$$

for IT and ET, respectively. For a given model of $\gamma_{\ddagger}^{\mathrm{IT}}$, there may be additional specific entropic contributions to the excess chemical potential landscape of the reaction mechanism, which could contribute to temperature dependence of the free energy barriers, $\Delta G_{\ddagger}^{\mathrm{red/ox}}$, derived below, although it is always possible to redefine $\gamma_{\ddagger}^{\mathrm{IT}}$ to incorporate all entropic contributions to the excess chemical potential of the transition state, $\mu_{\ddagger}^{\mathrm{ex}}$, consistent with eqn (6).

Substituting eqn (44) and (40) into eqn (38) and (39), we arrive at more familiar expressions for non-adiabatic reduction and oxidation rates in quantum electrochemistry,[25,26] first introduced by Gurney[42] and developed in detail by Levich, Dogonadze and Chizmadzhev:[26,27,36,48,50]

$$\tilde{k}_{\mathrm{red}} = \frac{\tilde{\kappa}_{\mathrm{e}}}{\gamma_{\ddagger}^{\mathrm{IT}}} \int_{-\infty}^{\infty} \mathrm{e}^{-\Delta G_{\ddagger}^{\mathrm{red}} / k_{\mathrm{B}} T} \tilde{n}_{\mathrm{e}} \rho_{\mathrm{e}} \mathrm{d}\varepsilon \tag{45}$$

$$\tilde{k}_{\mathrm{ox}} = \frac{\tilde{\kappa}_{\mathrm{e}}}{\gamma_{\ddagger}^{\mathrm{IT}}} \int_{-\infty}^{\infty} \mathrm{e}^{-\Delta G_{\ddagger}^{\mathrm{ox}} / k_{\mathrm{B}} T} \tilde{n}_{\mathrm{h}} \rho_{\mathrm{e}} \mathrm{d}\varepsilon \tag{46}$$

with an important new prefactor $(\gamma_{\ddagger}^{\mathrm{IT}})^{-1}$ that accounts for the entropic barrier (*e.g.* from excluded volume) for IT at the transition state.[24,103] The more standard appearance of $\tilde{n}_{\mathrm{e}}$ in the reduction rate and $\tilde{n}_{\mathrm{h}}$ in the oxidation rate corresponds to writing the net reduction reaction in the form of eqn (35), where an electron is replaced by a hole, when the faradaic reaction occurs. We have also made the standard approximation that the solvent polarization frequency, ν_{s}, and the electronic coupling, $H_{\mathrm{DA}}{}^{2}$, are independent of the IT coordinate ξ, which should be a good approximation for outer-sphere non-adiabatic ET. As such, the electron transmission coefficient, $\tilde{\kappa}_{\mathrm{e}}$, has been factored out of the integrals above.

3.3.2 Free energy barrier for nonadiabatic CIET. We postulate that the reaction complex in eqn (7) explores a landscape of excess chemical potential μ^{ex} driven by thermal noise.[24] Following Fraggedakis *et al.*,[103] we construct a two-dimensional landscape, $\mu^{\mathrm{ex}}(q,\xi)$, where ξ is again the IT reaction coordinate, and q is the ET reaction coordinate, which describes reorganization of the solvent (or more generally, the electronic environment), as shown in Fig. 5. Following Marcus,[33,37] we postulate separate, overlapping landscapes for two diabatic quantum states,[38] the initial state O + e^{-} and the final state R of the reduction reaction, making harmonic approximations of parabolic dependencies on the reorganization coordinate,

$$\mu_1^{\mathrm{ex}}(q,\xi) = \mu_1^{\mathrm{ex}}(q_{\mathrm{O}},\xi_{\mathrm{O}}) + f_1(q,\xi) + \frac{k_{\mathrm{O}}}{2}(q-q_{\mathrm{O}})^2 \tag{47}$$

$$\mu_2^{\mathrm{ex}}(q,\xi) = \mu_2^{\mathrm{ex}}(q_{\mathrm{R}},\xi_{\mathrm{R}}) + f_2(q,\xi) + \frac{k_{\mathrm{R}}}{2}(q-q_{\mathrm{R}})^2 \tag{48}$$

where $\mu_1^{\mathrm{ex}}(q,\xi) = \mu_{\mathrm{O}}^{\mathrm{ex}}(q,\xi) + \mu_{\mathrm{e}}^{\mathrm{ex}}(q,\xi)$ and $\mu_2^{\mathrm{ex}}(q,\xi) = \mu_{\mathrm{R}}^{\mathrm{ex}}(q,\xi)$. The functions, $f_1(q,\xi)$ and $f_2(q,\xi)$, describe the excess free energy of IT – without ET – in the diabatic basis starting from local minima at the oxidized state, $f_1(q_{\mathrm{O}},\xi_{\mathrm{O}}) = 0$, or the reduced state, $f_2(q_{\mathrm{R}},\xi_{\mathrm{R}}) = 0$, respectively. The excess free energy of reaction, eqn (33), is given by,

$$\Delta G^{\mathrm{ex}} = \mu_2^{\mathrm{ex}}(q_{\mathrm{R}},\xi_{\mathrm{R}}) - \mu_1^{\mathrm{ex}}(q_{\mathrm{O}},\xi_{\mathrm{O}}). \tag{49}$$

The set of possible ET transition states corresponds to the intersection of the two diabatic IT surfaces,

$$\mu_{\mathrm{ET}}^{\mathrm{ex}}(\xi) = \mu_1^{\mathrm{ex}}(q_{\ddagger},\xi) = \mu_2^{\mathrm{ex}}(q_{\ddagger},\xi). \tag{50}$$

The most likely CIET transition state corresponds to the minimum of $\mu_{\mathrm{ET}}^{\mathrm{ex}}(\xi)$, which is attained at the IT coordinate, $\xi_{\ddagger}$. At each IT coordinate ξ, ET can occur either non-adiabatically, by quantum tunneling at an excess chemical potential just below $\mu_{\mathrm{ET}}^{\mathrm{ex}}(\xi)$, or adiabatically, through a shared electronic state in the diabatic basis.[38] As

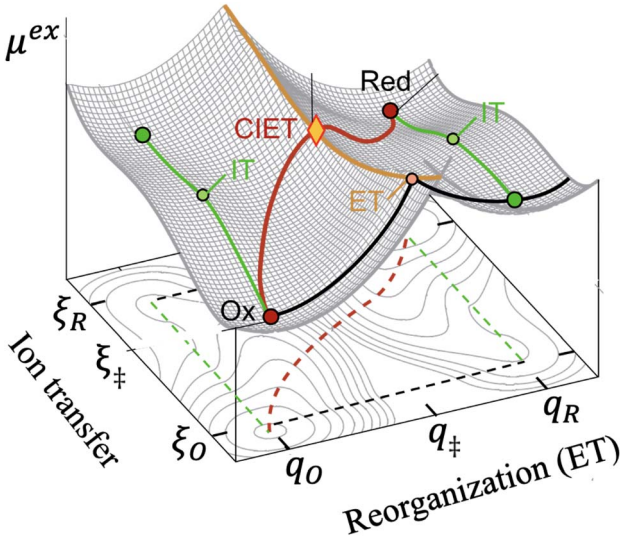

Fig. 5 Free energy landscape for coupled ion–electron transfer (CIET)[103] between diabatic reduced (Red) and oxidized (Ox) states.[38] The excess chemical potential of the reaction complex, $\mu^{ex}(\xi,q)$, is a function of the ion-transfer coordinate ξ (typically the position of a reactive ion) and the Marcus solvent reorganization coordinate, q. The oxidized ground state at (ξ_O,q_O) consists of the oxidized species and an electron in the electrode, and the reduced ground state at (ξ_R,q_R) corresponds to the reduced species. The green paths indicate ion transfer (IT) without electron transfer (ET), while the black paths indicate ET without IT. The orange activation barrier surface is formed by the intersection of Marcus parabolae at $q_\ddagger(\xi)$, where fast, iso-energetic ET is facilitated by slow IT. The lowest energy path in red corresponds to CIET over the saddle point at $q_\ddagger(\xi_\ddagger)$. [Adapted from Fig. 4b of Sood *et al.* (2021)[117] by Daniel Cogswell.]

long as the electron coupling is weak compared to the reorganization energy, $H_{DA}^2 \ll \lambda$, both limits lead to similar rate expressions, except for the prefactor. As noted above, the prefactor in eqn (45) and (46) is for non-adiabatic ET.

To further simplify the problem, we make several assumptions, which can be relaxed in some cases (below). Following most of the quantum electrochemistry literature, we assume symmetric ET with $k_O = k_R = k$, which ensures the existence of a unique transition state from the intersection of pairs of Marcus parabolae with the same curvature. We also assume a separable free energy with $f_1(q,\xi) \approx f_1(q_O,\xi)$ and $f_2(q,\xi) \approx f_2(q_R,\xi)$, which implies that ion transfer occurs independently from solvent relaxation. These are both good approximations, whenever ET and IT are physically separated at the Angstrom scale of quantum tunneling. For example, the reduced state could consist of a polaron (separated ion–electron pair) in an ion-intercalation electrode.[63,103] For electrodeposition or electrocatalysis at metal electrodes,[31] these approximations break down when the transferring ion is itself reduced for inner-sphere, adiabatic CIET,[118] but they may still hold for cases of outer-sphere or weakly adiabatic CIET.[119]

In principle, CIET theory can be extended (below) for the general case of asymmetric ET with $k_O \neq k_R$, but this requires circumventing the mathematical fact that parabolae with different curvatures may not intersect to determine a well-defined transition state. The most common theoretical framework for

asymmetric ET is based on asymmetric Marcus–Hush (AMH) theory.[51,57,58,61,120] The AMH theory expands the solvent reorganization landscape $\mu^{\mathrm{ex}}(q,\xi)$ for small overpotentials and large reorganization energies to obtain the first cubic corrections to the Marcus parabolae in the variable q. These terms are straightforward to add to the general CIET free energy landscape, eqn (47) and (48), but complicate the analysis and lose validity at large overpotentials, where the diabatic states do not cross. Let us thus postpone the discussion of AMH theory in CIET and focus on symmetric ET, $k_{\mathrm{O}} = k_{\mathrm{R}} = k$, while allowing for strong asymmetry in IT.

In the general case of symmetric ET and separable IT, we can solve for the ET activation barrier, $\mu^{\mathrm{ex}}_{\mathrm{ET}}(\xi)$, from the intersection of the Marcus parabolae, which occurs at the solvent reorganization coordinate,

$$q_{\ddagger}(\xi) = \frac{1}{2}(q_{\mathrm{O}} + q_{\mathrm{R}}) + \frac{\Delta G^{\mathrm{ex}} + f_2(q_{\mathrm{O}},\xi) - f_1(q_{\mathrm{R}},\xi)}{k(q_{\mathrm{R}} - q_{\mathrm{O}})}. \tag{51}$$

For small values of the driving force, $|\Delta G^{\mathrm{ex}}| < \lambda$, the barrier surface lies in the normal region, $q_{\mathrm{O}} < q_{\ddagger}(\xi) < q_{\mathrm{R}}$, as shown in Fig. 5. For large values of the driving force, $|\Delta G^{\mathrm{ex}}| > \lambda$, which are always possible for some range of electron energies, the barrier surface lies within the Marcus inverted region, where either $q_{\ddagger}(\xi) < q_{\mathrm{O}}$ or $q_{\ddagger}(\xi) > q_{\mathrm{R}}$ (not shown in the figure).

Substituting eqn (51) into eqn (47) and (48), we arrive at the ET activation barriers (at the diabatic crossings) for oxidation, eqn (24), and reduction, eqn (23), respectively:

$$\begin{aligned}\Delta G^{\mathrm{ET}}_{\mathrm{red}}(\xi) &= \mu^{\mathrm{ex}}_1(q_{\ddagger},\xi) - \mu^{\mathrm{ex}}_1(q_{\mathrm{O}},\xi_{\mathrm{O}}) \\ &= f_1(q_{\mathrm{O}},\xi) + \frac{1}{4\lambda}(\Delta G^{\mathrm{ex}} + f_2(q_{\mathrm{R}},\xi) - f_1(q_{\mathrm{O}},\xi) + \lambda)^2\end{aligned} \tag{52}$$

$$\begin{aligned}\Delta G^{\mathrm{ET}}_{\mathrm{ox}}(\xi) &= \mu^{\mathrm{ex}}_2(q_{\ddagger},\xi) - \mu^{\mathrm{ex}}_2(q_{\mathrm{R}},\xi_{\mathrm{R}}) \\ &= f_2(q_{\mathrm{R}},\xi) + \frac{1}{4\lambda}(\Delta G^{\mathrm{ex}} + f_2(q_{\mathrm{R}},\xi) - f_1(q_{\mathrm{O}},\xi) - \lambda)^2\end{aligned} \tag{53}$$

where we define the usual Marcus reorganization energy for ET,[37]

$$\lambda = \frac{k}{2}(q_{\mathrm{R}} - q_{\mathrm{O}})^2 \tag{54}$$

which arises from the general CIET theory, as a result of our assumptions of symmetric harmonic reorganization for ET and separable IT dependence in the free energy landscape. Under these approximations, the solvent polarization frequency can be expressed as $2\pi\nu_{\mathrm{s}} = \sqrt{k/m_{\mathrm{s}}}$,

$$\nu_{\mathrm{s}} = \frac{1}{2\pi}\sqrt{\frac{k}{m_{\mathrm{s}}}} = \frac{|q_{\mathrm{R}} - q_{\mathrm{O}}|}{\pi}\sqrt{\frac{\lambda}{2m_{\mathrm{s}}}} \tag{55}$$

where m_{s} is an effective mass for harmonic oscillations along the solvent reorganization coordinate, q.

For subsequent analysis, it is convenient to rewrite the CIET barriers as

$$\Delta G^{\mathrm{ET}}_{\mathrm{red/ox}} = \overline{f} + \frac{(\lambda \pm \Delta G^{\mathrm{ex}})^2}{4\lambda} + \frac{\Delta f^2}{4\lambda} \pm \frac{\Delta G^{\mathrm{ex}}\Delta f}{2\lambda} \tag{56}$$

in terms of the combined variables,

$$\bar{f}(\xi) = \frac{1}{2}(f_1(q_O,\xi) + f_2(q_R,\xi)) \tag{57}$$

$$\Delta f(\xi) = f_2(q_R,\xi) - f_1(q_O,\xi) \tag{58}$$

which correspond to the mean and difference of the IT barriers for reduction and oxidation, when ET occurs at a given IT coordinate ξ.

Fraggedakis *et al.*[103] postulated that $\Delta f(\xi_\ddagger) \approx 0$ at the CIET transition state, which leads to the original Marcus barriers for ET,

$$\Delta G_\ddagger^{\mathrm{red/ox}} = \Delta G_{\mathrm{red/ox}}^{\mathrm{ET}}(\xi_\ddagger) = \Delta G_\ddagger^{\mathrm{IT}} + \frac{(\lambda \pm \Delta G^{\mathrm{ex}})^2}{4\lambda} \tag{59}$$

but with an extra term for an effective IT barrier, $\Delta G_\ddagger^{\mathrm{IT}} = \bar{f}(\xi_\ddagger)$, which contributes a common Arrhenius prefactor to k_{red} and k_{ox}. However, no conditions were given to justify this postulate, and no formula was given for $\Delta G_\ddagger^{\mathrm{IT}}$. Instead, the effective IT barrier was expressed empirically as $\Delta G_\ddagger^{\mathrm{IT}} = \alpha_{\mathrm{IT}}\Delta E_{\mathrm{IT}}$ in terms of an overall ion transfer energy, ΔE_{IT}, multiplied by a phenomenological IT coefficient, $\alpha_{\mathrm{IT}} \approx 1/2$, inspired by the Butler–Volmer equation.[103] In this context, one might expect α_{IT} to be a symmetry factor,

$$\xi_\ddagger = \alpha_{\mathrm{IT}}\xi_O + (1 - \alpha_{\mathrm{IT}})\xi_R \tag{60}$$

reflecting the position of the effective IT barrier relative to that of the oxidized and reduced states.[6,7] However, it would still be unclear whether the energy ΔE_{IT} corresponds to reduction or oxidation, except in the symmetric case of equal IT energies with $\alpha_{\mathrm{IT}} = 1/2$. Of course, rather than making arbitrary postulates about the transition state, it would be more satisfying and consistent to derive such quantities systematically from the general theory.

In principle, the CIET free energy landscape $\mu^{\mathrm{ex}}(q,\xi)$ could be predicted by *ab initio* molecular dynamics (AIMD) quantum mechanical calculations, *e.g.* using constrained density functional theory (CDFT) to compute the diabatic states,[38,39,121–124] from which the most probable solvent reorganization coordinate, $q_\ddagger(\xi)$, and barriers, $\Delta G_\ddagger^{\mathrm{ox}}(\xi)$ and $\Delta G_\ddagger^{\mathrm{red}}(\xi)$, for CIET could be obtained numerically for each IT coordinate ξ and inserted into the integrals for the reduction and oxidation rates, k_{red} and k_{ox}. In general, the excess free energy landscapes for IT in the oxidized and reduced diabatic states, $f_1(q,\xi)$ and $f_2(q,\xi)$, respectively, may depend on the ET solvent reorganization coordinate q, as well as the IT coordinate ξ.

In the following sections, we consider three asymptotic limits of CIET theory, which correspond to rate limitation by either IT or (normal or inverted) ET. These universal limiting cases generalize and unify Butler–Volmer and Marcus kinetics, respectively. We then proceed to derive a simple, uniformly valid formula for all parameter values by asymptotic matching of these limits.

4 Marcus kinetics of electron-coupled ion transfer (ECIT)

4.1 Symmetric normal electron transfer

Here, we show that the Marcus IT barrier, eqn (59), augmented by a certain IT barrier, eqn (62), can be derived from the general CIET theory in the limit where the ET step is

rate limiting and the overpotential is small enough to remain in the normal region of Marcus kinetics. To be clear, nonadiabatic ET by quantum tunneling is still instantaneous and isoenergetic, but the prerequisite solvent reorganization is slow compared to IT, which may begin before ET but is rapidly completed after ET. We refer to this CIET reaction mechanism as "electron-coupled ion transfer" (ECIT).

In the regime of Normal ECIT, we require that both the effective IT free energy barrier, $\Delta G_{\ddagger}^{\mathrm{IT}}$, and the magnitude of the formal overpotential, $e|\eta_{\mathrm{f}}|$ (converted to an energy by the electron charge e), are smaller than the reorganization energy:

$$\lambda \gg \Delta G_{\ddagger}^{\mathrm{IT}}, e|\eta_{\mathrm{f}}|, k_{\mathrm{B}}T, \Delta_{\mathrm{e}} \text{ (Normal ECIT)} \tag{61}$$

where $\lambda \gg k_{\mathrm{B}}T$ is required by eqn (25) and $\Delta_{\mathrm{e}} \ll k_{\mathrm{B}}T$ for nonadiabatic ET. In this regime of CIET theory, we shall see that the IT barrier can be expressed explicitly in terms of the diabatic free energy landscapes as

$$\Delta G_{\ddagger}^{\mathrm{IT}} = \bar{f}(\xi_{\ddagger}) = \frac{1}{2}\min_{\xi}\{f_1(q_{\mathrm{O}},\xi) + f_2(q_{\mathrm{R}},\xi)\} \tag{62}$$

where $\xi = \xi_{\ddagger}$ is the IT coordinate of the transition state, which minimizes $\Delta G_{\ddagger}^{\mathrm{IT}}$. Given specific models for $f_1(q,\xi)$ and $f_2(q,\xi)$, such as the linear approximations introduced below, we can use eqn (62) to determine $\xi_{\ddagger}$ for a specific reaction.

For a given value of $\xi_{\ddagger}$, let us show that the CIET barriers, $\Delta G_{\ddagger}^{\mathrm{red/ox}}$, indeed approach the Marcus form proposed by Fraggedakis *et al.*, eqn (59), with $\Delta G_{\ddagger}^{\mathrm{IT}} = \bar{f}(\xi_{\ddagger})$ given by eqn (62) in the asymptotic limit of Normal ECIT, eqn (61). Our goal is to prove that the first two terms in eqn (56) dominate in the asymptotic limit of eqn (61). We begin by stating the triangle inequality, $|\Delta f| \leq 2\bar{f}$, since $f_1, f_2 \geq 0$, which helps us show that the third term in eqn (56) is asymptotically dominated by the first term:

$$\frac{(|\Delta f|/2)^2}{\lambda \bar{f}} \leq \frac{\bar{f}^2}{\lambda \bar{f}} = \frac{\bar{f}}{\lambda} \ll 1 \tag{63}$$

Bounding the fourth term, which directly couples the ET coordinate q and the IT coordinate ξ, is more subtle. By the same argument as in eqn (63), the fourth term in eqn (56) is also asymptotically dominated by the first term, but only in the limit of small driving force, $|\Delta G^{\mathrm{ex}}| \ll \lambda$, shown in Fig. 6(a). Given the definition, $\Delta G^{\mathrm{ex}} = e\eta_{\mathrm{f}} + \varepsilon_{\mathrm{F}} - \varepsilon$, this condition is satisfied at small formal overpotentials, $e|\eta_{\mathrm{f}}| \ll \lambda$, for the most probable electrons and holes participating in the reaction, which have energies near the Fermi surface in the assumed limit of small thermal energy, eqn (25).

On the other hand, if the driving force is large enough to enter the Marcus inverted region, $|\Delta G^{\mathrm{ex}}| \gg \lambda$, as shown in Fig. 6(c), then the approximation of Fraggedakis *et al.*, eqn (59) and (62), breaks down, although in a subtle way. In this regime, the fourth term becomes asymptotically dominated by the second term:

$$\frac{2|\Delta G^{\mathrm{ex}}\Delta f|}{(\lambda \pm \Delta G^{\mathrm{ex}})^2} \leq \frac{4\left|\bar{f}\right| \Big/ \left|\Delta G^{\mathrm{ex}}\right|}{(1 \pm \lambda/|\Delta G^{\mathrm{ex}}|)^2} \ll \frac{\lambda/|\Delta G^{\mathrm{ex}}|}{(1 \pm \lambda/|\Delta G^{\mathrm{ex}}|)^2} \ll 1 \tag{64}$$

where we use eqn (63) in the second step, which establishes the same approximation for almost all values of the parameters, seemingly even in the limit of large overpotentials. However, this is not correct, since the approximation always breaks down for electrons (or holes) whose energies are close to the point of

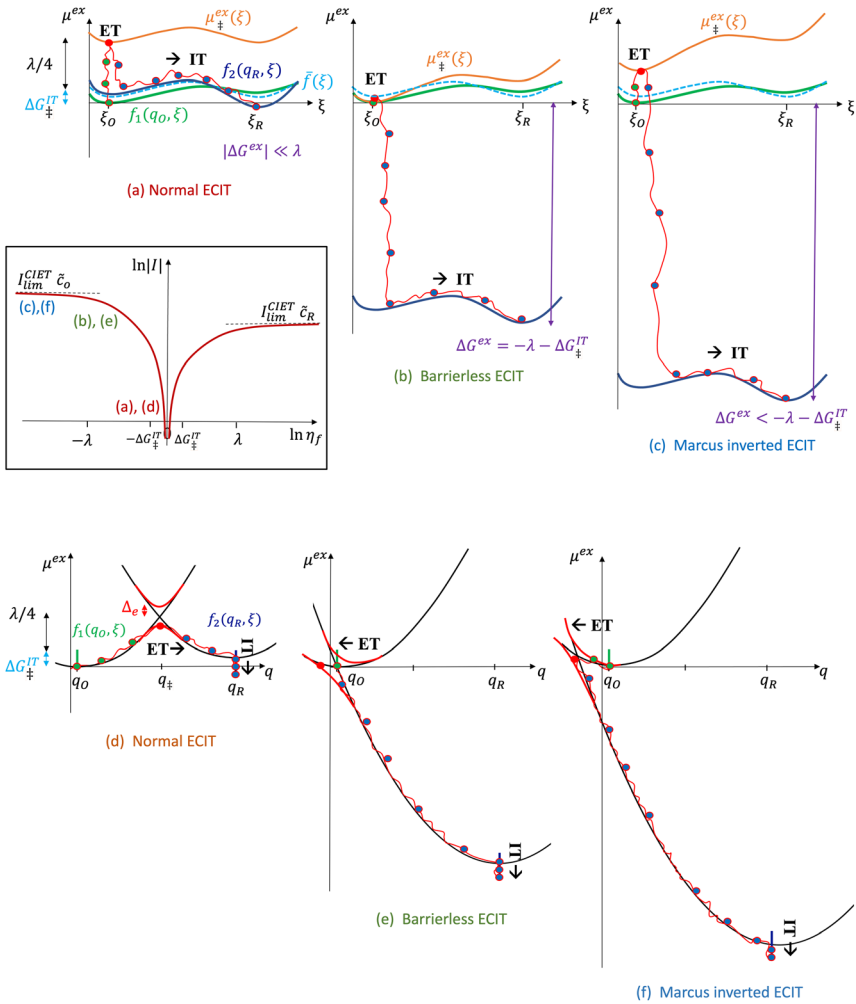

Fig. 6 Physics of ET-limited nonadiabatic CIET, or "electron-coupled ion transfer" (ECIT), at a metal electrode, where the Marcus reorganization energy λ is much larger than the ion transfer barrier, $\Delta G_{\ddagger}^{\mathrm{IT}}$, thermal energy $k_{\mathrm{B}}T$ and chemisorption function, Δ_{e}. The path of the reaction complex (red) is shown in the landscape of excess chemical potential $\mu^{\mathrm{ex}}(q,\xi)$ from Fig. 5 viewed along the IT coordinate ξ from the oxidized state ξ_{O} to the reduced state ξ_{R} in (a)–(c). The same paths are shown in (d)–(f) viewed along the ET reorganization coordinate q from q_{O} to q_{R}. The theory assumes that ET occurs close to the diabatic crossing, either by quantum tunneling or *via* adiabatic states with weak electronic coupling $H_{\mathrm{DA}} \ll \lambda$ (red curves in (d)). The oxidized state has IT energy $f_1(q_{\mathrm{O}},\xi)$ (green), and the reduced state has IT energy $f_2(q_{\mathrm{R}},\xi)$ (blue). The CIET barrier is $\mu_{\ddagger}^{\mathrm{ex}}(\xi) = \mu^{\mathrm{ex}}(q_{\ddagger},\xi)$ (orange). Three cases are depicted for the excess free energy of reaction, $\Delta G^{\mathrm{ex}} = e\eta_{\mathrm{f}} + \varepsilon_{\mathrm{F}} - \varepsilon$, the sum of the formal overpotential η_{f} and the electron energy ε below the Fermi level ε_{F}. In (a) and (d), for unbiased ECIT with $\Delta G^{\mathrm{ex}} = 0$, the rate limiting process is ET with a large barrier $\lambda/4$ (for symmetric ET) in addition to the small IT barrier $\Delta G_{\ddagger}^{\mathrm{IT}} \approx \bar{f}(\xi)$ (light blue). In (b) and (e), electrons at $\Delta G^{\mathrm{ex}} = -\lambda$ are able to make barrierless ET transitions, which dominate in the limit of large negative overpotentials, and facilitate IT at a constant rate. In (c) and (f), for $\Delta G^{\mathrm{ex}} < -\lambda$, the reaction complex enters the Marcus inverted region with a larger ET barrier and smaller contribution to the total current. (Inset) Tafel plot showing the scenarios (a)–(c)/(d)–(f) for reduction, where the Tafel slope is α_{ET} for the beginning of the negative reduction branch and $1 - \alpha_{\mathrm{ET}}$ for the positive oxidation branch. On both sides, the brief Tafel regime transitions to Marcus ECIT reaction limit current, when the overpotential exceeds the reorganization energy.

barrierless ET, where $\pm\Delta G^{\mathrm{ex}} \approx -\lambda$, shown in Fig. 6(b). In this case, the second term in eqn (56) vanishes, and, although the fourth term is still asymptotically bounded by the first term:

$$\frac{|\Delta G^{\mathrm{ex}}\Delta f|}{2\lambda\bar{f}} \approx \frac{\lambda|\Delta f|}{2\lambda\bar{f}} \leq 1 \tag{65}$$

(where we use the triangle inequality again), it cannot be neglected. While only a small range of electron or hole energies can complete barrierless ET, it is well known that these contributions dominate in the Marcus inverted region for an electrode. Below, we shall describe the new regime of inverted ECIT. For now, we have shown that in the regime of Normal ECIT, eqn (61), the integration over all electron energies ε in eqn (45) and (46) can be performed using only the first two terms of eqn (59) for the CIET barrier.

The resulting asymptotic rate expression for symmetric Normal ECIT is given by:

$$\tilde{k}_{\mathrm{red/ox}} = \frac{\tilde{\kappa}_{\mathrm{e}}}{\gamma_{\ddagger}^{\mathrm{IT}}} \mathrm{e}^{-\Delta\tilde{G}_{\ddagger}^{\mathrm{IT}}} \int_{-\infty}^{\infty} \frac{\mathrm{e}^{-\left(e\eta_{\mathrm{f}}+\varepsilon_{\mathrm{F}}-\varepsilon\pm\lambda\right)^2/4\lambda k_{\mathrm{B}}T}}{1+\mathrm{e}^{\pm(\varepsilon-\varepsilon_{\mathrm{F}})/k_{\mathrm{B}}T}} \rho_{\mathrm{e}}(\varepsilon)\mathrm{d}\varepsilon \quad \text{(Normal ECIT)} \tag{66}$$

where we define $\Delta\tilde{G}_{\ddagger}^{\mathrm{IT}} = \Delta G_{\ddagger}^{\mathrm{IT}}/k_{\mathrm{B}}T$. The Normal ECIT rate formula is identical to the Marcus expression for pure, symmetric ET at an electrode[36,51,60,86,125] ($\rho_{\mathrm{e}} =$ constant), except for an important new IT-dependent prefactor, which contains the activity coefficient γ^{IT} and effective free energy barrier $\Delta G_{\ddagger}^{\mathrm{IT}}$ for IT. Recall that the current is given by eqn (14) in terms of the k_{red} and k_{ox}.

For an ideal metal electrode with a uniform density of electronic states ($\rho_{\mathrm{e}} =$ constant), we recover the $\tilde{\eta}_{\mathrm{f}}$-dependence of MHC kinetics[85] with an IT-dependent Arrhenius prefactor,

$$\tilde{k}_{\mathrm{red/ox}} \approx \tilde{k}_0 \mathrm{e}^{-\Delta\tilde{G}_{\ddagger}^{\mathrm{IT}}} \tilde{k}_{\mathrm{red/ox}}^{\mathrm{MHC}} \quad \text{(Normal ECIT, metal)} \tag{67}$$

where we define the dimensionless characteristic rate constant,

$$\tilde{k}_0 = \frac{2\tilde{\kappa}_{\mathrm{e}}\tilde{\rho}_{\mathrm{e}}\sqrt{\pi\tilde{\lambda}}}{\gamma_{\ddagger}^{\mathrm{IT}}} = \frac{H_{\mathrm{DA}}{}^2\rho_{\mathrm{e}}}{\hbar\nu_{\mathrm{s}}\gamma_{\ddagger}^{\mathrm{IT}}} = \frac{\kappa_{\mathrm{T}}}{2\pi\nu_{\mathrm{s}}\gamma_{\ddagger}^{\mathrm{IT}}} \tag{68}$$

with dimensional form,

$$k_0 = \frac{\kappa_{\mathrm{T}}}{2\pi\gamma_{\ddagger}^{\mathrm{IT}}} = \frac{2}{\gamma_{\ddagger}^{\mathrm{IT}}}\frac{\Delta_{\mathrm{e}}}{h} \tag{69}$$

and where we adopt the uniformly valid approximation of Zeng *et al.*[60] for the integrals in eqn (67) to define the dimensionless MHC rate,

$$\tilde{k}_{\mathrm{red/ox}}^{\mathrm{MHC}} = \frac{1}{2(1+\mathrm{e}^{\pm\tilde{\eta}_{\mathrm{f}}})}\mathrm{erfc}\left(\frac{\tilde{\lambda}-\sqrt{1+\sqrt{\tilde{\lambda}}+\tilde{\eta}_{\mathrm{f}}{}^2}}{2\sqrt{\tilde{\lambda}}}\right) \tag{70}$$

in terms of the dimensionless variables, $\tilde{\eta}_{\mathrm{f}} = e\eta_{\mathrm{f}}/k_{\mathrm{B}}T$, $\tilde{\lambda} = \lambda/k_{\mathrm{B}}T$, and $\tilde{\rho}_{\mathrm{e}} = \rho_{\mathrm{e}}k_{\mathrm{B}}T$. Although various series expansions of the MHC integrals are available for different asymptotic limits of the parameters,[95,96] the closed-form approximation of eqn (70) has the advantage of being simpler and uniformly valid for all values of λ and η_{f}. Compared to the MHC integral, eqn (67), the maximum relative error of eqn (70) is around 5%, while maintaining high accuracy for large and small $\tilde{\lambda}$, as

well as large formal overpotentials, $\tilde{\eta}_f$, since it was derived by asymptotic matching of exact results for these limiting cases.[60]

The analytical approximation of the Normal ECIT rate for a metal electrode, eqn (67)–(70), is convenient for calculations of important quantities, such as the dimensionless exchange current,

$$\tilde{I}_0 = \frac{\tilde{k}_0}{4} e^{-\Delta\tilde{G}_\ddagger^{IT}} \left(\frac{\tilde{c}_O \tilde{c}_R}{\tilde{c}_O + \tilde{c}_R}\right) \mathrm{erfc}\left(\frac{\tilde{\lambda} - \sqrt{1 + \sqrt{\tilde{\lambda}} + \ln^2\left(\frac{\tilde{c}_O}{\tilde{c}_R}\right)}}{2\sqrt{\tilde{\lambda}}}\right) \quad \text{(Normal ECIT, metal)} \tag{71}$$

which is defined by the linear response, $\tilde{I} \sim \tilde{I}_0\tilde{\eta}$, where $\tilde{\eta} = \tilde{\eta}_f + \ln(\tilde{c}_R/\tilde{c}_O)$ is a small total overpotential, $|\tilde{\eta}| \ll 1$. In contrast to phenomenological BV theory, eqn (4), the exchange current for ECIT does not have simple power-law dependence on the reactant concentrations, $\tilde{c}_O$ and $\tilde{c}_R$. CIET kinetics is also non-separable, in the sense that the current cannot be expressed as a function of overpotential times a function of concentrations, in contrast to the separable form of the phenomenological BV equation, eqn (1). Note that for the typical low-temperature regime, $\tilde{\lambda} \gg 1$, the exchange current for symmetric ECIT has an Arrhenius temperature dependence, $\tilde{I}_0 \sim e^{-\Delta\tilde{G}_\ddagger^{ECIT}}$, with

$$\Delta\tilde{G}_\ddagger^{ECIT} = \Delta\tilde{G}_\ddagger^{IT} + \frac{\tilde{\lambda}}{4} \tag{72}$$

where the second term is the classical Marcus activation barrier for symmetric ET.

Eqn (66) is the main of Fraggedakis *et al.*,[103] but here we clarify its range of validity, eqn (61), and provide an explicit formula for the effective IT barrier in eqn (62). The analytical approximation for normal ECIT at metal electrode, eqn (67)–(70), has already been widely used in modeling Li-ion batteries,[98,99,104,105,126–128] metal electrodeposition[100–102] and solid-oxide fuel cells,[110] but without a clear understanding of its applicability and microscopic interpretation provided here. Since the (scaled) MHC rates tend to unity at large formal overpotentials,

$$\lim_{\tilde{\eta}_f \to -\infty} \tilde{k}_{red}^{MHC} = \lim_{\tilde{\eta}_f \to \infty} \tilde{k}_{ox}^{MHC} = 1, \tag{73}$$

the Normal ECIT rate for a metal electrode also extrapolates to a constant,

$$\lim_{\tilde{\eta}_f \to \mp\infty} \tilde{k}_{red/ox} = \tilde{k}_0\, e^{-\Delta\tilde{G}_\ddagger^{IT}} \quad \text{(Normal ECIT, metal)} \tag{74}$$

but it is important to recognize that this limit is not physically valid, since it exceeds the range of validity of Normal ECIT, $e|\eta_f| \ll \lambda$. Even when ET is slow compared to IT, $\Delta G_\ddagger^{IT} \ll \lambda$, a more general analysis of CIET theory is required to account for Inverted ECIT at large overpotentials, which leads to a somewhat different formula for the limiting reaction rate (below).

4.2 Asymmetric normal electron transfer

Although the vast majority of ET models are symmetric, as noted above, there has been growing interest in the asymmetric Marcus–Hush model,[51,120] led by Compton

et al.[57,58,129–131] for faradaic reactions involving inner-sphere ET. The AMH model introduces cubic terms in the free-energy landscape, which approximate the different nonlinear solvation characteristics of the reduced and oxidized states.[55,56] While the intersection of these diabatic surfaces is not always guaranteed at large overpotentials, the transition state always exists – by definition – for asymmetric Normal ECIT, by restriction to sufficiently small overpotentials.

For inner-sphere ET, the vibrational force constants are generally different for the reduced and oxidized states. In AMH theory,[51,120] this asymmetry is controlled by a new dimensionless parameter, γ, which can be expressed in terms of the inner-sphere reorganization energy λ_i as

$$\gamma = \frac{\lambda_i}{\lambda} \frac{\sum_s \overline{k}_s (\Delta q_s)^2 \Delta\tilde{k}}{\sum_s \overline{k}_s (\Delta q_s)^2} \tag{75}$$

where we define the dimensionless difference

$$\Delta\tilde{k} = \frac{k_{\mathrm{O},s} - k_{\mathrm{R},s}}{k_{\mathrm{O},s} + k_{\mathrm{R},s}} \tag{76}$$

and the harmonic mean

$$\overline{k}_s = \frac{2k_{\mathrm{O},s}k_{\mathrm{R},s}}{k_{\mathrm{O},s} + k_{\mathrm{R},s}} \tag{77}$$

of the inner-shell force constants, $k_{\mathrm{R},s}$ and $k_{\mathrm{O},s}$, of the reduced and oxidized states along the generalized solvent coordinate, Δq_s, of the sth phonon mode.[58] The sign of γ determines whether the larger force constants are in the oxidized ($\gamma > 0$) or reduced ($\gamma < 0$) states, while $\gamma = 0$ for the symmetric case.

For asymmetric Normal ECIT in the AMH approximation, the generalization of the quadratic CIET barrier, eqn (59), is a cubic function of ΔG^{ex}:

$$\Delta G_{\ddagger}^{\mathrm{red/ox}} = \Delta G_{\ddagger}^{\mathrm{IT}} + \frac{\lambda}{4}\left(1 \pm \frac{\Delta G^{\mathrm{ex}}}{\lambda}\right)^2 + \frac{\gamma}{4}(\Delta G^{\mathrm{ex}})\left[1 - \left(\frac{\Delta G^{\mathrm{ex}}}{\lambda}\right)^2\right] + \frac{\gamma^2\lambda}{16} \tag{78}$$

where the effective IT energy barrier is given by

$$\Delta G_{\ddagger}^{\mathrm{IT}} = \min_{\xi}\{(1-\alpha_{\mathrm{ET}})f_1(q_{\mathrm{O}},\xi) + \alpha_{\mathrm{ET}}f_2(q_{\mathrm{R}},\xi)\} \tag{79}$$

in terms of the ET symmetry factor

$$\alpha_{\mathrm{ET}} = \frac{1}{2} + \frac{\gamma}{4} \tag{80}$$

which is obtained by linearizing eqn (78) in the limit $|\Delta G^{\mathrm{ex}}| \ll \lambda$. A hallmark of CIET is that the weights for the IT energies of the reduced and oxidized states, $f_1(q_{\mathrm{O}},\xi)$ and $f_2(q_{\mathrm{R}},\xi)$, in the effective IT barrier $\Delta G_{\ddagger}^{\mathrm{IT}}$ are determined by the assumed symmetry of solvent reorganization controlling ET.

For a metal electrode, the rate integrals for asymmetric Normal ECIT can be approximately evaluated as

$$\tilde{k}_{\mathrm{red/ox}} \approx \tilde{k}_0 \mathrm{e}^{-\Delta\tilde{G}_{\ddagger}^{\mathrm{IT}}}\ \tilde{k}_{\mathrm{red/ox}}^{\mathrm{AMH}}\ \ (\text{asymmetric Normal ECIT, metal}) \tag{81}$$

using the asymptotic approximation of Zeng *et al.*[61] for AMH kinetics:

$$\tilde{k}^{\mathrm{AMH}}_{\mathrm{red/ox}} \approx \tilde{k}^{\mathrm{MHC}}_{\mathrm{red/ox}} \cdot \exp\left\{ -\frac{\gamma\tilde{\eta}_{\mathrm{f}}}{4\tilde{\lambda}}\left[1-\left(\frac{\tilde{\eta}_{\mathrm{f}}}{\tilde{\lambda}}\right)^2\right] - \frac{\gamma^2\tilde{\lambda}}{16}\right\} \tag{82}$$

which reduces to MHC kinetics for $\gamma = 0$.

Although nonlinear solvation effects in ET can break symmetry in the reduction and oxidation rates, they still cannot explain Tafel's law. The symmetry factor, α_{ET}, was derived by linearization for small values of ΔG^{ex} and does not hold at large formal overpotentials. In order to predict linear Tafel plots, one must consider CIET rate limitation by asymmetric IT.

5 Butler–Volmer kinetics of ion-coupled electron transfer (ICET)

Ion transfer tends to be asymmetric when coupled with nonadiabatic ET, since the compensating electron occupies different wavefunctions in the reduced and oxidized states, leading to differences in both the electrostatic energy and coordination chemistry of the ions. As such, we can generally characterize the IT barriers for reduction and oxidation with distinct free energy differences, β_{red} and β_{ox}, respectively. Without loss of generality, we assume $f_1(q,\xi) \leq \beta_{\mathrm{red}}$ and $f_2(q,\xi) \leq \beta_{\mathrm{red}}$ in the CIET landscape of excess chemical potential, eqn (47) and (48). Assuming the coupled ET is characterized by a reorganization energy, λ, we now turn our attention to the opposite limit of IT rate limitation,

$$\beta_{\mathrm{red/ox}} \gg \lambda, e|\eta_{\mathrm{f}}|, k_{\mathrm{B}}T, \Delta_{\mathrm{e}} \text{ (ICET)} \tag{83}$$

which we refer to as "ion-coupled electron transfer" (ICET), when ET occurs suddenly in response to slow IT, as shown in Fig. 7. (The term "ICET" was perhaps first used by Daniel Nocera in 2022, private communication.) Here we develop a detailed theory for the nonadiabatic case, but we argue below that similar results hold for adiabatic ICET. In contrast to ECIT, eqn (61), which corresponds to a regular limit of CIET theory, the ICET limit, eqn (83), is singular and must be treated with care.

As noted in the introduction, Butler[18] was the first to consider what we call "ICET" in the singular limit of infinitely fast ET, $\lambda \to 0$. In that case, as illustrated in Fig. 7, the parabolic ET contributions to the CIET activation barriers diverge in eqn (52) and (53) for all values of the IT coordinate ξ as $\lambda \to 0$:

$$\lim_{\lambda\to 0}\Delta G^{\mathrm{ET}}_{\mathrm{red}}(\xi) = \begin{cases} f_1(q_0,\xi_\ddagger) & \text{if } \xi = \xi_\ddagger \\ \infty & \text{if } \xi \neq \xi_\ddagger \end{cases} \tag{84}$$

$$\lim_{\lambda\to 0}\Delta G^{\mathrm{ET}}_{\mathrm{ox}}(\xi) = \begin{cases} f_2(q_{\mathrm{R}},\xi_\ddagger) & \text{if } \xi = \xi_\ddagger \\ \infty & \text{if } \xi \neq \xi_\ddagger \end{cases} \tag{85}$$

except at special values of $\xi = \xi_\ddagger$ where those terms identically vanish. These transition state values of the IT coordinate are determined implicitly by intersections of IT free energy landscapes for reduction and oxidation, shifted by the overpotential:

$$\Delta G^{\mathrm{ex}} + f_2(q_{\mathrm{O}},\xi_\ddagger) = f_1(q_{\mathrm{R}},\xi_\ddagger) \tag{86}$$

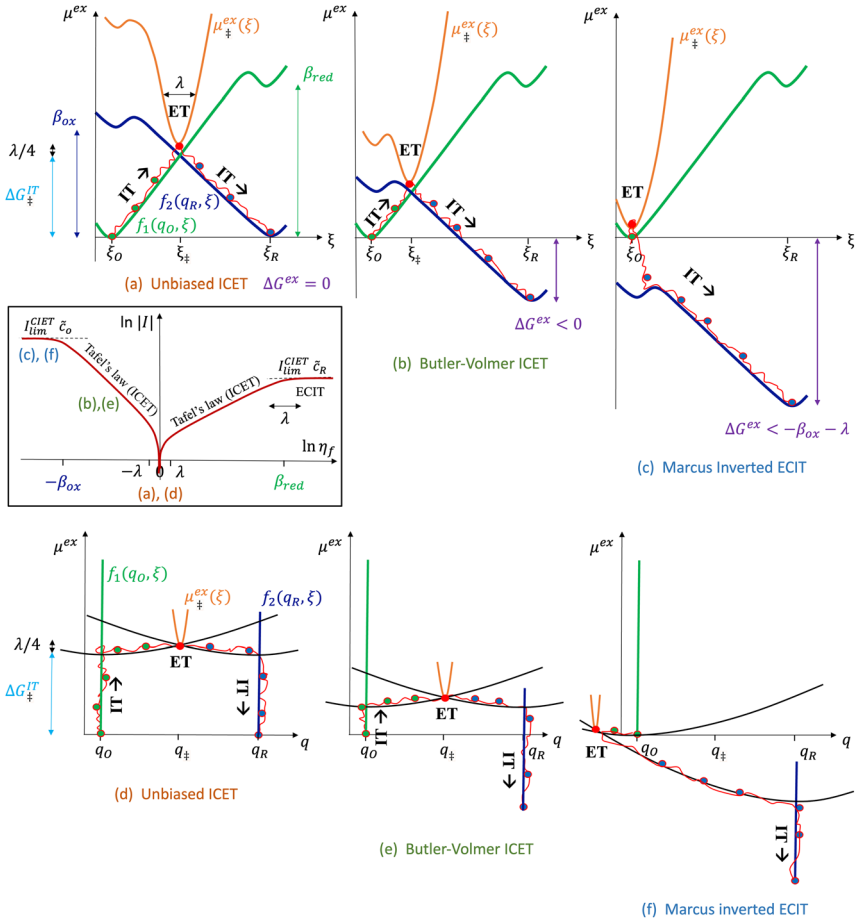

Fig. 7 Physics of IT-limited non-adiabatic CIET, or "ion-coupled electron transfer" (ICET), at a metal electrode, where the ion transfer barrier, $\Delta G^{\mathrm{IT}}_{\ddagger}$, exceeds the reorganization energy λ, thermal energy $k_{\mathrm{B}}T$ and chemisorption function, Δ_{e}. In this limit, the path of the reaction complex (red) is shown in the two dimensional landscape of excess chemical potential $\mu^{\mathrm{ex}}(q,\xi)$, shown in Fig. 5, viewed along the IT coordinate ξ from the oxidized state ξ_{O} to the reduced state ξ_{R}, in (a)–(c), and the dependence on the ET solvent reorganization coordinate q is shown for the same cases in (d)–(f). The oxidized state has IT energy $f_1(q_{\mathrm{O}},\xi)$ (green), and the reduced state has IT energy $f_2(q_{\mathrm{R}},\xi)$ (blue). The CIET barrier is $\mu^{\mathrm{ex}}_{\ddagger}(\xi) = \mu^{\mathrm{ex}}(q_{\ddagger},\xi)$ (orange). Three cases are depicted for the excess chemical potential applied between the reduced and oxidized states, $\Delta G^{\mathrm{ex}} = e\eta_{\mathrm{f}} + \varepsilon_{\mathrm{F}} - \varepsilon$, which is the sum of the formal overpotential η_{f} and the electron energy ε below the Fermi level ε_{F}, sampled from the band structure of the electrode $\rho_{\mathrm{e}}(\varepsilon)$ according to the Fermi–Dirac distribution $\tilde{n}_{\mathrm{e}}(\varepsilon)$: in (a) and (d) for unbiased ICET with $\Delta G^{\mathrm{ex}} = 0$, the rate limiting process is IT with a large barrier β_{ox} (in the reduction direction) in addition to the small ET barrier $\lambda/4$ (light blue). In (b) and (e) for moderate overpotentials, $\Delta G^{\mathrm{ex}} < 0$, Butler–Volmer kinetics holds for ICET. In (c) and (f) at even larger driving force, $\Delta G^{\mathrm{ex}} < -\beta_{\mathrm{ox}} - \lambda$, the reaction complex enters the Marcus inverted region of ECIT, as the ion sits at the oxidized state before ET triggers IT to complete the reaction. (Inset) Tafel plot showing the scenarios (a)–(c) for reduction, where the Tafel slope is $\alpha_{\mathrm{IT}} = \beta_{\mathrm{red}}/(\beta_{\mathrm{red}} + \beta_{\mathrm{ox}})$ for the negative reduction branch and $1 - \alpha_{\mathrm{IT}}$ for the positive oxidation branch. On both sides, the straight-line Tafel regime transitions to a reaction limited current for Inverted ECIT, when the overpotential exceeds the ion-transfer energy.

Of course, we must assume (for now) that such intersections exist, which is expected up to moderately large overpotentials, $-\beta_{ox} < \Delta G^{ex} < \beta_{red}$, and guaranteed if $f_1(q_O,\xi)$ and $f_2(q_R,\xi)$ are also monotonic functions.

The general formula eqn (86) determines the transition state IT coordinate, $\xi_\ddagger(\Delta G^{ex})$, for any intersecting $f_1(q_O,\xi)$ and $f_2(q_R,\xi)$ in the limit $\lambda \to 0$, but we now introduce a critical approximation, which leads to BV kinetics for sufficiently small but finite λ. Following Gurney[42] and Butler,[18] it is convenient to assume linear dependence of the IT free energy landscapes,

$$f_1(q_O,\xi) = \beta_{red}\left(\frac{\xi - \xi_O}{\xi_R - \xi_O}\right) \tag{87}$$

$$f_2(q_R,\xi) = \beta_{ox}\left(\frac{\xi_R - \xi}{\xi_R - \xi_O}\right) \tag{88}$$

as sketched in Fig. 8, but we make this approximation in the general quantum-mechanical framework of CIET theory, eqn (47) and (48). We assume asymmetric IT and symmetric IT with small but finite λ, in the ICET regime, eqn (83), for general situations as sketched in Fig. 7. Note that β_{red} and β_{ox} have units of energy, since we have rescaled the IT reaction coordinate ξ by the total displacement, $(\xi_R - \xi_O)$, from the oxidized state to the reduced state.

By minimizing the free energy barrier, we find that the transition state occurs at the following coordinates,

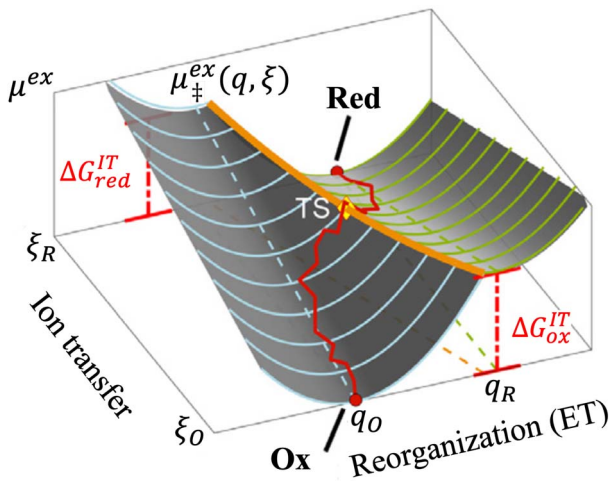

Fig. 8 Free energy landscape of IT-limited CIET, which we refer to as "ion-coupled electron transfer" (ICET), in the linear approximation of the ion-transfer coordinate ξ dependence of free energy of the diabatic reduced and oxidized states, eqn (87) and (88), respectively. For nonadiabatic ET, this approximation enables a quantum mechanical derivation of the Butler–Volmer equation, eqn (1), with the charge transfer coefficient (or symmetry factor), α, given by eqn (91) and the exchange current I_0 given by eqn (101) and (102). The quantum BV equation based on nonadiabatic CIET theory is valid for IT rate limitation, eqn (83), where the IT free energies $\beta_{red/ox}$ are much larger than the reorganization energy λ, thermal energy k_BT, formal overpotential $e|\eta_f|$, and electronic coupling $|H_{DA}|$. [Adapted from Fig. 5a of Fraggedakis *et al.* (2021).[103]]

$$q_{\ddagger} = \alpha_{\mathrm{IT}} q_{\mathrm{R}} + (1 - \alpha_{\mathrm{IT}}) q_{\mathrm{O}} \tag{89}$$

$$\xi_{\ddagger} = \alpha_{\mathrm{IT}} \xi_{\mathrm{O}} + (1 - \alpha_{\mathrm{IT}}) \xi_{\mathrm{R}} + \frac{(\lambda(1 - 2\alpha_{\mathrm{IT}}) + \Delta G^{\mathrm{ex}})(\xi_{\mathrm{R}} - \xi_{\mathrm{O}})}{(\beta_{\mathrm{red}} + \beta_{\mathrm{ox}})} \tag{90}$$

where the charge transfer coefficient (or symmetry factor) for IT takes the Gurney–Butler form,[7,18,42]

$$\alpha_{\mathrm{IT}} = \frac{\beta_{\mathrm{red}}}{\beta_{\mathrm{red}} + \beta_{\mathrm{ox}}}. \tag{91}$$

Using eqn (33), the free energy barriers for ICET can then be expressed in terms of the formal overpotential, η_{f}, and the electron energy relative to the Fermi level, $\varepsilon - \varepsilon_{\mathrm{F}}$:

$$\Delta G_{\ddagger}^{\mathrm{red}} = \alpha_{\mathrm{IT}} \Delta G^{\mathrm{ex}} + \Delta G_{\ddagger}^{\mathrm{ICET}} \tag{92}$$

$$\Delta G_{\ddagger}^{\mathrm{ox}} = -(1 - \alpha^{\mathrm{IT}}) \Delta G^{\mathrm{ex}} + \Delta G_{\ddagger}^{\mathrm{ICET}} \tag{93}$$

as well an overall activation energy for ICET controlling the reaction rate prefactor,

$$\Delta G_{\ddagger}^{\mathrm{ICET}} = \Delta G_{\ddagger}^{\mathrm{ET}} + \Delta G_{\ddagger}^{\mathrm{IT}} \tag{94}$$

which is the sum of a contribution from ET

$$\Delta G_{\ddagger}^{\mathrm{ET}} = \alpha_{\mathrm{IT}}(1 - \alpha_{\mathrm{IT}})\lambda = \frac{\beta_{\mathrm{red}} \beta_{\mathrm{ox}} \lambda}{(\beta_{\mathrm{red}} + \beta_{\mathrm{ox}})^2} \tag{95}$$

and another from IT

$$\Delta G_{\ddagger}^{\mathrm{IT}} = \alpha_{\mathrm{IT}}(1 - \alpha_{\mathrm{IT}})(\beta_{\mathrm{red}} + \beta_{\mathrm{ox}}) = \frac{\beta_{\mathrm{red}} \beta_{\mathrm{ox}}}{\beta_{\mathrm{red}} + \beta_{\mathrm{ox}}}. \tag{96}$$

The ET part of the ICET activation energy, eqn (95), is an asymmetric generalization of the Marcus barrier for symmetric ET, $\Delta G_{\ddagger}^{\mathrm{ET}} = \lambda/4$ for $\alpha_{\mathrm{IT}} = 1/2$, which also arises in our result for the ECIT barrier above in eqn (72). The IT part of the ICET activation energy, eqn (96), is likewise an asymmetric generalization of the activation energy for symmetric ECIT, eqn (62), since we have

$$\Delta G_{\ddagger}^{\mathrm{IT}} = (1 - \alpha_{\mathrm{IT}}) f_1(q_{\mathrm{O}}, \xi) + \alpha_{\mathrm{IT}} f_2(q_{\mathrm{R}}, \xi) \tag{97}$$

which does not depend on ξ in the linear approximation. This expression also matches the expected IT barrier for asymmetric ET-limited CIET, eqn (79), if we set $\alpha_{\mathrm{ET}} = \alpha_{\mathrm{IT}} = \alpha$, which supports the physical picture that IT is the dominant source of asymmetry in CIET.

Substituting into eqn (45) and (46) and using eqn (33) and (14), we can derive rate expressions for ICET,

$$\tilde{k}_{\mathrm{red}} = \left(\frac{\tilde{\kappa}_{\mathrm{e}}}{\gamma_{\ddagger}^{\mathrm{IT}}} \mathrm{e}^{-\tilde{\Delta} G_{\ddagger}^{\mathrm{ICET}}} \right) \mathrm{e}^{-\alpha e \eta_{\mathrm{f}} / k_{\mathrm{B}} T} \int_{-\infty}^{\infty} \mathrm{e}^{\alpha(\varepsilon - \varepsilon_{\mathrm{F}})/k_{\mathrm{B}} T} \tilde{n}_{\mathrm{e}}(\varepsilon) \rho_{\mathrm{e}}(\varepsilon) \mathrm{d}\varepsilon \quad (\mathrm{ICET}) \tag{98}$$

$$\tilde{k}_{\mathrm{ox}} = \left(\frac{\tilde{\kappa}_{\mathrm{e}}}{\gamma_{\ddagger}^{\mathrm{IT}}} \mathrm{e}^{-\tilde{\Delta} G_{\ddagger}^{\mathrm{ICET}}} \right) \mathrm{e}^{(1-\alpha) e \eta_{\mathrm{f}} / k_{\mathrm{B}} T} \int_{-\infty}^{\infty} \mathrm{e}^{-(1-\alpha)(\varepsilon - \varepsilon_{\mathrm{F}})/k_{B} T} \tilde{n}_{\mathrm{h}}(\varepsilon) \rho_{\mathrm{e}}(\varepsilon) \mathrm{d}\varepsilon \quad (\mathrm{ICET}) \tag{99}$$

where $\Delta\tilde{G}_{\ddagger}^{\mathrm{ICET}} = \Delta G_{\ddagger}^{\mathrm{ICET}}/k_{\mathrm{B}}T$. By converting from formal to total overpotential using eqn (9), we finally arrive at the BV equation (for one electron transfer),

$$\tilde{I}_{\mathrm{ICET}} = \tilde{I}_0^{\mathrm{ICET}}(\mathrm{e}^{-\alpha\tilde{\eta}} - \mathrm{e}^{(1-\alpha)\tilde{\eta}}) \tag{100}$$

with all parameters determined by the quantum theory of ICET. The charge transfer coefficient, $\alpha = \alpha_{\mathrm{IT}}$, is given by eqn (91), as predicted by Gurney–Butler theory,[7,18,42] but CIET theory also provides a quantum-mechanical formula for the BV exchange current for ICET, given by

$$\tilde{I}_0^{\mathrm{ICET}} = \tilde{\kappa}_{\mathrm{e}}\tilde{N}_{\mathrm{e}}(\alpha)\mathrm{e}^{-\Delta\tilde{G}_{\ddagger}^{\mathrm{ICET}}}\left(\frac{\tilde{c}_{\mathrm{O}}{}^{1-\alpha}\tilde{c}_{\mathrm{R}}{}^{\alpha}}{\gamma_{\ddagger}^{\mathrm{IT}}}\right) \tag{101}$$

where we define a dimensionless prefactor

$$\tilde{N}_{\mathrm{e}}(\alpha) = \int_{-\infty}^{\infty}\frac{\mathrm{e}^{\alpha(\varepsilon-\varepsilon_{\mathrm{F}})/k_{\mathrm{B}}T}}{1+\mathrm{e}^{(\varepsilon-\varepsilon_{\mathrm{F}})/k_{\mathrm{B}}T}}\rho_{\mathrm{e}}(\varepsilon)\mathrm{d}\varepsilon \tag{102}$$

which can be interpreted as the relative number of electronic states participating in ET as a function of α, the charge transfer coefficient for IT.

The quantum-mechanical BV exchange current density predicted by ICET theory, eqn (101) and (102), differs from that of phenomenological IT theory, eqn (4), in several fundamental ways. First, the activities a_{O} and a_{R} have been replaced by concentrations, $\tilde{c}_{\mathrm{O}}$ and $\tilde{c}_{\mathrm{R}}$, respectively. Second, the empirical lumped prefactor, $nek_0^{\mathrm{BV}}a_{\mathrm{e}}{}^{n(1-\alpha)}$, has been replaced by the product of the electron transmission coefficient $\tilde{\kappa}_{\mathrm{e}}$, the effective number of participating electronic states $\tilde{N}_{\mathrm{e}}(\alpha)$, and an Arrhenius prefactor, where the activation energy, $\Delta G_{\ddagger}^{\mathrm{ICET}}$, is expressed in terms of both the ET reorganization energy and the mean IT barrier.

The factor $N_{\mathrm{e}}(\alpha)$ rescales the BV reaction rate according to the number of accessible electronic states near the Fermi level in the band structure of the electrode, $\rho_{\mathrm{e}}(\varepsilon)$. It is also a sensitive function of the charge-transfer coefficient, α, because asymmetry in the IT energy landscape increases the range of electron and hole energies that can contribute to the rate for a given formal overpotential. In the case of a metallic electrode with $\rho_{\mathrm{e}} =$ constant, this integral can be evaluated by residue calculus,

$$\tilde{N}_{\mathrm{e}}(\alpha) = \tilde{\rho}_{\mathrm{e}}\int_{-\infty}^{\infty}\frac{\mathrm{e}^{\alpha\tilde{\varepsilon}}}{1+\mathrm{e}^{\tilde{\varepsilon}}}\mathrm{d}\tilde{\varepsilon} = \frac{\pi\tilde{\rho}_{\mathrm{e}}}{\sin(\pi\alpha)} \quad (\text{metal}) \tag{103}$$

to complete a simple analytical formula for the reaction rate. For symmetric IT, $\alpha = 1/2$, a minimum of $\tilde{N}_{\mathrm{e}} = \pi\tilde{\rho}_{\mathrm{e}}$ is attained, while $\tilde{N}_{\mathrm{e}} \to \infty$ for highly asymmetric IT, $\alpha \to 0$ or $\alpha \to 1$, as the number of electrons diverges due to the nearly flat IT energy landscape of either the reduced or the oxidized state. It is important to recognize that $\alpha \to 0, 1$ is a pathological limit of the ICET model using the Gurney–Butler linear approximation of the IT free energy landscapes, since the transition state $\xi_{\ddagger}$ for many electron levels will lie far outside the physically meaningful range, $\xi_{\mathrm{O}} \leq \xi \leq \xi_{\mathrm{R}}$.

CIET theory thus provides a rigorous, quantum-mechanical derivation of Butler–Volmer kinetics, including Tafel's limiting law, which clarifies its range of applicability and underlying physics (apparently for the first time). We see that the BV equation is valid for IT-limited CIET (or ICET) satisfying eqn (83), as long as the overpotential is not so large that Tafel's law breaks down. For a metal

electrode, the quantum-mechanical ICET exchange current has the following dimensional form:

$$I_0^{\mathrm{ICET}} = I_0^* \mathrm{e}^{-\Delta G_{\ddagger}^{\mathrm{ICET}}/k_{\mathrm{B}}T} \left(\frac{\tilde{c}_{\mathrm{O}}{}^{1-\alpha} \tilde{c}_{\mathrm{R}}{}^{\alpha}}{\gamma_{\ddagger}^{\mathrm{IT}}} \right) \tag{104}$$

where

$$\Delta G_{\ddagger}^{\mathrm{ICET}} = \alpha(1-\alpha)(\lambda + \beta_{\mathrm{red}} + \beta_{\mathrm{ox}}) \tag{105}$$

and

$$I_0^* = e\nu_{\mathrm{s}} \frac{A}{A_{\mathrm{s}}} \tilde{\kappa}_{\mathrm{e}} \tilde{N}_{\mathrm{e}}(\alpha) = \frac{e\Delta_{\mathrm{e}}}{h} \frac{A}{A_{\mathrm{s}}} \frac{1}{\sin(\pi\alpha)} \sqrt{\frac{\pi k_{\mathrm{B}} T}{\lambda}} \tag{106}$$

The importance of ET in quantum Butler–Volmer kinetics of ICET is underscored by the presence of the dimensionless Marcus reorganization energy, λ, in both the exchange current prefactor, I_0^*, and the activation barrier, $\Delta G_{\ddagger}^{\mathrm{ICET}}$.

6 Barrierless ECIT at the end of Tafel's law

"In spite of almost a century of confirming data, there is still a frontier in the study of Tafel's law. Is there an overpotential at which it will break down?" (*ibid.*, p. 1511).[7]

CIET theory is finally able to answer to this question. As shown in Fig. 8, the phenomenological derivation of the BV equation clearly breaks down when the formal overpotential exceeds the chemical barriers for IT. In that case, the transition state can no longer be identified without considering coupled Marcus kinetics of ET. The general definition of these barriers is given in terms of the diabatic free energy surfaces by

$$\begin{aligned} \beta_{\mathrm{red}} &= \max_{\xi_{\mathrm{O}} \le \xi \le \xi_{\mathrm{R}}} \{ f_1(q_{\mathrm{O}}, \xi) - f_2(q_{\mathrm{R}}, \xi) \} \\ \beta_{\mathrm{ox}} &= \max_{\xi_{\mathrm{O}} \le \xi \le \xi_{\mathrm{R}}} \{ f_2(q_{\mathrm{R}}, \xi) - f_1(q_{\mathrm{O}}, \xi) \} \end{aligned} \tag{107}$$

as shown in Fig. 7. If the formal overpotential further exceeds the following bounds set by the reorganization energy,

$$\begin{aligned} \Delta G^{\mathrm{ex}} &< -(\lambda + \beta_{\mathrm{ox}}) \\ \Delta G^{\mathrm{ex}} &> \lambda + \beta_{\mathrm{red}} \end{aligned} \qquad \text{(Inverted ECIT)} \tag{108}$$

then barrierless transitions become possible, which will dominate the current as usual, according to Marcus theory for metal electrodes.[25,51] CIET theory thus predicts a universal transition from either Marcus kinetics of Normal ECIT or Butler–Volmer kinetics of ICET to a new regime of "Inverted ECIT" at large overpotentials, where Tafel's law breaks down. In the case of ICET at a metal electrode, a constant reaction-limited current is attained, dominated by barrierless transitions, which are always possible at large overpotentials for some electrons deep within the Fermi sea. The scale of this transition region is set by λ for non-adiabatic CIET, but below we argue that the basic concept of a reaction-limited current beyond Tafel's law should still hold for adiabatic CIET with the scale set instead by Δ_{e}.

The basic physics of Inverted ECIT are sketched in Fig. 7 for the case of a transition from ICET at low overpotentials to Inverted ECIT at large overpotentials. When the free energy of reaction leaves the ICET range, $-\beta_{\mathrm{ox}} < \Delta G^{\mathrm{ex}} < \beta_{\mathrm{red}}$, the IT coordinate of the lowest-energy transition state becomes pinned at a value that

attains one of the bounds in eqn (107). If the diabatic curves are monotonic across the IT range, $\xi_O < \xi < \xi_R$, then the IT coordinate of the Inverted ECIT transition state is pinned at its equilibrium value (in the absence of any overpotential):

$$\xi_{\ddagger} \sim \begin{cases} \xi_O & \text{for } \Delta G^{ex} < -\beta_{ox} \\ \xi_R & \text{for } \Delta G^{ex} > \beta_{red} \end{cases} \tag{109}$$

as the ions await ET to trigger the ECIT reaction. For sufficiently large excess free energies of reaction satisfying, eqn (108), the diabatic IT curves, $f_1(q_O,\xi)$ and $f_2(q_R,\xi)$, no longer intersect, as shown in Fig. 7(c), and the transition state arises in the Marcus inverted region for ET, shown in Fig. 7(f).

Following our derivation of ECIT kinetics above, the corresponding activation barriers take the form,

$$\Delta G_{\ddagger}^{red} \approx \frac{(\lambda + \beta_{ox} + \Delta G^{ex})^2}{4\lambda} \quad \text{for } \Delta G^{ex} < -\beta_{ox} \tag{110}$$

$$\Delta G_{\ddagger}^{ox} \approx \frac{(\lambda + \beta_{red} - \Delta G^{ex})^2}{4\lambda} \quad \text{for } \Delta G^{ex} > \beta_{red} \tag{111}$$

Compared to the original Marcus theory for ECIT, eqn (59), the excess free energy of reaction, ΔG^{ex}, is now shifted by a certain IT free energy, β_{red} or β_{ox}, generally given by eqn (107). Although it may seem counter-intuitive, the reduction (or oxidation) rate for large negative (or positive) overpotentials is controlled by the opposite IT free energy for oxidation (or reduction), respectively, which sets the other side of the ECIT transition state, following ET and prior to IT.

For a metallic electrode (ρ_e = constant), the asymptotic activation barriers in eqn (110) and (112) imply that Tafel's law smoothly transitions to a reaction-limited current according to shifted Marcus ECIT curves, which are generally different for reduction

$$\tilde{I} \sim \tilde{k}_0 \tilde{c}_O \tilde{k}_{red}^{MHC}(\tilde{\lambda}, \tilde{\eta}_f + \tilde{\beta}_{ox}) \text{ for } \tilde{\eta}_f < -\tilde{\beta}_{ox} \tag{112}$$

and for oxidation

$$\tilde{I} \sim \tilde{k}_0 \tilde{c}_R \tilde{k}_{ox}^{MHC}(\tilde{\lambda}, \tilde{\eta}_f - \tilde{\beta}_{red}) \text{ for } \tilde{\eta}_f > \tilde{\beta}_{red} \tag{113}$$

based on different shifts of the MHC formula, eqn (70). Since $\tilde{k}_{red/ox}^{MHC} \to 1$ as $|\eta_f| \to \infty$, CIET theory thus predicts a universal limited reaction rate for metallic electrodes corresponding to barrierless ECIT,

$$\lim_{\tilde{\eta}_f \to \pm\infty} \tilde{I} = \tilde{I}_{lim}^{CIET} \tilde{c}_{R/O} \quad \text{(metal)} \tag{114}$$

where the dimensionless limiting current in the standard state, ($\tilde{c}_{R/O} = 1$), is given by $\tilde{I}_{lim}^{CIET} = \tilde{k}_0$, or, with units restored,

$$I_{lim}^{CIET} = \frac{eH_{DA}{}^2\rho_e}{\hbar\gamma_{\ddagger}^{IT}}\frac{A}{A_s} = \frac{e\kappa_T}{2\pi\gamma_{\ddagger}^{IT}}\frac{A}{A_s} = \frac{2\Delta_e}{h}\frac{e}{\gamma_{\ddagger}^{IT}}\frac{A}{A_s} \tag{115}$$

An important prediction of CIET theory for metal electrodes is that the universal limiting current is fully quantum mechanical with vanishing activation energy, *i.e.* no Arrhenius dependence on temperature. As anticipated above, the universal

CIET limiting current differs from the extrapolated limiting current of Normal ECIT, eqn (74), by the absence of the IT activation energy barrier, $\Delta G_{\ddagger}^{\mathrm{IT}} \to 0$, which has been overcome by the applied overpotential. Instead, the CIET limiting current is set by the quantum tunneling current, $e\kappa_{\mathrm{T}}$, for barrierless transitions between the donor and acceptor states and scales with the number of reacting surface sites A/A_{s} and the inverse activity coefficient of the IT transition state, $(\gamma_{\ddagger}^{\mathrm{IT}})^{-1}$, which is proportional to its excluded volume.

We expect that it would be difficult to unambiguously observe the CIET reaction-limited current for a given faradaic reaction experimentally. At such large overpotentials, exceeding all IT and ET barriers for the desired reaction, various side reactions would likely also be triggered, *e.g.* contributing to rapid growth of solid-electrolyte interphase (SEI) or bubble generation on the metal surface. Transport limitation leading to concentration polarization and ohmic drops from series resistances are also difficult to avoid, whenever large faradaic currents are achieved. The key to testing this prediction of CIET theory thus would be to find ways to slow down both IT and ET, for example with electrode compositions that suppress IT by enhancing ion crowding, $\gamma_{\ddagger}^{\mathrm{IT}} \gg 1$, and resistive electrode coatings to limit ET.

7 Uniformly valid approximation for CIET kinetics

In the preceding three sections, we have derived general limiting expressions for the faradaic current by CIET, regardless of the details of the diabatic free energy landscape, in three asymptotic limits:

(1) **Normal Marcus kinetics of ECIT** for $\lambda \gg \beta_{\mathrm{red/ox}}, e|\eta_{\mathrm{f}}|, k_{\mathrm{B}}T, \Delta_{\mathrm{e}}$ with a new IT-dependent prefactor,

(2) **Butler–Volmer kinetics of ICET** for $\beta_{\mathrm{red/ox}} \gg \lambda, e|\eta_{\mathrm{f}}|, k_{\mathrm{B}}T, \Delta_{\mathrm{e}}$ with a new quantum-mechanical formula for the exchange current, and

(3) **Inverted Marcus kinetics of ECIT** for $e|\eta_{\mathrm{f}}| > \beta_{\mathrm{red/ox}} + \lambda$ in a new "post-Tafel" regime, shifted by the red/ox IT energies.

Our CIET theoretical framework thus unifies and justifies the famous limits of BV kinetics for IT and Marcus kinetics for nonadiabatic ET. More importantly, it can also provide uniformly valid rate expressions that interpolate between these limits, for any specific model of the diabatic free-energy landscapes, which leads to a rich set of new kinetic models for CIET. For accurate predictions, the diabatic states can be modeled by CDFT or other *ab initio* quantum calculations, but it can be even more useful (at least for experimentalists and engineers) to develop simple, uniformly valid analytical approximations for the CIET reaction rates by asymptotic matching of the results above. The resulting alternatives to (and extensions of) the BV equation can then be fitted to experiments to infer microscopic parameters and/or used in engineering simulations of electrochemical systems.

Asymptotic matching requires finding mathematical expressions that uphold known asymptotic limits and interpolate smoothly between them, while balancing accuracy (to be checked against the full model and/or experimental data) and elegance (analytical simplicity for modeling and simulation). Uniformly valid asymptotic approximations of pure ET kinetics are already available in both symmetric (MHC)[61] and asymmetric (AMH)[61] forms and were used above to model the corresponding ECIT limits of CIET kinetics. It is more challenging to develop such approximations for the general CIET theory, because the free energy landscape is two-dimensional and must be described with sufficiently simple

approximations (*e.g.* low-order polynomials) to allow evaluation of the Fermi integrals. In order to do so and illustrate the overall form of a complete CIET theory, we shall make somewhat more restrictive assumptions, leaving open the possibility of deriving more accurate, general approximations in the future.

We consider the simplest possible approximation of the free energy landscape, which imposes strict constraints on the IT coordinate, $\xi_O \leq \xi \leq \xi_R$, in the model of ICET above, motivated by the transition to ECIT in eqn (109). We postulate that the diabatic free-energy surfaces are parabolic in the ET reorganization coordinate q and linear in the IT coordinate ξ,

$$f_1(q_O, \xi) = \beta_{red}\left(\frac{\xi - \xi_O}{\xi_R - \xi_O}\right), \quad \text{for } \xi_O \leq \xi \leq \xi_R \tag{116}$$

$$f_2(q_R, \xi) = \beta_{ox}\left(\frac{\xi_R - \xi}{\xi_R - \xi_O}\right), \quad \text{for } \xi_O \leq \xi \leq \xi_R \tag{117}$$

$$f_i(q,\xi) = \infty, \text{ for } \xi < \xi_R,\ \xi > \xi_O,\ i = 1, 2 \tag{118}$$

while diverging outside the allowed range of IT coordinates. These truncated linear approximations of the diabatic free energy surfaces allow us to derive uniformly valid asymptotic approximations of the CIET rates for both symmetric and asymmetric IT.

7.1 Symmetric nonadiabatic CIET

For symmetric IT, where $\beta_{red} = \beta_{ox} = \beta$, the free energy barriers in this model can be written compactly as

$$\Delta G_{\ddagger}^{red/ox} = \begin{cases} \frac{1}{4\lambda}(\lambda + \beta \pm \Delta G^{ex})^2 & \text{for } \mp\Delta G^{ex} > \beta \\ \frac{1}{2}\left(\frac{\lambda}{2} + \beta \pm \Delta G^{ex}\right) & \text{for } |\Delta G^{ex}| < \beta \\ \frac{1}{4\lambda}(\lambda + \beta \pm \Delta G^{ex})^2 \pm \Delta G^{ex} & \text{for } \pm\Delta G^{ex} > \beta \end{cases} \tag{119}$$

which satisfies the De Donder relation, eqn (27), in the form,

$$\Delta G_{\ddagger}^{red} - \Delta G_{\ddagger}^{ox} = \Delta G^{ex}. \tag{120}$$

These approximate barriers can be inserted into the Fermi integrals to obtain the CIET rates for a general electrode,

$$\tilde{k}_{red/ox} = \frac{\tilde{\kappa}_e}{\gamma_{\ddagger}^{IT}} \int_{-\infty}^{\infty} \frac{e^{-\Delta \tilde{G}_{\ddagger}^{red/ox}} \tilde{\rho}_e(\tilde{\varepsilon}) d\tilde{\varepsilon}}{1 + e^{\pm\tilde{\varepsilon}}} \tag{121}$$

where $\tilde{\varepsilon} = (\varepsilon - \varepsilon_F)/k_B T$. These uniformly valid approximations are nearly exact for the truncated linear models in eqn (116)–(118). They also reproduce the barriers derived above in the three asymptotic regimes of the general theory, while interpolating smoothly between them with continuously differentiable functions. After integration over the electron energies, the rate formulae in eqn (139) thus possess two continuous derivatives.

In order to obtain a simple formula, we consider the typical case of a metal electrode, $\tilde{\rho}_e$ = constant, and replace the Fermi–Dirac functions with Heaviside step functions,[25,60]

$$\frac{1}{1+e^{\pm\tilde{\varepsilon}}} \approx H(\mp\tilde{\varepsilon}) \tag{122}$$

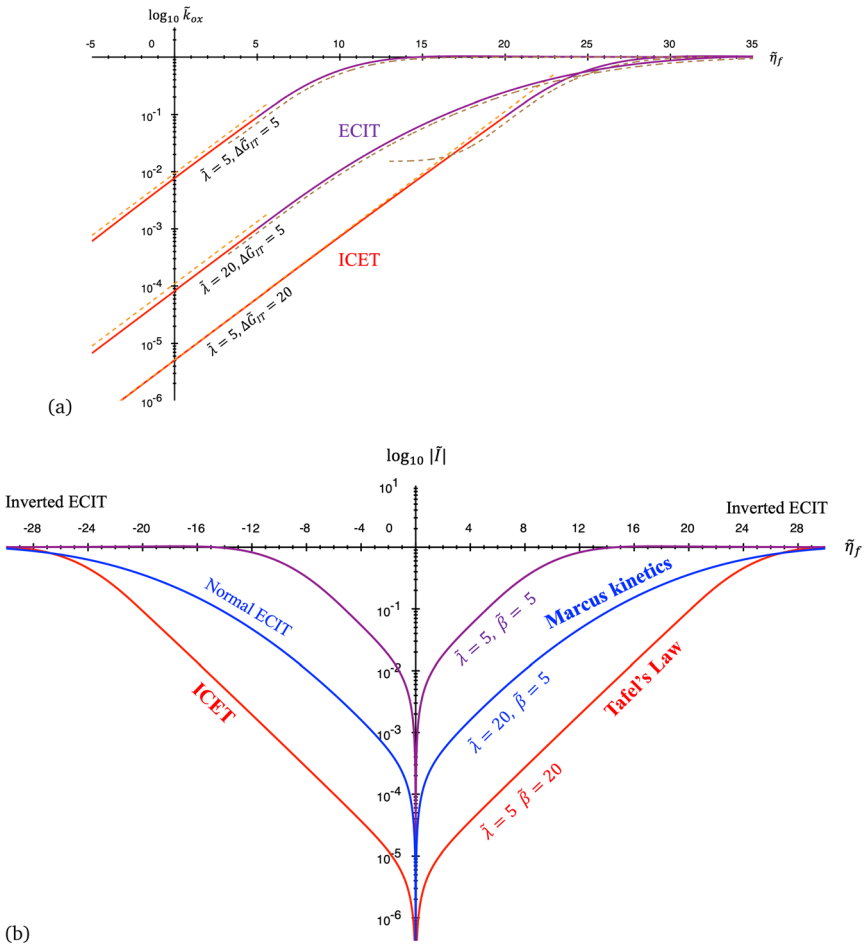

Fig. 9 Unification of Butler–Volmer and Marcus kinetics: uniformly valid approximation of symmetric nonadiabatic CIET kinetics at a metal electrode, eqn (123). (a) Linear–log plot of the dimensionless oxidation rate constant, $\tilde{k}_{ox}$, scaled to the universal limiting rate k_0 in the standard state ($\tilde{c}_O = \tilde{c}_R = 1$), *versus* dimensionless formal overpotential, $\tilde{\eta}_f$, scaled to k_BT/e, for three cases of reorganization energy, $\tilde{\lambda}$, and ion transfer free energy, $\tilde{\beta}$ (scaled to k_BT). Dashed curves show the asymptotic approximations for ICET for $\tilde{\eta}_f < \tilde{\beta}$ and for ECIT for $\tilde{\eta}_f > \tilde{\beta}$, which have been matched to obtain the uniformly valid approximations (solid curves). (b) Tafel plot of the absolute value of the CIET current, $|\tilde{I}|$, scaled to the limiting current, ek_0, *versus* dimensionless formal overpotential for the cases in (a), assuming standard conditions for the reactants, $\tilde{c}_O = \tilde{c}_R = 1$. For ICET over a wide range of formal overpotentials, $k_BT \ll e\eta_f \ll \beta$, the theory is able to exactly reproduce Tafel's law, eqn (2), and predict its breakdown, as explained in Fig. 7.

which is valid for low temperatures, $k_B T \ll \lambda, \beta$, as required for validity of transition state theory. We also neglect the high-energy Marcus tails for reverse bias ($\pm\Delta G^{ex} > \beta$) in eqn (119), which introduces only exponentially small errors, slightly violating the De Donder relation, eqn (120). This allows us to perform the integrals in eqn (139) to obtain closed-form uniformly valid approximations for the symmetric CIET rate constants (Fig. 9),

$$\frac{\tilde{k}^{\text{uni}}_{\text{red/ox}}}{\tilde{k}_0 M(\tilde{\eta}_f)} = \begin{cases} \text{Butler} - \text{Volmer ICET kinetics for } \mp\tilde{\eta}_f < \tilde{\beta}: \\ \dfrac{e^{-\tilde{\lambda}/4}}{\sqrt{\pi\tilde{\lambda}}} e^{-(\pm\tilde{\eta}_f+\tilde{\beta})/2} \\ \text{Marcus ECIT kinetics for } \mp\tilde{\eta}_f > \tilde{\beta}: \\ \dfrac{1}{2}\left[\text{erf}\left(\dfrac{\sqrt{\tilde{\lambda}}}{2}\right) - \text{erf}\left(\dfrac{\tilde{\lambda}+\tilde{\beta}\pm\tilde{\eta}_f}{2\sqrt{\tilde{\lambda}}}\right)\right] + \dfrac{e^{-\tilde{\lambda}/4}}{\sqrt{\pi\tilde{\lambda}}} \end{cases} \tag{123}$$

where we scale the rate constants to their universal limiting value k_0 in eqn (69) and introduce an asymptotic matching factor, $M(\tilde{\eta}_f)$, which interpolates between the exact prefactors for large and small overpotentials derived above. This factor is required for mathematical accuracy in the asymptotic limits, but could be set to $M = 1$ in most cases, given the crude physical accuracy of the truncated linear approximation of the diabatic free energy landscape, eqn (118).

If high mathematical accuracy is desired for this physical model, then the matching factor can be chosen to correct for small errors introduced in eqn (123) compared to the exact integral formula, eqn (139), resulting from the low-temperature approximation, eqn (122). At high formal overpotentials, $|\tilde{\eta}_f| \gg 1$, the approximation of eqn (123) reaches a limiting rate given by

$$\frac{1}{M_\infty} = \frac{1}{2}\left[\text{erf}\left(\frac{\sqrt{\tilde{\lambda}}}{2}\right) + 1\right] + \frac{e^{-\tilde{\lambda}/4}}{\sqrt{\pi\tilde{\lambda}}} \tag{124}$$

which slightly over-estimates the correct universal value, $\tilde{k}_{\text{red/ox}} \to \tilde{k}_0$, but rapidly converges in the relevant low-temperature limit, $\tilde{\lambda} \gg 1$. For example, $M_\infty^{-1} = 1.2$ for $\tilde{\lambda} = 1$, and $M_\infty^{-1} = 1.02$ for $\tilde{\lambda} = 4$. For small formal overpotentials, $|\tilde{\eta}_f| \ll 1$, we must set

$$M_0 = \frac{\pi}{2} \tag{125}$$

in order to recover the exact exchange current for ICET, eqn (101). The transition from this value to the limiting value should occur for $|\tilde{\eta}_f| > \tilde{\beta}$ over a range set by $\tilde{\lambda}$, so we could choose the matching function to be

$$M(\tilde{\eta}_f) = \frac{M_0 - M_\infty}{\left(1 + e^{-(\tilde{\eta}_f+\tilde{\beta})/\tilde{\lambda}}\right)\left(1 + e^{(\tilde{\eta}_f-\tilde{\beta})/\tilde{\lambda}}\right)} + M_\infty \tag{126}$$

where we control the transition with Fermi–Dirac functions (Fig. 10). The asymptotic matching prefactor factor, $M(\tilde{\eta}_f)$, introduces some curvature of the Tafel plot for ICET, even at low formal overpotentials, which physically corresponds to smoothing of the sharp minima in the truncated linear approximations of the diabatic free energy landscape.

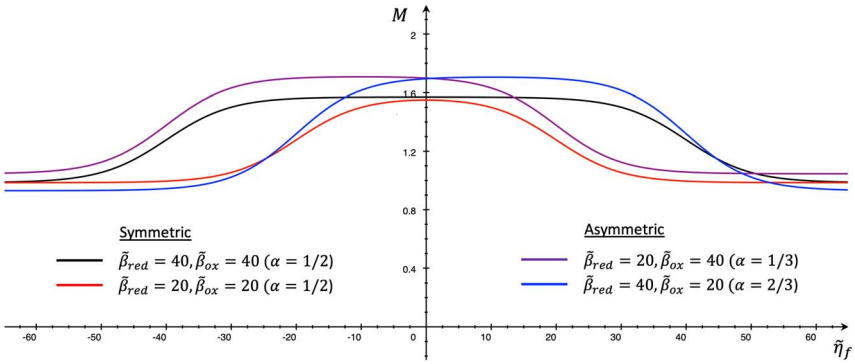

Fig. 10 Asymptotic matching function, $M(\tilde{\eta}_f)$, plotted for the ICET regime with parameters shown for symmetric cases, eqn (124)–(126), and asymmetric cases, eqn (130)–(132) with $\tilde{\lambda} = 5$.

As shown in Fig. 11, this formula smoothly interpolates between BV kinetics of ICET and Marcus kinetics of ECIT. The theory is thus able to predict Tafel's law from quantum electrochemistry. Unlike previous ET or IT theories, CIET theory predicts Tafel's law in the limit of IT rate limitation (ICET) across a wide range of formal overpotentials, $k_B T \ll |e\eta_f| \ll \beta$, while also predicting its failure by transition to ET limitation (Inverted ECIT) at large overpotentials, $|e\eta_f| \gg \beta$.

7.2 Asymmetric nonadiabatic CIET

For asymmetric IT, where $\beta_{red} \neq \beta_{ox}$ and thus $\alpha \neq 1/2$, we must find a simple approximation for the CIET barrier under the truncated linear approximations, eqn (116)–(118), which reproduces the BV equation and Tafel's law in the ICET regime of moderate overpotentials, while smoothly transitioning to the exact limiting current for barrierless ECIT at large overpotentials. As a generalization of the symmetric case, eqn (119), we propose the following approximations:

$$\Delta G_{\ddagger}^{red} = \begin{cases} \dfrac{\alpha}{4(1-\alpha)\lambda}(2(1-\alpha)\lambda + \beta_{ox} + \Delta G^{ex})^2 & \text{for } \Delta G^{ex} < -\beta_{ox} \\ \alpha((1-\alpha)\lambda + \beta_{ox} + \Delta G^{ex}) & \text{for } -\beta_{ox} < \Delta G^{ex} < \beta_{red} \\ \dfrac{1-\alpha}{4\alpha\lambda}(2\alpha\lambda + \beta_{red} - \Delta G^{ex})^2 + \Delta G^{ex} & \text{for } \Delta G^{ex} > \beta_{red} \end{cases}$$

$$\Delta G_{\ddagger}^{ox} = \begin{cases} \dfrac{\alpha}{4(1-\alpha)\lambda}(2(1-\alpha)\lambda + \beta_{ox} - \Delta G^{ex})^2 - \Delta G^{ex} & \text{for } \Delta G^{ex} < -\beta_{ox} \\ (1-\alpha)(\alpha\lambda + \beta_{red} - \Delta G^{ex}) & \text{for } -\beta_{ox} < \Delta G^{ex} < \beta_{red} \\ \dfrac{1-\alpha}{4\alpha\lambda}(2\alpha\lambda + \beta_{red} - \Delta G^{ex})^2 & \text{for } \Delta G^{ex} > \beta_{red} \end{cases} \tag{127}$$

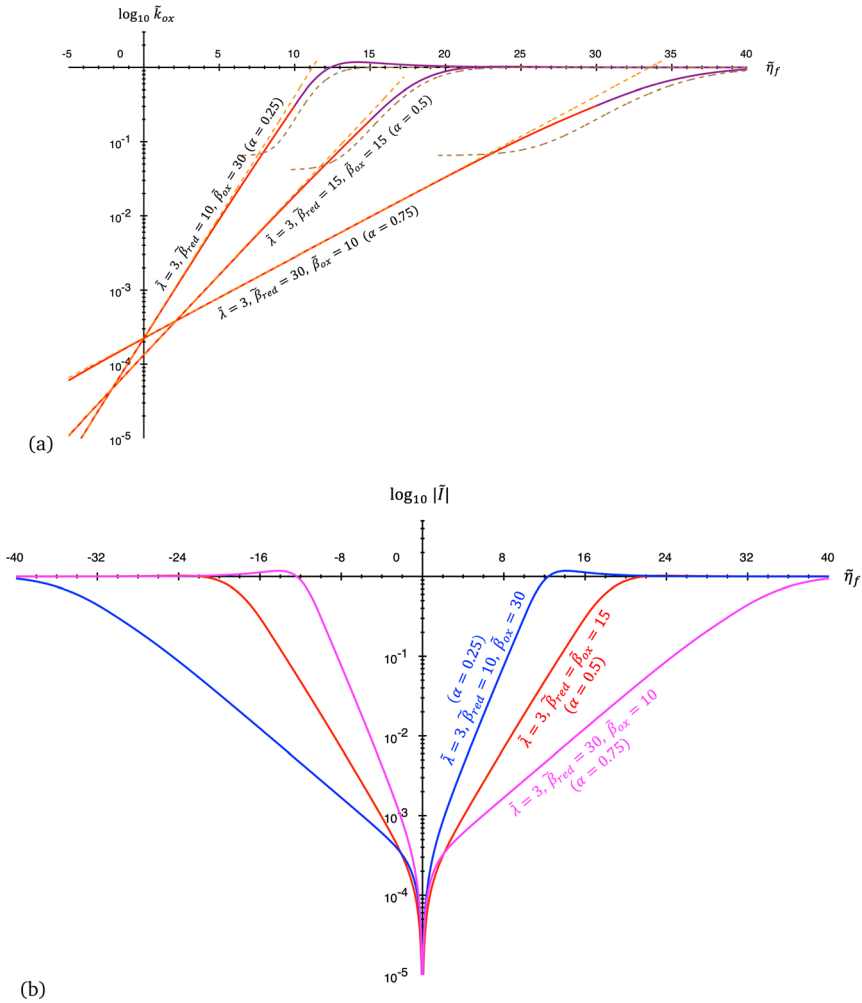

Fig. 11 Tafel's law and its breakdown at large overpotentials: uniformly valid approximation of asymmetric nonadiabatic ICET kinetics at a metal electrode, eqn (128) and (129). (a) Linear–log plot of the dimensionless oxidation rate constant, $\tilde{k}_{ox}$, ($\tilde{c}_O = \tilde{c}_R = 1$), *versus* dimensionless formal overpotential, $\tilde{\eta}_f$, for three cases of $\tilde{\lambda}$, $\tilde{\beta}_{red}$ and $\tilde{\beta}_{ox}$. Dashed curves show the asymptotic approximations for ICET ($-\tilde{\beta}_{ox} < \tilde{\eta}_f < \tilde{\beta}_{red}$) and for ECIT ($\tilde{\eta}_f < -\tilde{\beta}_{ox}$, $\tilde{\eta}_f > \tilde{\beta}_{red}$), which have been matched to obtain the uniformly valid approximations (solid curves). (b) Tafel plot of the absolute value of the dimensionless CIET current, $|\tilde{I}|$, *versus* $\tilde{\eta}_f$ for the cases in (a), assuming $\tilde{c}_O = \tilde{c}_R = 1$.

where below we shall again neglect the high-energy Marcus tails for reverse bias ($\Delta G^{ex} > \beta_{red}$ for reduction and $\Delta G^{ex} < -\beta_{ox}$ for oxidation) with exponentially small errors, violating the De Donder relation, eqn (120). These approximations of the barriers are continuously differentiable, so the associated reaction rate constants will be continuously twice differentiable after performing the Fermi integrals. In order to achieve such smooth approximations, we have modified the curvature of the Marcus parabolae, by replacing λ with $\alpha\lambda/(1-\alpha)$, but this

only affects the transition from the exact quantum Tafel's law to the barrierless ECIT limiting current. Moreover, this approximation effectively blurs the distinction between asymmetric ET and IT at large overpotentials, where we set $\alpha \approx \alpha_{\mathrm{IT}} \approx \alpha_{\mathrm{ET}}$ for the general case of asymmetric CIET.

Again, we take the low temperature limit of the Fermi–Dirac distributions, eqn (122), and perform the rate integrals, eqn (139), now using the approximate barriers in eqn (127) to obtain closed-form uniformly valid approximations for the asymmetric CIET rate constants for reduction,

$$\frac{k_{\mathrm{red}}^{\mathrm{uni}}}{k_0 M(\tilde{\eta}_{\mathrm{f}})} = \begin{cases} \text{Butler} - \text{Volmer ICET kinetics for } \tilde{\eta}_{\mathrm{f}} > -\tilde{\beta}_{\mathrm{ox}}: \\ \dfrac{\mathrm{e}^{-\alpha\left((1-\alpha)\tilde{\lambda}+\tilde{\beta}_{\mathrm{ox}}\right)}}{\sqrt{4\alpha(1-\alpha)\pi\tilde{\lambda}}}\,\mathrm{e}^{-\alpha\tilde{\eta}_{\mathrm{f}}} \\ \text{Marcus ECIT kinetics for } \tilde{\eta}_{\mathrm{f}} < -\tilde{\beta}_{\mathrm{ox}}: \\ \dfrac{1}{2}\left[\mathrm{erf}\left(\sqrt{\alpha(1-\alpha)\tilde{\lambda}}\right) - \mathrm{erf}\left(\dfrac{2(1-\alpha)\tilde{\lambda}+\tilde{\beta}_{\mathrm{ox}}+\tilde{\eta}_{\mathrm{f}}}{2\sqrt{(1-\alpha)\tilde{\lambda}/\alpha}}\right)\right] \\ +\dfrac{\mathrm{e}^{-\alpha(1-\alpha)\tilde{\lambda}}}{\sqrt{4\alpha(1-\alpha)\pi\tilde{\lambda}}} \end{cases} \tag{128}$$

and for oxidation,

$$\frac{k_{\mathrm{ox}}^{\mathrm{uni}}}{k_0 M(\tilde{\eta}_{\mathrm{f}})} = \begin{cases} \text{Butler} - \text{Volmer ICET kinetics for } \tilde{\eta}_{\mathrm{f}} < \tilde{\beta}_{\mathrm{red}}: \\ \dfrac{\mathrm{e}^{-(1-\alpha)\left(\alpha\tilde{\lambda}+\tilde{\beta}_{\mathrm{red}}\right)}}{\sqrt{4\alpha(1-\alpha)\pi\tilde{\lambda}}}\,\mathrm{e}^{(1-\alpha)\tilde{\eta}_{\mathrm{f}}} \\ \text{Marcus ECIT kinetics for } \tilde{\eta}_{\mathrm{f}} > \tilde{\beta}_{\mathrm{red}}: \\ \dfrac{1}{2}\left[\mathrm{erf}\left(\sqrt{\alpha(1-\alpha)\tilde{\lambda}}\right) - \mathrm{erf}\left(\dfrac{2\alpha\tilde{\lambda}+\tilde{\beta}_{\mathrm{red}}-\tilde{\eta}_{\mathrm{f}}}{2\sqrt{\alpha\tilde{\lambda}/(1-\alpha)}}\right)\right] \\ +\dfrac{\mathrm{e}^{-\alpha(1-\alpha)\tilde{\lambda}}}{\sqrt{4\alpha(1-\alpha)\pi\tilde{\lambda}}} \end{cases} \tag{129}$$

where we have multiplied the oxidation rate by $\sqrt{(1-\alpha)/\alpha}$ and the reduction rate by $\sqrt{\alpha/(1-\alpha)}$ in order to approximate the correct limiting behavior at large overpotentials. In particular, the dimensionless rate constants now tend to a limiting value,

$$\frac{1}{M_\infty} = \frac{1}{2}\left[\mathrm{erf}\left(\sqrt{\alpha(1-\alpha)\tilde{\lambda}}\right)+1\right] + \frac{\mathrm{e}^{-\alpha(1-\alpha)\tilde{\lambda}}}{\sqrt{4\alpha(1-\alpha)\pi\tilde{\lambda}}} \tag{130}$$

which approximates the barrierless ECIT rate, $k_{\mathrm{red/ox}}^{\mathrm{uni}} \to k_0$, in the low temperature limit, $\tilde{\lambda} \gg 1$. In order to recover the exact exchange current for ICET, eqn (101), we must also set

$$\frac{e^{-(1-\alpha)\left(\alpha\tilde{\lambda}+\tilde{\beta}_{\mathrm{red}}\right)}}{\sqrt{4\alpha(1-\alpha)\pi\tilde{\lambda}}}\,e^{(1-\alpha)\tilde{\eta}_{\mathrm{f}}} \tag{131}$$

which reproduces $M_0(1/2) = \pi/2$ for the symmetric case. Since $\sin(\pi\alpha) \approx 4\alpha(1-\alpha)$ for $0 < \alpha < 1$, the matching factor can be approximated as $M_0(\alpha)/M_0(1/2) \approx 1/2\sqrt{\alpha(1-\alpha)}$, which diverges in the limits of fully asymmetric charge transfer, $\alpha \to 0, 1$, and thus should be included in the uniformly valid approximation. The transition to the limiting value should occur for $\tilde{\eta}_{\mathrm{f}} < -\tilde{\beta}_{\mathrm{ox}}$ for reduction and $\tilde{\eta}_{\mathrm{f}} > \tilde{\beta}_{\mathrm{red}}$ for oxidation over a range set by $\tilde{\lambda}$. Once again controlling these transitions with Fermi–Dirac functions, we choose

$$M(\tilde{\eta}_{\mathrm{f}}) = \frac{M_0 - M_\infty}{\left(1+e^{-\left(\tilde{\eta}_{\mathrm{f}}+\tilde{\beta}_{\mathrm{ox}}\right)/\tilde{\lambda}}\right)\left(1+e^{\left(\tilde{\eta}_{\mathrm{f}}-\tilde{\beta}_{\mathrm{red}}\right)/\tilde{\lambda}}\right)} + M_\infty \tag{132}$$

With these matching factors (Fig. 10) included, the uniformly valid approximations, eqn (128) and (129), reproduce the exact asymptotic rates for large and small formal overpotentials and maintain small mathematical errors for all parameter values. Physically, these corrected approximations predict small curvatures of the Tafel plot in the ICET regime associated with smoothing the unphysically sharp minima of the diabatic free energy landscapes in the truncated linear approximations.

8 Distributions of electron energies in CIET

8.1 Gaussian statistics for symmetric ECIT

Following Gerischer,[25,31,132] we can interpret the non-adiabatic Normal ECIT rate probabilistically,

$$\tilde{k}_{\mathrm{red/ox}} = \frac{{H_{\mathrm{DA}}}^2}{\hbar\nu_{\mathrm{s}}\gamma_{\dagger}^{\mathrm{IT}}}e^{-\Delta\tilde{G}_{\ddagger}^{\mathrm{IT}}}\int_{-\infty}^{\infty} P_{\mathrm{red/ox}}^{\mathrm{ET}}(\varepsilon)\tilde{n}_{\mathrm{e/h}}(\varepsilon)\rho_{\mathrm{e}}(\varepsilon)\mathrm{d}\varepsilon \qquad (\mathrm{ECIT}) \tag{133}$$

as an integral over the conditional probability of ET for each available electron or hole state in the electrode,

$$P_{\mathrm{red/ox}}^{\mathrm{ET}}(\varepsilon) = \frac{\exp\left(-\dfrac{\left(e\eta_{\mathrm{f}}+\varepsilon_{\mathrm{F}}-\varepsilon\pm\lambda\right)^2}{4\lambda k_{\mathrm{B}}T}\right)}{\sqrt{4\pi\lambda k_{\mathrm{B}}T}} \tag{134}$$

The same statistics, $P_{\mathrm{red/ox}}^{\mathrm{ET}}(\varepsilon)$, apply to the limit of Inverted ECIT, which corresponds to $\Delta\tilde{G}_{\ddagger}^{\mathrm{IT}} = 0$ in eqn (133). From this perspective, the probability of nonadiabatic ET from/to state ε during reduction/oxidation has a normal Gaussian distribution with mean and variance,

$$\langle\varepsilon\rangle = e\eta_{\mathrm{f}} + \varepsilon_{\mathrm{F}} \pm \lambda \tag{135}$$

$$\mathrm{Var}(\varepsilon) = 2\lambda k_{\mathrm{B}}T \tag{136}$$

respectively, as shown in Fig. 12(b).

The Gaussian statistics of symmetric ECIT can also be derived directly from quantum mechanical transitions of displaced harmonic oscillators (DHO),[133,134] which represent the quantum analog of classical transitions between the Marcus parabolae for the diabatic states for inner-sphere ET, where λ is a thermally

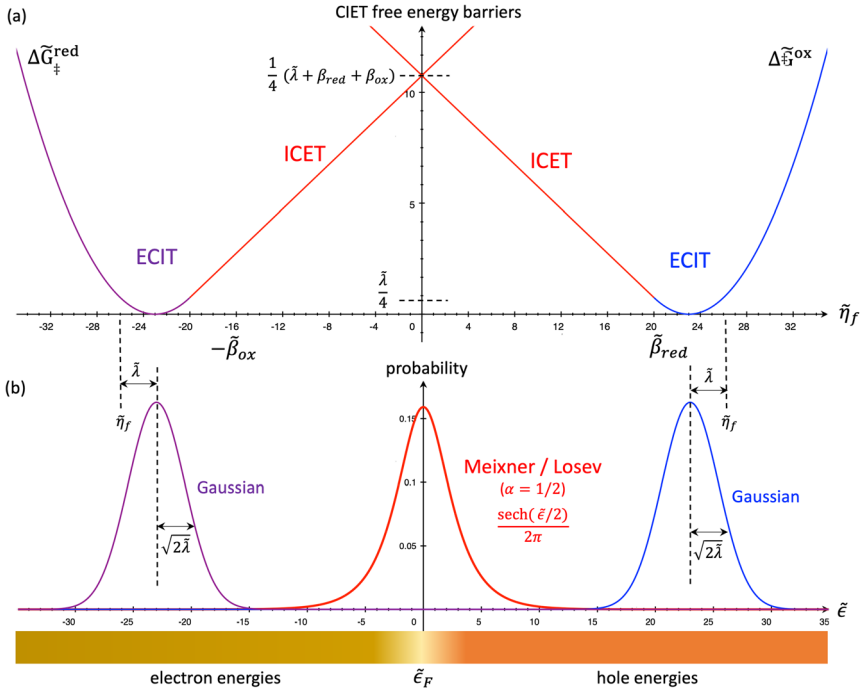

Fig. 12 Quantum statistics of transferring electron energies for symmetric ICET at a metal electrode. (a) Uniformly valid approximation of the CIET energy barriers for $\tilde{\beta}_{\mathrm{red}} = \tilde{\beta}_{\mathrm{ox}} = 20$ and $\tilde{\lambda} = 3$, and (b) corresponding electron energy distributions for $\tilde{\eta}_{\mathrm{f}} = -26, 0, 26$.

averaged spring constant for the vibrations. At finite temperature, the most probable electron transition occurs at the electron resonance of the Fermi level, shifted by the reorganization energy, as in eqn (135). It is important to stress, however, that Gerischer's interpretation with Gaussian statistics only holds for the symmetric Normal ECIT limit of the general CIET theory.

8.2 Modified Gaussian statistics for Asymmetric ECIT

In our general theory of CIET, the transition to ECIT at large overpotentials can lead to modified Gaussian statistics in the asymmetric case, $\alpha \neq 1/2$. In particular, our uniformly valid approximation of the asymmetric CIET barriers preserves the Gaussian shape of the distribution of transferring electron energies but predicts different means,

$$\langle \varepsilon \rangle = \begin{cases} e\eta_{\mathrm{f}} + \varepsilon_{\mathrm{F}} + \lambda(1-\alpha)/\alpha & \text{for } \eta_{\mathrm{f}} \ll -\beta_{\mathrm{ox}} \\ e\eta_{\mathrm{f}} + \varepsilon_{\mathrm{F}} - \lambda\alpha/(1-\alpha) & \text{for } \eta_{\mathrm{f}} \gg \beta_{\mathrm{red}} \end{cases} \tag{137}$$

and variances,

$$\mathrm{Var}(\varepsilon) = \begin{cases} 2\lambda k_{\mathrm{B}} T(1-\alpha)/\alpha & \text{for } \eta_{\mathrm{f}} \ll -\beta_{\mathrm{ox}} \\ 2\lambda k_{\mathrm{B}} T\alpha/(1-\alpha) & \text{for } \eta_{\mathrm{f}} \gg \beta_{\mathrm{red}} \end{cases} \tag{138}$$

for the reduction and oxidation reactions, respectively. Examples of these rescaled Gaussian distributions for ECIT are shown in Fig. 13(a) and compared with the

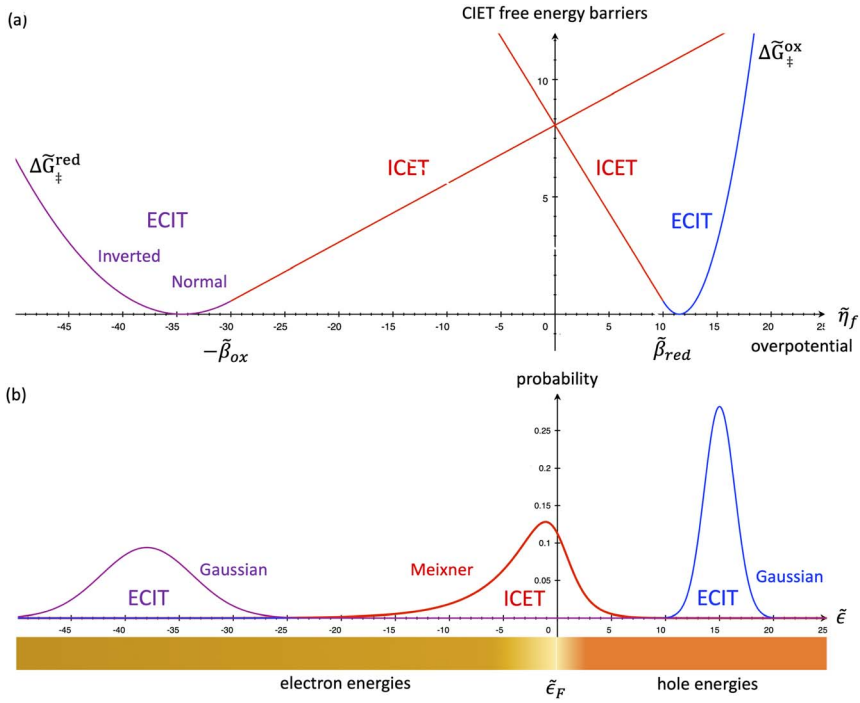

Fig. 13 Quantum statistics of transferring electron energies for asymmetric ICET at a metal electrode. (a) Uniformly valid approximation of the CIET free energy barriers for reduction and oxidation, eqn (127), for $\alpha = 0.25$, $\tilde{\beta}_{red} = 30$, $\tilde{\beta}_{ox} = 10$, $\tilde{\lambda} = 3$. Linear regions for ICET are shown in red, and quadratic regions for Normal and Inverted ECIT are shown in purple for reduction and blue for oxidation. (b) Probability distributions, $P_{red/ox}^{CIET}(\tilde{\varepsilon})$, for the dimensionless energy of the transferring electron or hole, $\tilde{\varepsilon} = (\varepsilon - \varepsilon_F)/k_BT$. Over the full range of formal overpotentials for ICET, $-\beta_{ox} < \eta_f < \beta_{red}$, the electrons or holes are sampled from a Meixner–Losev skewed hyperbolic secant distribution, eqn (141), which is peaked at the Fermi level with a fat tail in the direction of the flatter diabatic free energy landscape, *e.g.* for lower electron energies (or larger binding energies) if $\beta_{ox} > \beta_{red}$ or $\alpha < 1/2$ as shown. For large formal overpotentials in the Normal and Inverted regimes of ECIT, the electrons or holes are sampled from Gerischer's shifted Gaussian distributions, eqn (134), with rescaled parameters, shown for $\tilde{\eta}_f = -45, 15$.

CIET barriers. In this model, the reorganization energy under extreme overpotentials has been rescaled as $\lambda \to \lambda(1-\alpha)/\alpha$ for reduction and $\lambda \to \lambda\alpha/(1-\alpha)$ for oxidation, so that the local barriers for forward and backward ECIT smoothly transition from those of ICET and inherit the same asymmetry. This is a different way to model asymmetric ET compared to the AMH theory described above. Here, asymmetric solvent reorganization depends on over-potential, as a result of strong coupling with asymmetric IT.

8.3 General statistics of electron energies in CIET

Whenever IT is significantly coupled to ET, the quantum statistics of transferring electron energies are non-Gaussian. This can be seen by rewriting the CIET rate constants for a metal electrode, eqn (139), as

$$\tilde{k}_{\mathrm{red/ox}} = \frac{\tilde{\kappa}_{\mathrm{e}} Z_{\mathrm{red/ox}}}{\gamma_{\ddagger}^{\mathrm{IT}}} \int_{-\infty}^{\infty} P_{\mathrm{red/ox}}^{\mathrm{CIET}}(\tilde{\varepsilon}) \mathrm{d}\tilde{\varepsilon} \tag{139}$$

where we define the probability $P_{\mathrm{red/ox}}^{\mathrm{CIET}}(\tilde{\varepsilon})$ that an electron or hole with dimensionless energy $\tilde{\varepsilon} = (\varepsilon - \varepsilon_{\mathrm{F}})/k_{\mathrm{B}}T$ participates in the CIET reduction or oxidation reaction, respectively:

$$P_{\mathrm{red/ox}}^{\mathrm{CIET}} = \frac{1}{Z_{\mathrm{red/ox}}^{\mathrm{CIET}}} \frac{\mathrm{e}^{-\Delta \tilde{G}_{\ddagger}^{\mathrm{red/ox}}} \tilde{\rho}_{\mathrm{e/h}}(\tilde{\varepsilon})}{1 + \mathrm{e}^{\pm \tilde{\varepsilon}}} \tag{140}$$

which is normalized by $Z_{\mathrm{red/ox}}^{\mathrm{CIET}}$. For example, the uniformly valid approximations above correspond to different choices of the barriers, eqn (119) and (127), for symmetric or asymmetric IT, respectively, which smoothly transition between statistics of ICET and ECIT as $|\tilde{\eta}_{\mathrm{f}}|$ passes through $\tilde{\beta}_{\mathrm{red/ox}}$. It appears that the general CIET distributions have not been studied before in probability and statistics, and their mathematical properties await systematic characterization.

8.4 Meixner statistics of electron energies for ICET

In the symmetric ICET regime for a metal electrode, the conditional probability of ET is an exponential random variable, whose density multiplies the Fermi–Dirac distribution to obtain a Meixner distribution[135] of electron energies:

$$P_{\mathrm{red}}^{\mathrm{ICET}} = \frac{\sin(\pi\alpha)}{\pi} \frac{\mathrm{e}^{\alpha\tilde{\varepsilon}}}{1 + \mathrm{e}^{\tilde{\varepsilon}}} = P_{\mathrm{ox}}^{\mathrm{ICET}} = \frac{\sin(\pi\alpha)}{\pi} \frac{\mathrm{e}^{-(1-\alpha)\tilde{\varepsilon}}}{1 + \mathrm{e}^{-\tilde{\varepsilon}}} = \frac{\sin(\pi\alpha)}{\pi} \frac{1}{\mathrm{e}^{-\alpha\tilde{\varepsilon}} + \mathrm{e}^{(1-\alpha)\tilde{\varepsilon}}}. \tag{141}$$

The normalization factor is given by

$$Z_{\mathrm{red/ox}}^{\mathrm{ICET}} = \frac{\pi \mathrm{e}^{-\Delta \tilde{G}_{\ddagger}^{\mathrm{ICET}}} \tilde{\rho}_{\mathrm{e}}(\tilde{\varepsilon})}{\sin(\pi\alpha)} \tag{142}$$

where $\Delta \tilde{G}_{\ddagger}^{\mathrm{ICET}}$ is given by eqn (155). In contrast to ECIT, the Fermi level ($\tilde{\varepsilon} = 0$) is always close to the most probable energy for electrons or holes involved in reduction or oxidation by ICET at a metal electrode, respectively, regardless of the overpotential or reorganization energy. For the symmetric ICET ($\alpha = 1/2$), the electron energy (for reduction) or hole energy (for oxidation) are sampled from the hyperbolic secant distribution

$$P_{\mathrm{red/ox}}^{\mathrm{ICET}} = \frac{1}{2\pi} \operatorname{sech}\left(\frac{\tilde{\varepsilon}}{2}\right) \tag{143}$$

which has mean and variance,

$$\langle \varepsilon \rangle = \varepsilon_{\mathrm{F}} \tag{144}$$

$$\mathrm{Var}(\varepsilon) = (\pi k_{\mathrm{B}} T)^2 \tag{145}$$

respectively, and excess kurtosis, 2. The latter indicates that the distribution is leptokurtotic, meaning that it has fat tails and a more sharply peaked central region compared to a normal (or Gaussian) distribution.

The limiting electron energy distributions are shown in Fig. 12 for symmetric ICET and in Fig. 13 for asymmetric ICET. For symmetric ICET, eqn (145), the participating electrons and holes lie within a few $k_{\mathrm{B}}T$ of the Fermi level, but for

asymmetric ICET, eqn (141), the distribution of transferring electron energies is strongly skewed with a fat tail to favor either electrons far below the Fermi level for $\alpha \to 0$ or holes far above the Fermi level for $\alpha \to 1$. As noted above, these are singular limits associated with diverging faradaic reaction rates, as the number of participating electrons $\tilde{N}_e$ diverges for $\alpha \to 0, 1$.

It would be interesting to develop quantum mechanical models for the non-Gaussian statistics of electron energies participating in nonadiabatic CIET, generalizing the DHO model for Marcus kinetics of nonadiabatic ET.[133,134] The most natural quantum model would involve "displaced linear oscillators", where the IT coordinate is described, for example, by the truncated linear wells of eqn (118). One could also assume bilinear wells of the form,

$$f_1(q_O, \xi) = \beta_{red}\left|\frac{\xi - \xi_O}{\xi_R - \xi_O}\right| \tag{146}$$

$$f_2(q_R, \xi) = \beta_{ox}\left|\frac{\xi_R - \xi}{\xi_R - \xi_O}\right| \tag{147}$$

or other, more realistic models of the diabatic states with smoothed parabolic minima in the IT coordinate, in addition to the harmonic approximation for the solvent reorganization coordinate q in eqn (47) and (48). In the ICET limit, we expect that such quantum models would yield Meixner statistics of electron transfer, eqn (141), from first-order perturbation theory in the semi-classical limit, while also providing a fully quantum mechanical derivation of the Butler–Volmer equation.

8.5 CIET effects in photo-electron spectroscopy

The ICET distribution of electron energies, eqn (141), is an example of a generalized hyperbolic secant distribution[136] from the Meixner family of stochastic processes.[135,137,138] These distributions have received relatively little attention in statistics,[139] although they are used to describe non-Gaussian fluctuations of stock prices in financial mathematics.[140] In physics, skewed hyperbolic secant distributions have been proposed to fit asymmetric peaks in X-ray photoelectron spectroscopy (XPS) by Losev,[141,142] but without any physical justification. The electron energy distribution for ICET appears to be the first case of Meixner–Losev statistics derived from a physical model.

Asymmetric line shapes are commonly observed in both XPS[143,144] and Auger electron spectroscopy (AES)[145,146] of metal surfaces, and they are fitted to either cascades of symmetric line shapes or various skewed functions.[141,147,148] In XPS of simple metals, asymmetric line shapes are usually fitted to the skewed Lorentzian shape of Doniach and Šunjić[149] (with power-law tails) and attributed to many-body interactions between conduction electrons and the final-state core hole.[144,150,151] For chemically-oxidized metal surfaces, similar asymmetric line shapes are also observed if the oxide film has a wide band of conducting states near the Fermi level to accept shake-up electrons, while more symmetric line shapes are observed for insulating oxide films.[143,152] Interestingly, the Losev line shape[141,142] (with exponential tails) has also been shown to fit XPS line shapes for conducting oxide and sulphide films on metal surfaces.[153]

The final state of core-electron photo-emission is an ionized atom (with a core hole), which feels a strong Coulomb attraction to the metal surface, as it draws in electrons (and repels holes) in the conduction band near the Fermi level to form a meta-stable ion-image polaron pair near the surface. This shake-up process of polaron formation can be viewed as a CIET reaction, where ionized atom transfer into the surface is coupled with electron transfer from the bulk conduction band to a nearby, weakly-coupled orbital. The binding energy of the transferring electron (relative to the Fermi energy) is subtracted from the emitted photo-electron energy, resulting in a larger apparent binding energy for the original core electron.

CIET theory provides a simple alternative explanation for the observed trends in XPS line shapes on metal surfaces. For insulating surface films, the ET step is rate limiting and leads to the Gerischer–Marcus Gaussian line shape of ECIT. For conducting surface films, the IT step is rate limiting and leads to the Meixner–Losev line shape of ICET. In that case, the relative ease of reduction, $\beta_{\mathrm{red}} < \beta_{\mathrm{ox}}$, (resulting from the core hole) explains the skew of the distribution to larger binding energies, $\alpha < 1/2$, as shown in Fig. 13(b).

Stronger signatures of CIET should be apparent in AES, where ionic relaxation is known to play an important role in spectra with asymmetric line shapes.[145,146] Auger electron photo-emission creates a doubly-ionized atom (with core and valence holes), which can attract two conduction electrons to form a divalent polaron by CIET. Given the larger ion transfer energies for divalent ions, the AES shake-up process is even more likely influenced by ICET, which again skews the line shape to larger binding energies.

9 Adiabatic ICET and electrocatalysis

The mathematical theory of CIET developed here is strictly valid only for nonadiabatic ET with weak electronic coupling, $\Delta_{\mathrm{e}} \ll k_{\mathrm{B}}T$, but we expect some of its key predictions to be universally valid, even in the opposite limit of strong coupling, $\Delta_{\mathrm{e}} \gg k_{\mathrm{B}}T$, where ET is adiabatic, involving electrons that are shared in hybrid orbitals between the diabatic states. In the weakly adiabatic regime, where the electronic coupling is much smaller than the reorganization energy, $k_{\mathrm{B}}T < \Delta_{\mathrm{e}} \ll \lambda$, the level splitting partly lowers the ET free energy barriers, $\Delta G_{\mathrm{ET}}^{\mathrm{red/ox}}$, compared to the non-adiabatic CIET theory, as shown in Fig. 6(c)–(e), although the prefactor changes and becomes roughly independent of the electronic coupling.[25,31,154] As such, we expect similar functional forms for the limits of ECIT and ICET kinetics, but with a modified prefactor that could in principle be derived from quantum calculations. In the strongly adiabatic regime, typical of electrocatalysis, the electronic coupling may become comparable to or exceed the reorganization energy, $\Delta_{\mathrm{e}} > \lambda$, effectively eliminating the Marcus ET barrier, and a modified approach becomes necessary.

Schmickler[67] first proposed a unified quantum theory of adiabatic ET coupled with IT across the double layer at an electrode/electrolyte interface, based on a model Hamiltonian with electronic and solvent contributions, $H = H_{\mathrm{e}} + H_{\mathrm{sol}}$, each of which depend on the distance ξ of the ionic reactant from the electrode surface. The electronic part of the Hamiltonian $H_{\mathrm{e}}(\xi)$ is adapted from the Anderson–Newns model for chemisorption on metal surfaces for the case of one electronic state on the reactant exchanging electrons with the electrode, where the coupling matrix elements depend on ξ. The solvent Hamiltonian $H_{\mathrm{sol}}(\xi)$ describes

quantum harmonic oscillators for inner-sphere and outer-sphere modes perturbed by a linear interaction of the reactant and each solvent mode, where the coupling constants again depend on position ξ. For a particular choice of the dominant solvent mode, q, the model predicts a two-dimensional (q,ξ) energy landscape, which allows the activation barrier to be calculated, either by a simple analytical model or a more realistic quantum computation. However, the model does not account for the applied overpotential, so it is mainly used to predict trends in the exchange current prefactor with microscopic properties, *e.g.* explaining why silver electrodeposition is so fast, despite its large solvation energy (as a result of close approach of the solvated ion facilitating ET).[118]

Building on ideas of Savéant,[155,156] Koper and Voth extended Schmickler's adiabatic ET/IT model to account for bond-breaking electron transfer (BBET) between the reactant and the electrode, influenced by the overpotential.[69] Similar to the earliest models of Gurney[42] and Butler,[18] they used Morse potentials in ξ for the bond-breaking interactions coupling the reactant electron to the electrode. They also postulated that the energy of the anti-bonding orbital was equal to the inner-sphere reorganization energy plus the experimental overpotential, $\varepsilon_a = \lambda + \eta$, for small overpotentials $|\eta| \ll \lambda$. In this limit, the curved Tafel plot (characteristic of all ET theories) could be linearized to derive the charge transfer coefficient α as the degree of electron occupation of the anti-bonding orbital at the transition state,[69] similar to Hush's original interpretation of α for adiabatic outer-sphere ET reactions.[45] As noted in the Introduction, however, such ET theories are not able to explain the persistence of BV kinetics at higher potentials leading to Tafel's law.

In summary, since adiabatic ET models must take into account the molecular details of the electrode/electrolyte interface, they struggle to predict the charge transfer coefficient, let alone the full overpotential dependence of the reaction rate:

"The potential-energy surface will change when the electrode potential is varied; consequently the energy of activation will change too. These changes will depend on the structure of the double layer, so we cannot predict the transfer coefficient α unless we have a detailed model for the distribution of potential in the double layer." – Schmickler and Santos (2010).[25]

From the perspective of CIET theory, it would indeed seem difficult to make any general predictions about the form of the reaction rate for strongly adiabatic ECIT, where $\Delta_e > \lambda \gg \beta_{red/ox}$, since the electronic coupling overwhelms all other barriers and invalidates any use of transition state theory, but this is not the most common situation.

It is more typical for the IT free energies to be the largest in the system, $\beta_{red/ox} > \Delta_e, \lambda, k_B T$, since they include energies of solvation-shell shedding and chemical-bond breaking and thus often exceed 1 eV. Chemisorption functions for ET, by contrast, are usually much smaller, with the ET rate transitioning from non-adiabatic to weakly adiabatic around $\Delta_e \approx 1$ meV and to strongly adiabatic for electrocatalysis around $\Delta_e \approx 150$ meV,[154] which may exceed λ in some cases. Most systems are thus in the regime of ICET, already noted above in eqn (83), where the effect of adiabaticity is relatively small and only becomes important close to the transition state.

As shown in Fig. 14, whenever the linear approximations of the ξ-dependence of the diabatic free energy landscapes are valid, we expect BV kinetics to hold for adiabatic ICET, until a reaction-limited current is reached. Even for strongly adiabatic ICET with $\beta_{red/ox} \gg \Delta_e > \lambda$, the same functional form of the ICET rate should hold, since the kinetics are dominated by slow classical IT in the diabatic

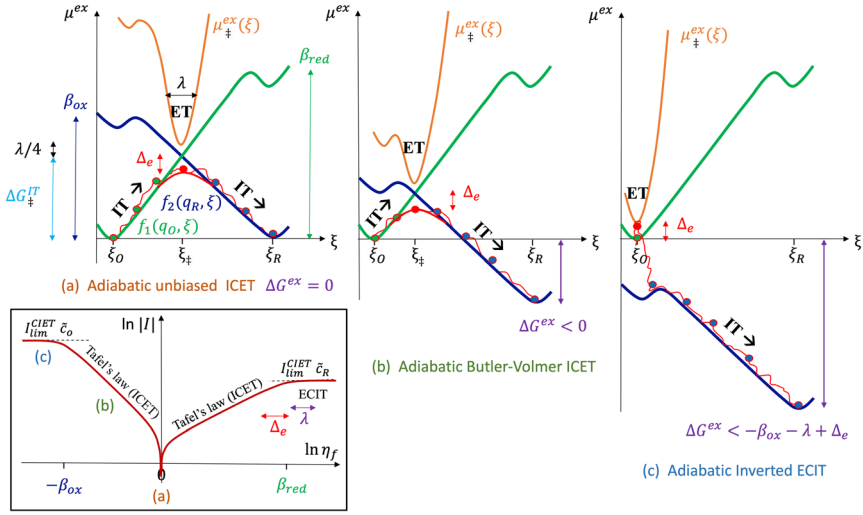

Fig. 14 Physics of strongly adiabatic ion-coupled electron transfer (ICET), where the chemisorption function (or electronic coupling) is larger than the reorganization energy and thermal energy, $\Delta_e > \lambda, k_BT$, but smaller than the ion-transfer free energies, $\Delta_e \ll \beta_{red/ox}$. In normal adiabatic ICET (a) and (b), the transferring electron remains in one of the diabatic states during IT until thermal fluctuations along the coordinate ξ activate the reduced and oxidized states to within Δ_e of the Gurney–Volmer diabatic crossing, yielding Butler–Volmer kinetics of ICET. (In contrast, for weakly adiabatic ICET (Fig. 7) or ECIT (Fig. 6), the orbitals mainly hybridize along the reorganization coordinate q, as in adiabatic ET theory.) During adiabatic ICET, Tafel's law may hold over a wide range of formal overpotentials, where the linear approximations of the ξ-dependence of the IT diabatic states holds, as shown in (b). At large formal overpotentials, $\eta_f < -\beta_{ox} - \lambda + \Delta_e$ for reduction or $\eta_f > \beta_{red} + \lambda - \Delta_e$ for oxidation, there is a transition to adiabatic Inverted ECIT shown in (c), which, for a metal electrode, leads to the universal limiting current dominated by barrierless transitions below the Fermi level.

states, except within Δ_e of the transition state, where the reduced and oxidized states create hybrid orbitals along the ξ axis to lower the effective barrier for fast adiabatic ET, as shown in Fig. 14(a) and (b). In contrast, for weakly adiabatic ICET (Fig. 7) or ECIT (Fig. 6), the red/ox hybridization occurs preferentially along the solvent reorganization coordinate, q, blurring the intersection of the Marcus parabolae. As long as the IT barriers are large, however, the main effect of adiabaticity is to lower the ICET activation barrier by Δ_e:

$$\Delta G_{\ddagger}^{\mathrm{ICET}} \approx \alpha(1-\alpha)(\lambda + \beta_{\mathrm{red}} + \beta_{\mathrm{ox}}) - \Delta_e \tag{148}$$

where Δ_e is constant in the wide band approximation for a metal electrode. The adiabatic correction in eqn (148) is valid as long as the overall barrier exceeds the thermal energy

$$\Delta G_{\ddagger}^{\mathrm{ICET}} > k_B T \tag{149}$$

in order to justify the use of classical transition state theory in the CIET derivation. We may expect a similar lowering of the IT barrier by Δ_e to hold for weakly adiabatic ECIT, eqn (72), as long as the corrected barrier is larger than the thermal energy.

As with nonadiabatic CIET, whenever barrierless transitions become energetically favorable, they will also dominate the response of a metallic electrode for adiabatic ICET. At large formal overpotentials, $\eta_f < -\beta_{ox} - \lambda + \Delta_e$ for reduction or $\eta_f > \beta_{red} + \lambda - \Delta_e$ for oxidation, we thus also expect a transition from adiabatic ICET to Inverted ECIT shown in Fig. 14(c). For a metal electrode, this again leads to the universal limiting current. In the transition regime, the ICET barrier, eqn (148), vanishes over a range of formal overpotentials $e|\Delta\eta_f| \approx \Delta_e + \lambda$, in order to first overcome the remaining IT barrier reduced by adiabaticity and as well as the reorganization energy required to achieve the dominant barrierless transition.

Recent progress in quantum electrochemistry has opened the possibility that *ab initio* calculations may soon be able to test these predictions and further develop the theory of adiabatic CIET to enable evaluation of its parameters from first principles. Chan and Nørskov proposed a simple approximation to convert from constant charge to constant potential for the electrode, by dividing the free energy along the reaction path into a chemical part and an electrostatic part, given by $\frac{1}{2}\Delta Q\Delta V$, where the charge ΔQ can be obtained by density functional theory (DFT) and ΔV is the electrode potential relative to computational vacuum (on the other side of the electrolyte).[157,158] Although this approach neglects the polarization of interfacial dipoles and various details of the electric double layers, it provides a means to compute the free energy landscape of adiabatic CIET as a function of electrode potential. In a "computational tour de force",[31] Kronberg and Laasonen recently used DFT-based constrained MD simulations to calculate the adiabatic free energy barrier *versus* applied potential for hydrogen evolution on a platinum electrode, the Volmer reaction on Pt(111), albeit with relatively large values compared to experiments.[159] Over some range of electrode potentials at different surface coverages, the free energy barriers vary almost linearly with formal overpotential, which would be consistent with BV kinetics of ICET, and there are also quadratic terms, perhaps similar to those arising in the more general CIET theory.

10 Summary of CIET kinetics for metal electrodes

In this section, we summarize the key predictions of CIET theory for faradaic reaction rates at metal electrodes in wide-band approximation ($\rho_e \approx$ constant), which is the most relevant limit for electrochemical engineering. Based on our analysis, we propose to replace phenomenological BV kinetics, eqn (1)–(4), with one of the following approximations, which correspond to different ordering of the three characteristic energies in the model, β_{red},β_{ox},$\lambda > k_BT$. The theory was developed for non-adiabatic CIET, $\Delta_e \ll k_BT$, but corrections for weakly adiabatic CIET are possible if the electronic coupling Δ_e is much smaller than at least one of three energies governing CIET (β_{red}, β_{ox} and λ).

10.1 Butler–Volmer kinetics of ICET

Ion-coupled electron transfer (ICET) at a metal electrode, illustrated in Fig. 7, is the most important limit of the general CIET theory, since the free energies of ion transfer are larger than the other energies in the model for most faradaic reactions:

$$\beta_{\mathrm{red/ox}} \gg \lambda, e|\eta_{\mathrm{f}}|, \Delta_{\mathrm{e}}, k_{\mathrm{B}}T \text{ (ICET)} \tag{150}$$

In the ICET regime, for formal overpotentials in the range,

$$-(\tilde{\beta}_{\mathrm{ox}} + \tilde{\lambda}) \ll \tilde{\eta}_{\mathrm{f}} \ll \tilde{\beta}_{\mathrm{red}} + \tilde{\lambda}, \tag{151}$$

the uniformly valid approximation of the CIET current at a metal electrode has the asymptotic form of the BV equation,

$$I = I_0^{\mathrm{ICET}} M(\tilde{\eta}_{\mathrm{f}})(\mathrm{e}^{-\alpha\tilde{\eta}} - \mathrm{e}^{(1-\alpha)\tilde{\eta}}) \tag{152}$$

multiplied by the matching function, $M(\tilde{\eta}_{\mathrm{f}})$, given by eqn (130)–(132), which imparts slight curvature to the Tafel plot controlled by λ. In most cases, one can set $M(\tilde{\eta}_{\mathrm{f}}) \approx M(0) = M_0(\alpha) = \pi\sqrt{\alpha(1-\alpha)}/\sin(\pi\alpha)$to recover the pure BV equation, which is exact in the limit of negligible reorganization energy, $\lambda/\beta_{\mathrm{ox/red}} \to 0$.

The charge-transfer coefficient is given by

$$\alpha = \frac{\beta_{\mathrm{red}}}{\beta_{\mathrm{red}} + \beta_{\mathrm{ox}}} \tag{153}$$

The parameters β_{red} and β_{ox} are IT free energies, which generally depend on temperature. In contrast, the Marcus reorganization energy λ has negligible temperature dependence. These are important predictions of CIET theory that can be tested experimentally.

The ICET exchange current (including the matching function) is given by

$$\begin{aligned} I_0 &= I_0^{\mathrm{ICET}} M\left(\ln\frac{\tilde{c}_{\mathrm{O}}}{\tilde{c}_{\mathrm{R}}}\right) \\ &= \frac{e\Delta_{\mathrm{e}}}{h}\frac{A}{A_{\mathrm{s}}}\mathrm{e}^{-\Delta\tilde{G}_{\ddagger}^{\mathrm{ICET}}}\frac{\tilde{c}_{\mathrm{O}}{}^{1-\alpha}\tilde{c}_{\mathrm{R}}{}^{\alpha}}{\gamma_{\ddagger}^{\mathrm{IT}}}\left(\frac{M\left(\ln\frac{\tilde{c}_{\mathrm{O}}}{\tilde{c}_{\mathrm{R}}}\right)}{\sqrt{\pi\alpha(1-\alpha)\tilde{\lambda}}}\right) \end{aligned} \tag{154}$$

The ICET activation energy is

$$\Delta G_{\ddagger}^{\mathrm{ICET}} = \alpha(1-\alpha)(\beta_{\mathrm{red}} + \beta_{\mathrm{ox}} + \lambda) - \Delta_{\mathrm{e}} \tag{155}$$

$$\Delta G_{\ddagger}^{\mathrm{ICET}} = \left(\frac{\beta_{\mathrm{red}}\beta_{\mathrm{ox}}}{\beta_{\mathrm{red}} + \beta_{\mathrm{ox}}}\right)\left(1 + \frac{\lambda}{\beta_{\mathrm{red}} + \beta_{\mathrm{ox}}}\right) - \Delta_{\mathrm{e}} \tag{156}$$

where we have added the simple correction for adiabatic ICET introduced above, which lowers the ICET barrier by Δ_{e} and thus amplifies the reaction rate. Using eqn (131) and (132), the factor in parentheses in eqn (154) can be replaced by

$$\frac{M\left(\ln\frac{\tilde{c}_{\mathrm{O}}}{\tilde{c}_{\mathrm{R}}}\right)}{\sqrt{\pi\alpha(1-\alpha)\tilde{\lambda}}} \to \frac{1}{\sin(\pi\alpha)}\sqrt{\frac{\pi}{\tilde{\lambda}}} \tag{157}$$

in the ICET limit, $\lambda/\beta_{\mathrm{ox/red}} \to 0$, consistent with eqn (106).

10.2 Marcus kinetics of normal ECIT

As shown in Fig. 6, for rate-limiting Normal ECIT at large reorganization energies,

$$\lambda \gg \beta_{\mathrm{red/ox}}, |e\eta_{\mathrm{f}}|, \Delta_{\mathrm{e}}, k_{\mathrm{B}}T \text{ (Normal ECIT)} \tag{158}$$

over the range of formal overpotentials,

$$e|\eta_{\mathrm{f}}| \ll \lambda, \tag{159}$$

the Faradaic current at a metal electrode can be approximated as

$$I_{\mathrm{ECIT}} = \frac{e\Delta_{\mathrm{e}}}{h}\frac{A}{A_{\mathrm{s}}}\frac{\mathrm{e}^{-\Delta\tilde{G}_{\ddagger}^{\mathrm{IT}}}}{\gamma_{\ddagger}^{\mathrm{IT}}}\left(\frac{\tilde{c}_O}{1+\mathrm{e}^{\tilde{\eta}_{\mathrm{f}}}} - \frac{\tilde{c}_{\mathrm{R}}}{1+\mathrm{e}^{-\tilde{\eta}_{\mathrm{f}}}}\right)\mathrm{erfc}\left(\frac{\tilde{\lambda} - \sqrt{1+\sqrt{\tilde{\lambda}}+\tilde{\eta}_{\mathrm{f}}{}^2}}{2\sqrt{\tilde{\lambda}}}\right). \tag{160}$$

The IT energy barrier is generally defined as the mean of the diabatic IT free energies,

$$\Delta G_{\ddagger}^{\mathrm{IT}} = \frac{1}{2}\min_{\xi}\{f_1(q_{\mathrm{O}},\xi) + f_2(q_{\mathrm{R}},\xi)\} - \Delta_{\mathrm{e}} \tag{161}$$

where the first term reduces to $\frac{1}{2}\min\{\beta_{\mathrm{red}}, \beta_{\mathrm{ox}}\}$ for the truncated linear approximation, eqn (118), and $\frac{1}{4}(\beta_{\mathrm{red}} + \beta_{\mathrm{ox}})$ for the uniformly valid approximation of CIET kinetics, and the second term is a weakly adiabatic correction.

The exchange current is given by

$$I_0^{\mathrm{ECIT}} = \frac{e\Delta_{\mathrm{e}}}{h}\frac{A}{A_{\mathrm{s}}}\frac{\mathrm{e}^{-\Delta\tilde{G}_{\ddagger}^{\mathrm{IT}}}}{\gamma_{\ddagger}^{\mathrm{IT}}}\frac{1}{2}\left(\frac{\tilde{c}_{\mathrm{R}}\tilde{c}_{\mathrm{O}}}{\tilde{c}_{\mathrm{R}}+\tilde{c}_{\mathrm{O}}}\right)\mathrm{erfc}\left(\frac{\tilde{\lambda} - \sqrt{1+\sqrt{\tilde{\lambda}}+\ln^2\left(\frac{\tilde{c}_{\mathrm{O}}}{\tilde{c}_{\mathrm{R}}}\right)}}{2\sqrt{\tilde{\lambda}}}\right) \tag{162}$$

Note that we have set $M = 1$ for the asymptotic limit, $\tilde{\lambda} \gg \tilde{\beta}_{\mathrm{red/ox}}$, corresponding to ECIT. Considering the low-temperature expansion of I_0^{ECIT}, the total activation barrier at low overpotentials is given by eqn (72), which is the symmetric case of eqn (155) for $\alpha = 1/2$.

10.3 Reaction-limited current for inverted ECIT

In the limit of large overpotentials,

$$e|\eta_{\mathrm{f}}| \gg \beta_{\mathrm{red/ox}}, \lambda, \Delta_{\mathrm{e}}, k_{\mathrm{B}}T \text{ (Inverted ECIT)} \tag{163}$$

a metal electrode will exhibit a constant reaction-limited current given by

$$\lim_{\eta\to\pm\infty} I = I_{\mathrm{lim}}^{\mathrm{CIET}}\tilde{c}_{\mathrm{R/O}} \tag{164}$$

where

$$I_{\mathrm{lim}}^{\mathrm{CIET}} = \frac{e\Delta_{\mathrm{e}}}{h}\frac{A}{A_{\mathrm{s}}}\frac{2}{\gamma_{\ddagger}^{\mathrm{IT}}} \tag{165}$$

is the quantum-mechanical limiting current corresponding to barrierless nonadiabatic ECIT in the limit of weak electronic coupling, using Fermi's golden rule. Further developments in the theory of adiabatic CIET will be required to refine the prediction of the limiting current for more general situations, especially for electrocatalysis. However, we expect our theoretical framework of CIET to

correctly predict the conditions for the breakdown of either MHC kinetics of Normal ECIT or BV kinetics of ICET, including Tafel's law, when the reaction passes to the Inverted ECIT regime.

10.4 Uniformly valid approximation for CIET

Whenever an experimental system is able to reach large overpotentials and probe the transition to reaction-limited current, we propose using the uniformly valid approximation of CIET kinetics, eqn (128)–(132). This may be the simplest possible analytical approximation that exactly reproduces all of the preceding limiting cases and smoothly transitions between them. It is strictly valid for nonadiabatic CIET with small electronic coupling, $\Delta_e \ll k_B T \ll \lambda, \beta_{red/ox}$, but may also hold with barriers reduced by Δ_e for weakly adiabatic CIET, $k_B T < \Delta_e \ll \lambda, \beta_{red/ox}$ and perhaps even strongly adiabatic ICET, $k_B T < \lambda < \Delta_e \ll \beta_{red/ox}$, as long as the classical IT barriers are large and dominate the reaction rate.

11 Application to lithium iron phosphate

In this section, we briefly illustrate the application of CIET theory to our motivating problem of lithium ion intercalation in LFP. For the reduction of a monovalent ion such as Li^+ by intercalation into a solid electrode, we let $\tilde{c}_R = \tilde{c}$ be the dimensionless intercalated ion concentration (or filling fraction) in the solid and $\tilde{c}_O = \tilde{c}_+$ be the dimensionless adsorbed surface concentration (or surface coverage) given by the adsorption isotherm, eqn (20). As noted above, the key requirement for ion intercalation is that the CIET transition state excludes one solid site, or equivalently, involves one vacancy, $\gamma_{\ddagger}^{IT} = (1 - \tilde{c})^{-1}$. From this theoretical perspective, we revisit the existing data for the rate dependence on overpotential, temperature and solid concentration.

11.1 Overpotential and temperature dependence

First, we consider the limiting case of Normal ECIT. As described in the introduction, CIET theory was born out of the hypothesis that ET from a metal coating (or surface contact) could limit the rate of ion intercalation in a poorly conducting solid electrode, such as LFP.[63] By interpreting the non-monotonic chronoamperometry data for LFP porous electrodes (Fig. 4) using a statistical model of reaction-limited phase transformations,[160] Bai and Bazant[63] constructed Tafel plots (Fig. 3) for the rate constants for LFP intercalation *versus* overpotential (averaging over the microscopic concentration dependence) and found excellent agreement with MHC kinetics of ET (using the original integral form[87] just before the analytical approximation of Zeng *et al.*[60] became available). As shown in Fig. 3(b) and 15(a), the Tafel data over a wide range of overpotentials and three different temperatures was shown to fit the MHC equation with a single value of the reorganization energy, $\lambda = 214 \pm 1$ meV ($\tilde{\lambda} = 8.3$ at room temperature) and independently fitted prefactors for each branch of Tafel data, shown in Fig. 15(b). The small uncertainty (0.5%) in the fitted reorganization energy indicates that the overpotential dependence of ECIT for a metal surface, eqn (160), captures the shape of these Tafel curves very well. As noted by the authors, the fact that all of the Tafel curvatures can be accurately fitted (with 0.5% uncertainty) by a single, temperature-independent reorganization energy provides strong support for the hypothesis of

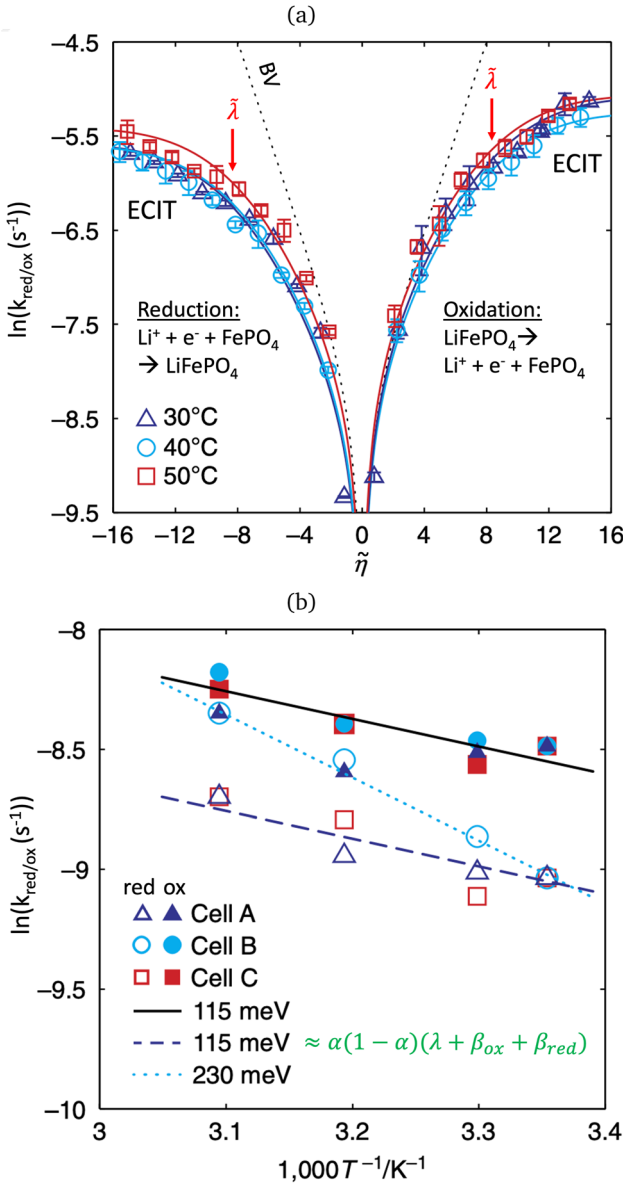

Fig. 15 Quantitative evidence for LFP intercalation by ECIT. (a) Tafel plots of rate constants, $k_{red/ox}$, measured at different temperatures from the population dynamics of phase separation (assuming reaction limitation) and fitted to the MHC equation for ECIT (solid lines) with a single value of the reorganization energy, $\lambda = 214 \pm 1$ meV and independently fitted prefactors for each Tafel branch. (b) Arrhenius plots of $k_{red/ox}$ revealing activation energies consistent with the prediction of nonadiabatic CIET theory at low overpotentials. [Adapted from Bai and Bazant (2014).[63]]

ET limitation in these experiments. In contrast, any fitted series resistances, which are routinely invoked to curve Tafel plots with BV kinetics,[88] must be temperature dependent, if they are to represent either ionic or electronic transport processes.

Further support for the ECIT hypothesis comes from the temperature dependence, shown in Fig. 15(b). Bai and Bazant[63] noted that the observed activation barriers for LFP intercalation in the range 115–230 meV were much larger than the Marcus prediction, $\lambda/4 = 53.5$ meV for MHC kinetics. CIET theory is now able to attribute this discrepancy to the additional barrier $\Delta G_{\ddagger}^{\mathrm{IT}}$ for ion transfer.[103] In the truncated linear approximation, the general formula for the IT barrier in ECIT, eqn (161), implies $\beta_{\min} = \min\{\beta_{\mathrm{red}}, \beta_{\mathrm{ox}}\} = 2\Delta G_{\ddagger}^{\mathrm{IT}} = 123$–$353$ meV, where we assume weak electronic coupling ($\Delta_{\mathrm{e}} \ll \lambda, \beta_{\mathrm{red/ox}}$) for nonadiabatic ECIT. The best fitting activation energy barrier (115 meV) corresponds to an ion transfer energy, $\beta_{\min} = 123$ meV, which is indeed much smaller than the reorganization energy, $\lambda = 214$ meV, obtained from the Tafel data, consistent with the hypothesis of ECIT. Even the highest activation energy (230 meV) would imply $\beta_{\min} \approx \lambda$, so we conclude that LFP intercalation kinetics in the original experiments[63] were consistent with CIET under at least partial ET limitation, $\lambda \geq \beta_{\mathrm{red/ox}}$.

Despite this consistent theoretical interpretation, the experimental data in Fig. 15 deviates from symmetric ECIT kinetics, eqn (67), since the rate constant for oxidation (Li^+ extraction) is somewhat larger than that of reduction (Li^+ insertion) by roughly a factor of $e^{0.5} = 1.65$. There could be several reasons for the small, observed asymmetry. The diabatic free energy landscapes, eqn (47) and (48), could have different force constants, k_{O} and k_{R}, approximated by the generalized AMH model of asymmetric ECIT, eqn (82). Alternatively, we could assume symmetric ET, $k_{\mathrm{O}} = k_{\mathrm{R}} = k$, and shift the formal overpotential by $\Delta\tilde{\eta} = \Delta\ln(\tilde{c}_+/\tilde{c}) \approx 1$, which would imply a larger surface coverage$\tilde{c}_+$ by a factor of $e \approx 2.7$ for oxidation versus reduction, assuming the slowest dynamics occurs for $\tilde{c} \to 1$ (since concentrations were not measured). Both models would slightly distort the excellent fit of the Tafel plots with MHC kinetics.

Next, we consider the ICET limit of the theory. Although the Tafel data in Fig. 15 is well fitted by MHC kinetics of ECIT, another study of LFP intercalation kinetics by Heubner, Schneider and Michaelis[88] based on nonlinear impedance spectroscopy found good agreement with nearly symmetric BV kinetics ($\alpha = 0.55$) up to 200 meV overpotentials, after subtracting various series resistances and neglecting any concentration heterogeneity from phase separation.[88] These experiments could also be consistent with CIET theory in the ICET regime, if $\beta_{\mathrm{ox}} > \beta_{\mathrm{red}} \gg 200$ meV $\gg \lambda$, provided that the nonlinear current pulses are large enough to suppress phase separation by driven auto-inhibitory reactions.[82,105,106] Unfortunately, temperature dependence was not measured, so we cannot perform this consistency check. Using eqn (155), we can at least estimate a consistent lower bound on the non-adiabatic ICET activation barrier, $\Delta G_{\ddagger}^{\mathrm{ICET}} \gg (200\ \mathrm{meV})/2 + \lambda/4$, which could fall in the range of activation energies from Fig. 15(b) assuming a small reorganization energy, $\lambda \ll 200$ meV, theoretically consistent with the ICET hypothesis. It is possible to have two different LFP electrodes exhibit different regimes of CIET kinetics, *e.g.* if the carbon coating and surface roughness are different, and we shall see that both ICET and ECIT lead to similar solid concentration dependence.

Regardless whether ET or IT is rate limiting, further evidence in favor of the general CIET theory is provided by the values of the inferred parameters, λ and $\beta_{\mathrm{red/ox}}$, which are quantitatively consistent with microscopic theories of charge transfer. In support of the ECIT hypothesis, the original paper noted that the fitted reorganization energy, $\lambda = 214$ meV, is identical to the Marcus outer-sphere

value calculated from the dielectric properties and crystal structure of LFP,[63] according to the reaction mechanism in Fig. 3(a). Here, we also infer the IT free energies, $\beta_{\min} = 123$–353 meV for ECIT or $\beta_{\min} > 200$ meV for ICIT, which are comparable to *ab initio* calculations of the diffusion barriers for Li^+/e^- polaron hopping in the bulk LFP (200–300 meV)[161,162] as well as the (adiabatic) oxidation barriers to extract Li^+ from charge-stabilized surface sites (150–200 meV).[163] The fact that surface modification of LFP by sulfur or nitrogen anions lowers the calculated energy barriers for IT, while also exhibiting faster charge-transfer kinetics in experiments,[163] also supports the hypothesis that CIET is rate limiting.

11.2 Solid concentration dependence

A major challenge in studying reaction kinetics in LFP is its strong tendency to separate into stable phases of high and low lithium ion concentration,[24,90,106] which makes it impossible to know the active area and surface concentration profile in order to interpret electrochemical measurements quantitatively. Experiments are further confounded by reaction heterogeneities associated with fast and slow regions on the surface,[106] *e.g.* due to variations in surface coatings of active materials. These effects can only be unraveled by direct imaging of the local surface concentration under driven reactions and learning optimal models to fit the data.

Recently, H. Zhao *et al.* overcame this challenge by learning the physics of heterogeneous intercalation kinetics in LFP nanoparticles directly from a massive dataset from *in operando* scanning tunneling X-ray microscopy (STXM) images,[105] building on the earlier experiments of Lim *et al.*[106] Using inverse learning methods (PDE-constrained optimization, Markov-chain Monte Carlo and Bayesian inference), the unknown constitutive relations were obtained from the STXM data for a general modeling framework based on electrochemical nonequilibrium thermodynamics,[24] which had previously been applied to LFP nanoparticles using classical models for reaction kinetics and phase separation dynamics.[84,93,94,102] The learned model was able to reproduce over 180 000 pixels of X-ray image data from 63 nanoparticles, each cycled through complete reduction (Li^+ insertion) and oxidation (Li^+ extraction), with only 7% global error across all pixels. Since the intercalation kinetics of carbon-coated LFP nanoparticles are famously fast along the *b*-axis of the LFP crystal exposed by the active (010) facet of the platelets,[165,166] the experiments were limited to small overpotentials, on the order of several k_BT/e. As such, the inverse learning process could not discern the overpotential dependence (assumed to be Butler–Volmer), but it was able to accurately extract the concentration dependence. Nanoscale spatial heterogeneities in the reaction rate constant were also learned from the STXM images and correlated with variations in carbon coating thickness, thereby enabling precise measurement of the underlying intercalation reaction kinetics.

The concentration dependence of the exchange current learned from the X-ray data is shown in Fig. 16 and compared to theoretical predictions. In a striking validation of the theory, the CIET exchange current *versus* concentration predicts the learned asymmetric profile to within the experimental error for all of the parameters estimated from the electrochemical data above. The ECIT limit, eqn (162), which provides the best fit of the Tafel plots in Fig. 15, also fits the exchange current very well for most choices of concentrations, as illustrated by the values $\tilde{c}_+ = 0.3$ and $\tilde{c} \to 1$ for the slowest reduction reaction dominating the transient

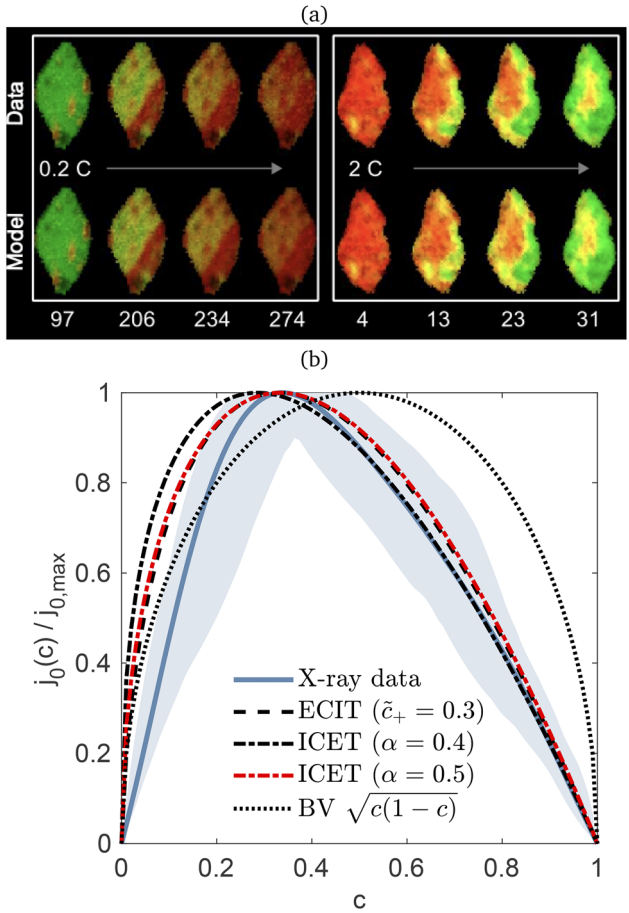

Fig. 16 Learning heterogeneous reaction kinetics of CIET from *operando* scanning tunneling X-ray microscopy (STXM)[106] by solving inverse problems for the best model that fits all pixels of the X-ray image data.[105] (a) Experimental images (top row) of LFP platelet nanoparticles undergoing driven phase transformations at different currents (0.2C and 2C with times shown below in minutes), compared with the learned model simulations with BV reaction kinetics (bottom row). (b) The normalized exchange current density profile learned from the X-ray images is shown as the solid blue curve with shaded blue range of uncertainty *versus* inserted lithium filling fraction, $\tilde{c}_R = c$, and compared with the theoretical predictions for ECIT, eqn (162), and ICET, eqn (154), using parameters that are also consistent with the Tafel data in Fig. 15. For comparison, the standard BV model with $I_0 \sim \sqrt{c(1-c)}$ widely used in Li-ion battery simulations[9,10,164] is not consistent with the experimental data. [Figure courtesy of Hongbo Zhao, adapted from Zhao *et al.* (2023).[105]]

response. The ICET formula, eqn (154), almost perfectly fits the learned kinetics at high concentration using the same value of $\alpha = 0.4$ inferred above from electrochemical data, while symmetic ICET with $\alpha = 0.5$ provides an even better overall fit. Overall, the analysis supports the picture of lithium intercalation in carbon-coated LFP as a process limited by comparable barriers for ET and IT.

An important general prediction of our CIET theory of ion intercalation kinetics is that the exchange current is proportional to the ion vacancy concentration in the electrode, $\tilde{I}_0 \propto (1 - \tilde{c})$. This linear trend is seen in both ECIT and

ICET formulae, in excellent agreement with the X-ray data in Fig. 16. This prediction holds regardless of whether ET or IT is rate-limiting because it comes from the universal activity coefficient of the IT transition state for intercalation, which must capture the exclusion of one site,[24], $(\gamma_{\ddagger}^{\mathrm{IT}})^{-1} = 1 - \tilde{c}$. In contrast, the standard empirical model of intercalation kinetics, used in popular porous electrode theory models and battery simulation software, postulates $\tilde{I}_0 \propto \sqrt{\tilde{c}(1-\tilde{c})}$, which scales with the square root of the vacancy concentration.[9,164] This model is inconsistent with the X-ray data, as well as the fundamental theory of CIET.

12 Conclusion and outlook

In summary, we have developed a theoretical framework of coupled ion–electron transfer (CIET) integrating the quantum physics of electron transfer (ET) with the non-equilibrium thermodynamics of ion transfer (IT). The theory can be applied to arbitrary diabatic free energy landscapes for the donor and acceptor states, but its scaling is controlled by six characteristic energies: the excess free energy of reaction, ΔG^{ex}, the thermal energy, $k_{\mathrm{B}}T$, the donor–acceptor electronic coupling, H_{DA}, the Marcus reorganization energy of ET, λ, and the free energies of IT, β_{ox} and β_{red}, in the donor and acceptor states, prior to oxidation and reduction, respectively.

Although CIET theory can be applied to chemical reactions in isolated molecules or bulk materials, our focus has been on faradaic reactions at electrode/electrolyte interfaces, where the reaction rate is controlled by the applied (formal) overpotential η_{f}. The thermodynamic driving force felt by electrons of energy ε relative to the Fermi level ε_{F} is given by $\Delta G^{\mathrm{ex}} = e\eta_{\mathrm{f}} + \varepsilon_{\mathrm{F}} - \varepsilon$. For semiconductor electrodes, there are additional energy scales having to do with the band structure, but in the usual case of metal electrodes, we make the wide-band approximation and replace H_{DA} with the chemisorption function, Δ_{e}. The physics of CIET are set by the relative magnitudes of the six characteristic energies, $e\eta_{\mathrm{f}}$, $k_{\mathrm{B}}T$, Δ_{e}, λ, β_{red} and β_{ox}. The theory assumes thermally activated transitions ($k_{\mathrm{B}}T \ll \lambda, \beta_{\mathrm{red}}, \eta_{\mathrm{ox}}$) and nonadiabatic ET ($\Delta_{\mathrm{e}} \ll k_{\mathrm{B}}T$), but does not constrain the other parameters. For weakly adiabatic CIET ($\Delta_{\mathrm{e}} \ll \lambda, \beta_{\mathrm{red}}, \beta_{\mathrm{ox}}$), activation energies are effectively lowered by Δ_{e}.

For metal electrodes, we considered three asymptotic limits leading to simple rate expressions (summarized in Section 10), each corresponding to a distinct reaction mechanism. First, we showed that the original CIET theory[103] tacitly assumed ET-limited reactions at small overpotentials ($\eta_{\mathrm{f}}, \beta_{\mathrm{red}}, \beta_{\mathrm{ox}} \ll \lambda$), leading to normal Marcus kinetics of electron-coupled ion transfer (Normal ECIT). Second, we considered IT-limited reactions ($\lambda \ll \beta_{\mathrm{red}}, \beta_{\mathrm{ox}}$) and derived the Butler–Volmer (BV) equation as the fundamental rate expression for ion-coupled electron transfer (ICET). This appears to be the first quantum mechanical derivation of BV kinetics, which reproduces Tafel's limiting law over a wide range of overpotentials ($-\beta_{\mathrm{ox}} \ll e\eta_{\mathrm{f}} \ll \beta_{\mathrm{red}}$). The ICET formula also connects the phenomenological BV parameters, α and I_0, to microscopic properties of the electrode/electrolyte interface, which can be measured experimentally or predicted by quantum computation. The theory also predicts that the transferring electron energy in ICET is selected from a fat-tailed Meixner (skewed hyperbolic secant) distribution, rather than the Gaussian distribution of ECIT from Gerischer–Marcus theory.

These electron energy distributions may find applications in describing asymmetric XPS and AES line shapes. Third, we predicted a universal transition to inverted Marcus kinetics of ECIT (Inverted ECIT) for large overpotentials ($\eta_f \ll -\beta_{ox}$ or $\eta_f \gg \beta_{red}$). For a metal electrode, the possibility of barrierless transitions during Inverted ECIT leads to a quantum-mechanical reaction-limited current with vanishing activation energy. Finally, we derived uniformly valid asymptotic approximations that smoothly interpolate between these three regimes, which are useful for intermediate cases where $\lambda \approx \beta_{red} \approx \beta_{ox}$.

One such intermediate case appears to be lithium intercalation in lithium iron phosphate (LFP), a popular cathode material for Li-ion batteries. We revisited the original data revealing ET rate limitation in LFP ($\lambda \approx 215$ meV)[63] and concluded that there was indeed a somewhat smaller barrier for IT in those experiments ($\beta_{min} \approx 123$ meV). If the kinetics lie closer to ICET than ECIT, however, due to different interfacial properties, this could help explain a subsequent study consistent with Butler–Volmer kinetics up to moderate overpotentials.[88] The key to this analysis, which could be replicated in other studies, was to seek consistency between theoretical predictions of both overpotential dependence (Tafel plots) and temperature dependence (Arrhenius plots) of the CIET rate. It was also compelling to confirm that the parameters are consistent with barriers predicted by Marcus theory, as well as quantum calculations.

Since it is difficult to isolate faradaic currents at large overpotentials without causing side reactions or transport limitation, it is important to test other predictions of the model. Besides temperature dependence, the model makes falsifiable predictions about concentration dependence, in particular, that the intercalation rate vanishes linearly with vacancy concentration in the solid at high filling fractions. For LFP, the predicted concentration profiles of both ICET and ECIT exchange currents are in excellent agreement with X-ray image-based learning of reaction kinetics,[105] lending further support to the hypothesis of CIET rate limitation for ion intercalation.

The new theory may find applications to other faradaic reactions in electrochemical engineering, such as electrodeposition and electrocatalysis. Since LFP is an electrical insulator exhibiting polaronic conduction of ion–electron pairs, it makes sense that ET from a metallic surface contact could contribute to CIET rate limitation. The situation is similar to metal electrodeposition from a ceramic solid electrolyte, which was recently shown by Williams *et al.* to be consistent with CIET theory[100] (in the ECIT limit) for sodium plating from NaSICON solid electrolyte in solid-state Na-ion batteries.[167] In contrast, most other Li-ion battery active materials, such as graphite anodes and transition metal oxide cathodes, are themselves metallic, and thus not as likely to exhibit ET rate limitation. Future studies of intercalation kinetics in these materials should also consider BV kinetics of ICET and test the predicted dependence on temperature, concentrations, and interfacial properties. The general features of limiting current and linear dependence on vacancy concentration may be quite robust, which may explain why ECIT theory helps explain the onset of lithium plating upon lattice saturation in graphite.[98,168] A recent study of lithium electrodeposition from liquid electrolytes by Boyle *et al.* also showed evidence of ET limitation *via* curved Tafel plots measured with microelectrodes,[107] but the data may be more consistent with ICET, which should explain the observed electrolyte dependence of the activation barrier better than my earlier theory based on ET limitation.[24]

Electrocatalysis normally involves strong electronic coupling leading to adiabatic ET, but we noted here that CIET theory may still apply if $\Delta_e \ll \beta_{red/ox},\lambda$. In a recent study of Bayesian model selection from experimental Tafel data for CO_2 reduction to CO on gold surfaces in aqueous electrolytes, out of many models, the best fit was found by MHC kinetics of ECIT.[169] Electrolysis of water and other electrocatalytic reactions also provide some of the clearest examples of Tafel's law,[62] which can now be explained by adiabatic or nonadiabatic ICET theory in the limit of large IT free energies. Williams *et al.* recently generalized nonadiabatic ECIT theory for protons tunneling between quantized energy levels in response to slow ET, a reaction mechanism we would call "electron-coupled proton transfer" (ECPT).[110] The theory accounts for electrostatic surface potentials and adsorbed proton dipole moments on mixed proton–electron conductor surfaces, such as Ni/galadonium-doped ceria, and predicts ECPT reaction rates of water electrolysis and hydrogen evolution in solid-oxide fuel cells (SOFC).[110]

Our theory also provides a useful framework for multiscale computation, to connect atomistic properties of electrode/electrolyte interfaces to faradaic reaction kinetics in electrochemical systems. Constrained density functional theory (CDFT),[39] which has already been used to predict ET kinetics using Marcus theory, would be the ideal method to calculate *ab initio* diabatic energy surfaces[38] for use in CIET theory. The advantage of the theory is its simplicity, in identifying a few key parameters and providing a convenient formula, *e.g.* for use in coarse-grained engineering models.[104]

Conflicts of interest

There are no conflicts to declare.

Acknowledgements

This work builds on over a decade of research on ET/CIET kinetics in batteries with key contributions by Dimitrios Fraggedakis, Peng Bai, Yi Zeng, Nicholas Williams, Raymond Smith, Michael McEldrew, Yamini Krishnan, and Hongbo Zhao primarily funded by Toyota Research Institute *via* the D3BATT Center for Data-Driven Design of Rechargeable Batteries. The recent advances sprang from a collaboration funded by Shell with Yirui Zhang, Shakul Pathak, Armando Neto, Cristina Grosu and Yang Shao-Horn, who also provided useful comments on the manuscript. The author thanks Shakul for proofreading the equations, as well as Gisela Scott and the editors accommodating some revisions after the conference.

Notes and references

1 E. Kaxiras, *Atomic and electronic structure of solids*, 2003.
2 A. Urban, D.-H. Seo and G. Ceder, *npj Comput. Mater.*, 2016, **2**, 16002.
3 D. Bedrov, J.-P. Piquemal, O. Borodin, A. D. MacKerell Jr, B. Roux and C. Schröder, *Chem. Rev.*, 2019, **119**, 7940–7995.
4 L. Scalfi, M. Salanne and B. Rotenberg, *Annu. Rev. Phys. Chem.*, 2021, **72**, 189–212.
5 V. G. Levich and C. W. Tobias, *J. Electrochem. Soc.*, 1963, **110**, 251C.

6 A. J. Bard and L. R. Faulkner, *Electrochemical Methods*, J. Wiley & Sons, Inc., New York, NY, 2001.
7 J. O. Bockris, A. K. N. Reddy and M. E. Gamboa-Aldeco, *Modern electrochemistry 2B: electrodics in chemistry, engineering, biology and environmental science*, Springer Science & Business Media, 1998, vol. 2.
8 J. O. Bockris, B. E. Conway and R. E. White, *Modern aspects of electrochemistry*, Springer Science & Business Media, 1992, vol. 22.
9 J. Newman and N. P. Balsara, *Electrochemical systems*, John Wiley & Sons, 2021.
10 T. F. Fuller and J. N. Harb, *Electrochemical engineering*, John Wiley & Sons, 2018.
11 J. A. V. Butler, *Trans. Faraday Soc.*, 1932, **28**, 379–382.
12 T. Erdey-Grúz and M. Volmer, *Z. Phys. Chem.*, 1931, **157A**, 165.
13 J. Tafel, *Z. Phys. Chem.*, 1905, **50**, 641–712.
14 G. Burstein, *Corros. Sci.*, 2005, **47**, 2858–2870.
15 J. A. V. Butler, *Trans. Faraday Soc.*, 1924, **19**, 659–665.
16 J. A. V. Butler, *Trans. Faraday Soc.*, 1924, **19**, 729–733.
17 J. A. V. Butler, *Trans. Faraday Soc.*, 1924, **19**, 734–739.
18 J. A. V. Butler, *Proc. R. Soc. London, Ser. A*, 1936, **157**, 423–433.
19 F. P. Bowden, *Proc. R. Soc. London, Ser. A*, 1929, **125**, 446–462.
20 T. Erdey-Grúz and M. Volmer, *Z. Phys. Chem.*, 1930, **150**, 203–213.
21 R. G. Compton and C. E. Banks, *Understanding voltammetry*, World Scientific, 2018.
22 A. Frumkin, *Z. Phys. Chem.*, 1933, **164A**, 121–133.
23 P. Biesheuvel, M. Van Soestbergen and M. Z. Bazant, *Electrochim. Acta*, 2009, **54**, 4857–4871.
24 M. Z. Bazant, *Acc. Chem. Res.*, 2013, **46**, 1144–1160.
25 W. Schmickler and E. Santos, *Interfacial electrochemistry*, Springer Science & Business Media, 2010.
26 A. M. Kuznetsov and J. Ulstrup, *Electron Transfer in Chemistry and Biology: An Introduction to the Theory*, Wiley, 1999.
27 V. Levich and R. Dogonadze, *Dokl. Akad. Nauk SSSR*, 1959, **124**, 123–126.
28 M. Z. Bazant, K. T. Chu and B. J. Bayly, *SIAM J. Appl. Math.*, 2005, **65**, 1463–1484.
29 P. Biesheuvel, M. van Soestbergen and M. Bazant, *Electrochim. Acta*, 2009, **54**, 4857–4871.
30 R. A. Marcus and N. Sutin, *Biochim. Biophys. Acta, Rev. Bioenerg.*, 1985, **811**, 265–322.
31 E. Santos and W. Schmickler, *Chem. Rev.*, 2022, **122**, 10581–10598.
32 R. R. Nazmutdinov, M. D. Bronshtein, T. T. Zinkicheva and D. V. Glukhov, *Int. J. Quantum Chem.*, 2016, **116**, 189–201.
33 R. A. Marcus, *J. Chem. Phys.*, 1956, **24**, 966–978.
34 R. Marcus, *J. Chem. Phys.*, 1957, **26**, 867–871.
35 R. Marcus, *J. Chem. Phys.*, 1957, **26**, 872–877.
36 R. A. Marcus, *Annu. Rev. Phys. Chem.*, 1964, **15**, 155–196.
37 R. A. Marcus, *Rev. Mod. Phys.*, 1993, **65**, 599–610.
38 T. Van Voorhis, T. Kowalczyk, B. Kaduk, L.-P. Wang, C.-L. Cheng and Q. Wu, *Annu. Rev. Phys. Chem.*, 2010, **61**, 149–170.
39 B. Kaduk, T. Kowalczyk and T. Van Voorhis, *Chem. Rev.*, 2012, **112**, 321–370.

40 J. Weiss, *Proc. R. Soc. London, Ser. A*, 1954, **222**, 128–141.
41 R. A. Marcus, *Discuss. Faraday Soc.*, 1960, **29**, 21–31.
42 R. W. Gurney, *Proc. R. Soc. London, Ser. A*, 1931, **134**, 137–154.
43 M. Chatenet, B. G. Pollet, D. R. Dekel, F. Dionigi, J. Deseure, P. Millet, R. D. Braatz, M. Z. Bazant, M. Eikerling, I. Staffell, *et al.*, *Chem. Soc. Rev.*, 2022, **51**, 4583–4762.
44 N. S. Hush, *Ber. Bunsenges. Phys. Chem.*, 1957, **61**, 734–738.
45 N. S. Hush, *J. Chem. Phys.*, 1958, **28**, 962–972.
46 N. S. Hush, *Trans. Faraday Soc.*, 1961, **57**, 557–580.
47 V. G. Levich, in *Advances in Electrochemistry and Electrochemical Engineering*, ed. P. Delahay and C. W. Tobias, Interscience, New York, 1966, vol. 4, pp. 249–371.
48 R. R. Dogonadze and Y. A. Chizmadzhev, *Dokl. Akad. Nauk SSSR*, 1962, **145**, 848–851.
49 R. R. Dogonadze, A. M. Kuznetsov and A. A. Chernenko, *Russ. Chem. Rev.*, 1965, **34**, 759–775.
50 R. Dogonadze, A. Kuznetsov and M. Vorotyntsev, *J. Electroanal. Chem. Interfacial Electrochem.*, 1970, **25**, A17–A19.
51 R. A. Marcus, *J. Chem. Phys.*, 1965, **43**, 679.
52 R. Marcus, *J. Chem. Soc., Faraday Trans.*, 1996, **92**, 3905–3908.
53 D. F. Calef and P. G. Wolynes, *J. Phys. Chem.*, 1983, **87**, 3387–3400.
54 D. F. Calef and P. G. Wolynes, *J. Chem. Phys.*, 1983, **78**, 470–482.
55 D. V. Matyushov and G. A. Voth, *J. Chem. Phys.*, 2000, **113**, 5413–5424.
56 D. V. Matyushov, *J. Chem. Phys.*, 2009, **130**, 234704.
57 E. Laborda, M. C. Henstridge and R. G. Compton, *J. Electroanal. Chem.*, 2012, **667**, 48–53.
58 E. Laborda, M. C. Henstridge, C. Batchelor-McAuley and R. G. Compton, *Chem. Soc. Rev.*, 2013, **42**, 4894–4905.
59 J. Newman and K. E. Thomas-Alyea, *Electrochemical Systems*, John Wiley and Sons, Hoboken, New Jersey, 3rd edn, 2004.
60 Y. Zeng, R. B. Smith, P. Bai and M. Z. Bazant, *J. Electroanal. Chem.*, 2014, **735**, 77–83.
61 Y. Zeng, P. Bai, R. B. Smith and M. Z. Bazant, *J. Electroanal. Chem.*, 2015, **748**, 52–57.
62 S. U. Khan and J. O. Bockris, *J. Phys. Chem.*, 1983, **87**, 2599–2603.
63 P. Bai and M. Z. Bazant, *Nat. Commun.*, 2014, **5**, 3585.
64 J. M. Savéant, *J. Am. Chem. Soc.*, 2008, **130**, 4732–4741.
65 R. Cukier, *J. Phys. Chem.*, 1994, **98**, 2377–2381.
66 R. I. Cukier and D. G. Nocera, *Annu. Rev. Phys. Chem.*, 1998, **49**, 337–369.
67 W. Schmickler, *Chem. Phys. Lett.*, 1995, **237**, 152–160.
68 W. Schmickler, *Electrochim. Acta*, 1996, **41**, 2329–2338.
69 M. T. Koper and G. A. Voth, *Chem. Phys. Lett.*, 1998, **282**, 100–106.
70 C. Hartnig and M. T. Koper, *J. Am. Chem. Soc.*, 2003, **125**, 9840–9845.
71 S. Hammes-Schiffer, *Acc. Chem. Res.*, 2001, **34**, 273–281.
72 M. H. V. Huynh and T. J. Meyer, *Chem. Rev.*, 2007, **107**, 5004–5064.
73 E. Santos, K. Pötting and W. Schmickler, *Faraday Discuss.*, 2009, **140**, 209–218.
74 E. Santos, A. Lundin, K. Pötting, P. Quaino and W. Schmickler, *Phys. Rev. B*, 2009, **79**, 1–10.
75 S. Y. Reece and D. G. Nocera, *Annu. Rev. Biochem.*, 2009, **78**, 673–699.

76 S. Hammes-Schiffer and A. V. Soudackov, *J. Phys. Chem. B*, 2008, **112**, 14108–14123.
77 S. Horvath, L. E. Fernandez, A. V. Soudackov and S. Hammes-Schiffer, *Proc. Natl. Acad. Sci. U. S. A.*, 2012, **109**, 15663–15668.
78 M. M. Melander, *J. Electrochem. Soc.*, 2020, **167**, 116518.
79 J.-M. Savéant, *Annu. Rev. Anal. Chem.*, 2014, **7**, 537–560.
80 S. Hammes-Schiffer, *Acc. Chem. Res.*, 2018, **51**, 1975–1983.
81 G. A. Parada, Z. K. Goldsmith, S. Kolmar, B. P. Rimgard, B. Q. Mercado, L. Hammarström, S. Hammes-Schiffer and J. M. Mayer, *Science*, 2019, **364**, 471–475.
82 M. Z. Bazant, *Faraday Discuss.*, 2017, **199**, 423–463.
83 K. Singh, H. Bouwmeester, L. de Smet, M. Bazant and P. Biesheuvel, *Phys. Rev. Appl.*, 2018, **9**, 064036.
84 P. Bai, D. A. Cogswell and M. Z. Bazant, *Nano Lett.*, 2011, **11**, 4890–4896.
85 M. C. Henstridge, C. Batchelor-McAuley, R. Gusmão and R. G. Compton, *Chem. Phys. Lett.*, 2011, **517**, 108–112.
86 R. Kurchin and V. Viswanathan, *J. Chem. Phys.*, 2020, **153**, 134706.
87 C. E. Chidsey, *Science*, 1991, **251**, 919–922.
88 C. Heubner, M. Schneider and A. Michaelis, *J. Power Sources*, 2015, **288**, 115–120.
89 W. Dreyer, J. Jamnik, C. Guhlke, R. Huth, J. Moškon and M. Gaberšček, *Nat. Mater.*, 2010, **9**, 448–453.
90 T. R. Ferguson and M. Z. Bazant, *Electrochim. Acta*, 2014, **146**, 89–97.
91 L. Li, Y.-c. K. Chen-Wiegart, J. Wang, P. Gao, Q. Ding, Y.-S. Yu, F. Wang, J. Cabana, J. Wang and S. Jin, *Nat. Commun.*, 2015, **6**, 6883.
92 G. K. Singh, G. Ceder and M. Z. Bazant, *Electrochim. Acta*, 2008, **53**, 7599–7613.
93 D. A. Cogswell and M. Z. Bazant, *ACS Nano*, 2012, **6**, 2215–2225.
94 D. A. Cogswell and M. Z. Bazant, *Nano Lett.*, 2013, **13**, 3036–3041.
95 B. Mamedov, *J. Math. Chem.*, 2013, **51**, 2699–2703.
96 K. B. Oldham and J. C. Myland, *J. Electroanal. Chem.*, 2011, **655**, 65–72.
97 R. B. Smith, E. Khoo and M. Z. Bazant, *J. Phys. Chem. C*, 2017, **121**, 12505–12523.
98 T. Gao, Y. Han, D. Fraggedakis, S. Das, T. Zhou, C.-N. Yeh, S. Xu, W. C. Chueh, J. Li and M. Z. Bazant, *Joule*, 2021, **5**, 393–414.
99 D. Zhuang and M. Z. Bazant, *J. Electrochem. Soc.*, 2022, **169**, 100536.
100 N. J. Williams, E. Quérel, I. D. Seymour, S. J. Skinner and A. Aguadero, *Chem. Mater.*, 2023, **35**, 863–869.
101 D. Fraggedakis and M. Z. Bazant, *J. Chem. Phys.*, 2020, **152**, 184703.
102 D. A. Cogswell, *Phys. Rev. E: Stat., Nonlinear, Soft Matter Phys.*, 2015, **92**, 011301(R).
103 D. Fraggedakis, M. McEldrew, R. B. Smith, Y. Krishnan, Y. Zhang, P. Bai, W. C. Chueh, Y. Shao-Horn and M. Z. Bazant, *Electrochim. Acta*, 2021, **367**, 137432.
104 R. B. Smith and M. Z. Bazant, *J. Electrochem. Soc.*, 2017, **164**, E3291–E3310.
105 H. Zhao, H. D. Deng, A. E. Cohen, J. Lim, Y. Li, D. Fraggedakis, B. Jiang, B. D. Storey, W. C. Chueh, R. D. Braatz and M. Z. Bazant, *Nature*, 2023, in press.
106 J. Lim, Y. Li, D. H. Alsem, H. So, S. C. Lee, P. Bai, D. A. Cogswell, X. Liu, N. Jin, Y.-s. Yu, N. J. Salmon, D. A. Shapiro, M. Z. Bazant, T. Tyliszczak and W. C. Chueh, *Science*, 2016, **353**, 566–571.

107 D. T. Boyle, X. Kong, A. Pei, P. E. Rudnicki, F. Shi, W. Huang, Z. Bao, J. Qin and Y. Cui, *ACS Energy Lett.*, 2020, **5**, 701–709.
108 G. K. Singh, G. Ceder and M. Z. Bazant, *Electrochim. Acta*, 2008, **53**, 7599–7613.
109 Y. Fu, S. Poizeau, A. Bertei, C. Qi, A. Mohanram, J. Pietras and M. Z. Bazant, *Electrochim. Acta*, 2015, **159**, 71–80.
110 N. J. Williams, R. E. Warburton, I. D. Seymour, A. E. Cohen, M. Z. Bazant and S. J. Skinner, *J. Chem. Phys.*, 2023, **158**, 244107.
111 G. H. Vineyard, *J. Phys. Chem. Solids*, 1957, **3**, 121–127.
112 N. G. Van Kampen, *Stochastic processes in physics and chemistry*, Elsevier, 1992, vol. 1.
113 W. Schmickler, *J. Electroanal. Chem.*, 1986, **204**, 31–43.
114 J. Muscat and D. Newns, *Prog. Surf. Sci.*, 1978, **9**, 1–43.
115 S. W. Feldberg and N. Sutin, *Chem. Phys.*, 2006, **324**, 216–225.
116 M. Z. Bazant, M. S. Kilic, B. D. Storey and A. Ajdari, *Adv. Colloid Interface Sci.*, 2009, **152**, 48–88.
117 A. Sood, A. D. Poletayev, D. A. Cogswell, P. M. Csernica, J. T. Mefford, D. Fraggedakis, M. F. Toney, A. M. Lindenberg, M. Z. Bazant and W. C. Chueh, *Nat. Rev. Mater.*, 2021, **6**, 847–867.
118 L. M. Pinto, E. Spohr, P. Quaino, E. Santos and W. Schmickler, *Angew. Chem., Int. Ed.*, 2013, **52**, 7883–7885.
119 P. Quaino, N. Luque, R. Nazmutdinov, E. Santos and W. Schmickler, *Angew. Chem., Int. Ed.*, 2012, **51**, 12997–13000.
120 N. S. Hush, *J. Electroanal. Chem.*, 1999, **460**, 5–29.
121 Q. Wu and T. Van Voorhis, *J. Chem. Phys.*, 2006, **125**, 164105.
122 M. Melander, E. Jónsson, J. J. Mortensen, T. Vegge and J. M. García Lastra, *J. Chem. Theory Comput.*, 2016, **12**, 5367–5378.
123 N. Holmberg and K. Laasonen, *J. Chem. Theory Comput.*, 2017, **13**, 587–601.
124 A. Hashemi, P. Peljo and K. Laasonen, *J. Phys. Chem. C*, 2023, **127**, 3398–3407.
125 M. C. Henstridge, E. Laborda, N. V. Rees and R. G. Compton, *Electrochim. Acta*, 2012, **84**, 12–20.
126 M. D. Berliner, D. A. Cogswell, M. Z. Bazant and R. D. Braatz, *J. Electrochem. Soc.*, 2021, **168**, 090504.
127 G. Galuppini, M. D. Berliner, D. A. Cogswell, D. Zhuang, M. Z. Bazant and R. D. Braatz, *J. Power Sources*, 2023, **573**, 233009.
128 G. Galuppini, M. D. Berliner, H. Lian, D. Zhuang, M. Z. Bazant and R. D. Braatz, *J. Power Sources*, 2023, **580**, 233272.
129 M. C. Henstridge, E. Laborda, Y. Wang, D. Suwatchara, N. Rees, Á. Molina, F. Martinez-Ortiz and R. G. Compton, *J. Electroanal. Chem.*, 2012, **672**, 45–52.
130 E. E. Tanner, L. Xiong, E. O. Barnes and R. G. Compton, *J. Electroanal. Chem.*, 2014, **727**, 59–68.
131 E. E. L. Tanner, E. O. Barnes, C. B. Tickell, P. Goodrich, C. Hardacre and R. G. Compton, *J. Phys. Chem. C*, 2015, **119**, 7360–7370.
132 H. Gerischer, *Z. Phys. Chem.*, 1960, **26**, 223–247.
133 J. Jortner, *J. Chem. Phys.*, 1976, **64**, 4860–4867.
134 A. Nitzan, *Chemical dynamics in condensed phases: relaxation, transfer and reactions in condensed molecular systems*, Oxford University Press, 2006.
135 J. Meixner, *Journal of the London Mathematical Society*, 1934, **1**, 6–13.
136 D. C. Vaughan, *Commun. Stat. Theory Methods*, 2002, **31**, 219–238.

137 C. Lai, *Math. Chron.*, 1977, **6**, 6–20.
138 B. Grigelionis, *Lithuanian Mathematical Journal*, 1999, **39**, 33–41.
139 P. Ding, *Am. Stat.*, 2014, **68**, 32–35.
140 M. J. Fischer, *Generalized hyperbolic secant distributions: with applications to finance*, Springer Science & Business Media, 2013.
141 A. Losev, *Surf. Interface Anal.*, 1989, **14**, 845–849.
142 A. Losev, *Appl. Spectrosc.*, 1994, **48**, 1289–1290.
143 D. J. Morgan, *Surf. Interface Anal.*, 2023, 1–5.
144 G. Wertheim and P. Citrin, in *Photoemission in solids I: general principles*, M. Cardona and L. Ley, Springer Berlin, Heidelberg, 2005, pp. 197–236.
145 D. E. Ramaker, *Crit. Rev. Solid State Mater. Sci.*, 1991, **17**, 211–276.
146 H. Madden, *Surf. Sci.*, 1983, **126**, 80–100.
147 B. Moeini, M. R. Linford, N. Fairley, A. Barlow, P. Cumpson, D. Morgan, V. Fernandez and J. Baltrusaitis, *Surf. Interface Anal.*, 2022, **54**, 67–77.
148 M. Schmid, H.-P. Steinrück and J. M. Gottfried, *Surf. Interface Anal.*, 2014, **46**, 505–511.
149 S. Doniach and M. Šunjić, *J. Phys. C: Solid State Phys.*, 1970, **3**, 285.
150 P. H. Citrin and T. D. Thomas, *J. Chem. Phys.*, 1972, **57**, 4446–4461.
151 S. Hüfner and G. Werthaim, *Phys. Rev. B: Solid State*, 1975, **11**, 678.
152 M. J. Acres, H. Hussain, M. S. Walczak, M. Nikiel, C. Sewell, C. Rafols i Belles, E. A. Ahmad, A. S. Walton, C. A. Muryn, N. M. Harrison and R. Lindsay, *Surf. Interface Anal.*, 202, **52**, 507–512.
153 A. Galtayries and J. Grimblot, *J. Electron Spectrosc. Relat. Phenom.*, 1999, **98**, 267–275.
154 W. Schmickler and J. Mohr, *J. Chem. Phys.*, 2002, **117**, 2867–2872.
155 J. M. Savéant, *Acc. Chem. Res.*, 1993, **26**, 455–461.
156 J. M. Saveant, *J. Am. Chem. Soc.*, 1987, **109**, 6788–6795.
157 K. Chan and J. K. Nørskov, *J. Phys. Chem. Lett.*, 2015, **6**, 2663–2668.
158 K. Chan and J. K. Nørskov, *J. Phys. Chem. Lett.*, 2016, **7**, 1686–1690.
159 R. Kronberg and K. Laasonen, *ACS Catal.*, 2021, **11**, 8062–8078.
160 P. Bai and G. Tian, *Electrochim. Acta*, 2013, **89**, 644–651.
161 T. Maxisch, F. Zhou and G. Ceder, *Phys. Rev. B: Condens. Matter Mater. Phys.*, 2006, **73**, 104301.
162 G. K. P. Dathar, D. Sheppard, K. J. Stevenson and G. Henkelman, *Chem. Mater.*, 2011, **23**, 4032–4037.
163 K.-S. Park, P. Xiao, S.-Y. Kim, A. Dylla, Y.-M. Choi, G. Henkelman, K. J. Stevenson and J. B. Goodenough, *Chem. Mater.*, 2012, **24**, 3212–3218.
164 M. Doyle, T. F. Fuller and J. Newman, *J. Electrochem. Soc.*, 1993, **140**, 1526–1533.
165 R. Malik, F. Zhou and G. Ceder, *Nat. Mater.*, 2011, **10**, 587–590.
166 R. Malik, D. Burch, M. Bazant and G. Ceder, *Nano Lett.*, 2010, **10**, 4123–4127.
167 E. Quérel, N. J. Williams, I. D. Seymour, S. J. Skinner and A. Aguadero, *Chem. Mater.*, 2023, **35**, 853–862.
168 H. Lian and M. Z. Bazant, *chemRxiv*, 2023, preprint.
169 S. M. Brown, M. Orella, Y. W. Hsiao, Y. Román-Leshkov, Y. Surendranath, M. Z. Bazant and F. Brushett, *chemRxiv*, 2020, preprint, DOI: **10.26434/chemrxiv.13244906.v1**.